TonB-dependent transport of Ferric Enterobactin through FepA in Gram negative bacteria

by

Aritri Majumdar

M.Sc., Jadavpur University, India, 2010

AN ABSTRACT OF A DISSERTATION

submitted in partial fulfillment of the requirements for the degree

DOCTOR OF PHILOSOPHY

Department of Biochemistry and Molecular Biophysics
College of Arts and Sciences

KANSAS STATE UNIVERSITY
Manhattan, Kansas

2018

Abstract

Siderophore uptake systems are one the most prominent methods of Fe^{3+}-iron acquisition in Gram negative bacteria. The catecholate siderophore enterobactin is synthesized and utilized by many members of *Enterobacteriaceae* as well as several of the ESKAPE pathogens. The outer membrane (OM) transporter of ferric enterobactin (FeEnt), FepA is a ligand-gated porin (LGP) that requires interaction with the inner membrane (IM) protein TonB in order to accomplish active transport. TonB is thought to transduce the electrochemical energy created by the proton gradient across the IM to LGPs like FepA in the OM, to promote siderophore transport through their occluded channels. However, we do not yet have a clear picture of either how TonB transfers energy to FepA, or what kind of conformational changes occur in the occluding domain of FepA to allow ligand passage. The experiments described herein investigate these two questions, building on previously outlined models and observations. Using fluorescence labeling of strategically substituted cysteines in the surface loops of FepA, we unraveled a hierarchy of loop motion during binding of FeEnt to FepA. Additionally, by rendering parts of the FepA protein immobile as a result of engineered disulfide bonds, I identified residues or regions within its occluding domain that may normally unfold to open a size-specific channel for FeEnt. I also elucidated the role of the peptidoglycan polymer beneath the OM a framework for protein-protein interactions between IM and OM proteins. This includes the proposed interaction between a rotating TonB and FepA, or other LGPs, that may transfer kinetic energy to the OM transporter.

The role of iron in microbial survival and pathogenesis makes iron-uptake pathways an attractive target for therapeutic intervention. Using the FeEnt-FepA uptake

system as a model, we used a fluorescence based high-throughput screening method to identify novel small molecule inhibitors of TonB action in *E. coli*. The approach used can be potentially adopted to screen bigger chemical libraries as well as used to find inhibitors of ESKAPE pathogens that use FeEnt such as, *Acinetobacter baumannii*, *Klebsiella pneumoniae* or *Pseudomonas aeruginosa*. Finally, we discoverd a TonB-dependent OM transporter of heme/hemoglobin called HutA in the oligotrophic bacterium *Caulobacter crescentus*.

TonB-dependent transport of Ferric Enterobactin through FepA in Gram negative bacteria

by

Aritri Majumdar

M.Sc., Jadavpur University, India, 201

A DISSERTATION

submitted in partial fulfillment of the requirements for the degree

DOCTOR OF PHILOSOPHY

Department of Biochemistry and Molecular Biophysics
College of Arts and Sciences

KANSAS STATE UNIVERSITY
Manhattan, Kansas

2018

Approved by:

Major Professor
Prof. Phillip E. Klebba

Copyright

Abstract

Siderophore uptake systems are one the most prominent methods of Fe^{3+}-iron acquisition in Gram negative bacteria. The catecholate siderophore enterobactin is synthesized and utilized by many members of *Enterobacteriaceae* as well as several of the ESKAPE pathogens. The outer membrane (OM) transporter of ferric enterobactin (FeEnt), FepA is a ligand-gated porin (LGP) that requires interaction with the inner membrane (IM) protein TonB in order to accomplish active transport. TonB is thought to transduce the electrochemical energy created by the proton gradient across the IM to LGPs like FepA in the OM, to promote siderophore transport through their occluded channels. However, we do not yet have a clear picture of either how TonB transfers energy to FepA, or what kind of conformational changes occur in the occluding domain of FepA to allow ligand passage. The experiments described herein investigate these two questions, building on previously outlined models and observations. Using fluorescence labeling of strategically substituted cysteines in the surface loops of FepA, we unraveled a hierarchy of loop motion during binding of FeEnt to FepA. Additionally, by rendering parts of the FepA protein immobile as a result of engineered disulfide bonds, I identified residues or regions within its occluding domain that may normally unfold to open a size-specific channel for FeEnt. I also elucidated the role of the peptidoglycan polymer beneath the OM a framework for protein-protein interactions between IM and OM proteins. This includes the proposed interaction between a rotating TonB and FepA, or other LGPs, that may transfer kinetic energy to the OM transporter.

The role of iron in microbial survival and pathogenesis makes iron-uptake pathways an attractive target for therapeutic intervention. Using the FeEnt-FepA uptake

system as a model, we used a fluorescence based high-throughput screening method to identify novel small molecule inhibitors of TonB action in *E. coli*. The approach used can be potentially adopted to screen bigger chemical libraries as well as used to find inhibitors of ESKAPE pathogens that use FeEnt such as, *Acinetobacter baumannii*, *Klebsiella pneumoniae* or *Pseudomonas aeruginosa*. Finally, we discoverd a TonB-dependent OM transporter of heme/hemoglobin called HutA in the oligotrophic bacterium *Caulobacter crescentus*.

Table of Contents

List of Figures……ix
List of Tables……xiv
Acknowledgements……xv
Dedications……..xvii
Chapter 1: Acquisition of iron in bacteria……1
1.1 Introduction……..1
1.1.1 Iron and bacterial pathogenesis……1
1.1.2 Bacterial iron uptake systems……...2
1.1.3 Siderophores……5
1.1.4 Regulation of iron uptake systems……...8
1.1.5 The Gram-negative bacterial cell envelope……10
1.1.6 Outer membrane channel transporters……13
1.1.7 Ferric enterobactin permease A (FepA)……19
1.1.8 TonB-ExbBD complex……...24
1.1.9 Role of the TonB IM complex in energy dependent iron uptake……...26
1.1.10 ROSET model of TonB action……...29
1.2 Significance of work……..32
Chapter 2: Materials and methods……33
2.1 Bacterial strains plasmids and culture conditions……..33
2.2 Preparation of plasmid DNA……..35
2.3 Preparation of $CaCl_2$ competent cells and heat shock transformation……...35
2.4 Preparation of electrocompetent cells and electroporation……36
2.5 One step gene replacement using PCR products……37
2.6 Site-directed mutagenesis……...38
2.7 Siderophore nutrition assay……39
2.8 Expression of FepA……39
2.9 Colicin sensitivity test……40
2.10 Siderophore accumulation over time……40
2.11 Siderophore binding assay……41
2.12 Siderophore transport……42
Chapter 3: Mechanism of Ferric enterobactin internalization by FepA……43
3.1 Introduction……43
3.2 Methods……..46
3.2.1 Creating double cysteine mutants……...46
3.2.2 Siderophore nutrition tests……..47
3.2.3 [^{59}Fe]Ent uptake assays……..47
3.2.4 Binding capacity screening……47
3.2.5 Spectroscopic measurement of FeEnt uptake by universal assay……..48
3.3 Results……48
3.3.1 Construction of double Cys mutants in FepA……48
3.3.2 Siderophore nutrition tests of double Cys mutants……50
3.3.3 [^{59}Fe]Ent accumulation studies……..53
3.3.4 Expression of FepA in Cys-Cys mutants……...55
3.3.5 Effect of disulfide bond formation on binding capacity……56

3.3.6 Spectroscopic measurement of FeEnt uptake by universal assay……..58
3.4 Discussion……...59
Chapter 4: Role of peptidoglycan in TonB dependent transport of ferric enterobactin by FepA.67
4.1 Introduction……67
4.2 Methods……...73
4.2.1 Transformation and expression of SAR endolysins in *E. coli*……...73
4.2.2 Preparation of spheroplasts……74
4.2.3 Expression of FepA in spheroplasts……...76
4.2.4 Siderophore nutrition tests……..76
4.2.5 Uptake of [^{59}Fe]Ent and [^{14}C]lactose……76
4.2.6 Live cell count assay……..77
4.2.7 MacConkey lactose utilization assay……77
4.2.8 Epifluorescence microscopy……..78
4.2.9 iPALM/dSTORM……...78
4.3 Results……82
4.3.1 Siderophore nutrition test with cells expressing SAR endolysins……..82
4.3.2 Survival ans stability of spheroplasts……85
4.3.3 Epifluorescence observation of FepA and TonB in spheroplasts……...89
4.3.4 [^{59}Fe]Ent uptake by spheroplasts……92
4.3.5 Proton motive force dependent transport via LacY……95
4.3.6 iPALM/dSTORM observation of FepA and TonB……..100
4.4 Discussion……102
Chapter 5: Concerted loop motion triggers induced fit of FepA to ferric enterobactin……...112
5.1 Introduction……...112
5.2 Methods……113
5.3 Results and discussion……...115
5.3.1 Site-directed fluorescence labeling of Cys substitutions in the surface loops of FepA……115
5.3.2 Loop motion during FeEnt binding and transport by FepA……118
5.3.3 Correspondence between fluorescence spectroscopic and radioisotopic measurement of FeEnt uptake……..119
5.3.4 Effects of ΔtonB on ligand adsorption to FepA in vivo……...121
5.3.5 Rates of FM quenching in different loops of FepA……..121
5.3.6 Bulk observations of FeEnt transport in living cells……123
Chapter 6: TonB-dependent Heme/Hemoglobin utilization by *Caulobacter crescentus* HutA..125
6.1 Introduction……...125
6.2 Methods……126
6.3 Results and discussion……...129
6.3.1 Siderophore nutrition tests with *C. crescentus*……129
6.3.2 Growth in iron-deficient media……130
6.3.3 Identificcation of potential iron transporters……130
6.3.4 Iron-regulated cell envelope proteins……...132
6.3.5 HutA is a receptor for heme/hemoglobin……134
6.3.6 Radioisotopic measurements of iron binding and transport……135
Chapter 7: Fluorescence high-throughput screening for inhibitors of TonB action……138
7.1 Introduction……...138

7.2 Methods……140
7.3 Results and discussion……...144
7.3.1 FLHTS for inhibitors of TonB-dependent FeEnt transport by FepA……...144
7.3.2 Identification and characterization of FeEnt transporter of *A. baumannii*...148
7.3.3 Fluorescence observations of FeEnt transport in AbaFepA Cys mutants…150
8. References……154

List of Figures

Figure 1-1: Iron availability and uptake systems in Gram negative and Gram positive bacteria…4

Figure 1-2: Siderophores…….6

Figure 1-3: Enterobactin: An Archetype for Microbial IronTransport……8

Figure 1-4: Alternative interpretations of the Fur box……...…….9

Figure 1-5: Arrangement of PG glycan strands…….13

Figure 1-6: Gram negative outer membrane β-barrel proteins……..15

Figure 1-7: Structure of FepA……20

Figure 1-8: Conformational changes in FepA during Ferric enterobactin binding and transport.22

Figure 1-9: Structure of TonB-ExbBD complex……...26

Figure 1-10: Schematic model of the arrangement of the PG-associated OM with OM proteins.29

Figure 1-11: ROSET model of TonB action……..31

Figure 3-1: Proposed model of FeEnt transport through FepA…….44

Figure 3-2: Location of of Cys-Cys mutants in the N-domain of FepA……49

Figure 3-3: Siderophore nutrition test for the N- to N-domain mutant G27C/R126C……...51

Figure 3-4: Siderophore nutrition test in N-domain and N- to C-domain mutants……52

Figure 3-5: Accumulation of [^{59}Fe]Ent over time in FepA Cys-Cys mutants……...54

Figure 3-6: [^{125}I]-Protein A immunoblot of N-domain Cys-Cys mutants…….55

Figure 3-7: Capacity screening of N-domain Cys-Cys mutants……57

Figure 3-8: Binding capacity at higher concentration of βME……..57

Figure 3-9: Spectroscopic observation of effect of disulfide bonds on FeEnt transport……..60

Figure 4-1: Schematic representation of the Gram-negative cell envelope……...69

Figure 4-2: TonB-GFP fusion construct……70

Figure 4-3: Plasmid map of pJFLyz……..75

Figure 4-4: Plasmid map of pGTFA698C…….81

Figure 4-5: Siderophore nutrition tests with Ferric ferrichrome and Ferric enterobactin……..84

Figure 4-6: Growth, percentage of spheroplast formation and survival of spheroplasts……...86

Figure 4-7: [^{125}I]-ProteinA immunoblot showing expression of FepA in whole cells and spheroplasts……88

Figure 4-8: Spectrophotometric observation of stability of spheroplasts in different media……89

Figure 4-9: Epifluorescence observation……...91

Figure 4-10: Accumulation of [^{59}Fe]Ent by KNK00 and KNK05……93

Figure 4-11: Accumulation of [^{59}Fe]Ent by BN1071……94

Figure 4-12: MacConkey lactose utilization assay by whole cells and spheroplasts……96

Figure 4-13: Vmax transport of [^{3}H]TMG by KNK00 whole cells and spheroplasts……...98

Figure 4-14: Accumulation of [^{14}C]lactose in KNK05 whole cells and spheroplasts……...99

Figure 4-15: iPALM/dSTORM observation in whole cells and spheroplasts……101

Figure 5-1: FM labeling reactions……....116

Figure 5-2: FeEnt-induced quenching of FepA surface loop–FM fluorescence, and recovery from FeEnt transport…….117

Figure 5-3: Concentration dependence of FeEnt quenching and recovery……..119

Figure 5-4: Rapid mixing stopped-flow measurements of FeEnt binding to FepA…….122

Figure 5-5: Observation of FeEnt binding and transport by Confocal microscopy…….124

Figure 6-1: Siderophore nutrition tests with *C. crescentus*……..129

Figure 6-2: Growth of *C. crescentus* NA1000 in iron-deficient media……...131

Figure 6-3: SDS-PAGE of iron regulated proteins……..133

Figure 6-4: Siderophore nutrition test……..135

Figure 6-5: Binding and uptake of [^{59}Fe]Fc and [^{59}Fe]Cit by *C. crescentus*……...136

Figure 7-1: Secondary screening for TonB-dependent inhibitors……146

Figure 7.2: Inhibition of [59Fe]Ent and [14C]lactose uptake in *E. coli* MG1655……...149

Figure 7-3: FeEnt transport by *A. baumannii*……..151

Figure 7-4: The proposed Cys residues in the Aba FepA……153

List of Tables

Table 1-1: TonB-dependent receptors encoded by the *E. coli* K-12 genome……17

Table 1-2: OM receptors utilized by colicins and bacteriophages to colonize Gram negative bacteria……..18

Table 2-1: List of strains used……....33

Table 2-2: List of plasmids used……34

Table 3-1: Summary of results from different assays for FeEnt transport due to the formation of the disulfide bonds…….65

Table 4-1: SAR endolysin plasmids used in the study……..73

Table 4-2: Number of clusters of FepA or mEos-TonB per cell vs cluster size……..102

Table 5-1: Binding and transport by cells expressing FepA Cys substitutions……...120

Table 5-2: Differential rates of FM quenching in extracellular loops of FepA……...123

Table 7-1: Summary of primary screen results……145

Table 7-2: Secondary screening of top 20 compounds against *E. coli* and *A. baumannii*……...147

Acknowledgements

I came to the United States of America to pursue my dream of higher education in science. Getting selected in Prof. Phillip E. Klebba's laboratory provided me a great opportunity to do that. In the past 6 years of working in his lab, I learnt a great deal about scientific research, evolved myself as a biochemist under his constant guidance and inspiration. Our co-advisor, Prof. Sally Newton, provided equal learning opportunities, at the same time making working in the lab a fun experience with her tremendous jovial demeanor. Over the course of time that I have been associated with them, they not only were great mentors but ultimately became my lighthouse of hope in a foreign country.

I would also like to thank my past lab mates, Dr. Lorne Jordan, Dr. Brittany Nairn, Dr. Yan Shipelskyi and the current members, Dr. Somnath Chakravorty, Asish Somvanshi, Taihao Yang for their help and support over the years. As a teaching assistant, I would like to extend my gratitude to all my students for making my teaching sessions, a fun and learning experience. The ever-helping departmental staff member, Melinda Bainter and technical genius, David Manning provided vital support in working through graduate school. I would like to thank from the bottom of my heart, the departmental head, and my committee member, Prof. Michael Zolkiewski along with all the faculty members of the department, for their help and support. I would like to extend my gratitude to Prof. Philip Hardwidge, who as a committee member, provided valuable insights on my thesis and research.

My acknowledgement will be incomplete without mentioning the contribution of my family in my life. My parents had to overcome unsurmountable obstacle in placing me where I am today and hence, they deserve equal share in my success. Last but not the least, the contributions

of my husband, Dr. Somnath Chakravorty in my daily and professional lives has kept me going through the ups and downs of the life of a graduate student.

Dedication

This work is dedicated to my mother Shyamasree and my husband Somnath

Chapter 1: Acquisition of iron in bacteria

1.1 Introduction

1.1.1 Iron and Bacterial pathogenesis

An unlimited supply of nutrients is a pre-requisite for profuse proliferation of bacteria. Thus, host organisms adopt mechanisms to limit the supply of nutrients like carbon sources, vitamins and metal ions from pathogens as a first line of defense. This is referred to as 'nutritional immunity'. While bacteria can adapt their metabolic pathways to suit the respective carbon and nitrogen availability, shortage of metal ions is often reflected as "stress-response" in *in-vivo* transcriptomic studies of bacteria from infection sites (Motley et al., 2004; Szafranzka et al., 2014; Nuss et al., 2017). The best studied example is of the dependence on iron, because of the ubiquitous role of iron in cell survival and proliferation. For most microorganisms and all animals, iron is indispensable as a red-ox agent, and also in catabolic pathways, peroxide reduction and DNA biosynthesis. Iron bound to heme helps in the transportation of oxygen. However, despite being one of the most abundant metals on the earth's crust, the availability of free iron in the extracellular milieu is limited (10^{-18} M) (Bullen et al., 1978). Iron readily oxidizes in aqueous environment to form large insoluble hydroxide polymers which are not suitable for uptake by living organisms. Furthermore, free iron in body fluids is cytotoxic. Hence, mammalian hosts complex free iron from body fluids using proteins like transferrin, lactoferrin, ferritin, haptoglobin further reducing the concentration of available iron to 10^{-24} M (Kretchmar et al.,1988). Therefore, microorganisms including pathogens must elaborate biosynthetic and transport systems to be able to acquire the metal from their environments as well as within their plant or animal hosts.

1.1.2 Bacterial Iron Uptake Systems

The chief sources of iron for bacteria are either free extracellular Fe^{2+} under anaerobic-microaerophillic conditions (Cao et al., 2007)), heme or Fe^{3+}-chelates. Depending on the cell wall architecture, Gram positive and Gram negative bacteria produce distinct iron receptors/transporters and binding proteins that enable the passage of the iron bound molecules through the different layers of the cell envelope into the cytosol. Free Fe^{2+} is rarely present in the host, except under conditions where the redox potential or the pH are disturbed, such as ischemia caused by a trauma or following reduction of the environment by proliferating bacteria (Bullen et al., 2005). In bacteria, Fe^{2+} enters the periplasm through non-specific porins and is delivered to the cytoplasm through different transporters such as FeoB in a GTP-dependent manner. To access iron from heme, bacteria either directly uptake heme or use hemophore-mediated heme transport proteins. Direct heme uptake systems are exemplified by Phu system (Pseudomonas heme uptake) and Isd (Iron-regulated surface determinant) system (Sharp et al., 2007; Reniere et al., 2007) in *Pseudomonas aeruginosa* and *Staphylococcus aureus* respectively. They possess cell surface receptors that directly bind hemoglobin (e.g. PhuR or, IsdH and IsdB) or hemoglobin-haptoglobin, extract heme from them and transfer it to other binding proteins (e.g. PhuT in the periplasm or, IsdC in peptidoglycan). The second heme-uptake system relies on hemophores, which are bacterial secreted proteins (e.g. HasA (heme acquisition system) in *Serratia marcescens*) (Letoffe et al., 1999) capable of scavenging porphyrin or heme from hemoglobin or hemoglobin-haptoglobin and hemopexin. Once they are shuttled to the cell surface, they are bound by hemophore-specific receptors (e.g. HasR). Subsequently, the extracted

heme is transported across the cell membrane via membrane transport systems (e.g. IsdDEH) or ABC-type transporters (e.g. PhuSTUVW) to the cytosol where heme is finally degraded by oxygenases and Fe^{2+} is extracted. Large number of bacteria are reported to comprise multiple heme uptake systems for example, *Neisseria meningitides* (Perkins-Balding et al., 2004), *Helicobacter pylori* (Worst et al., 1999), *Haemophilus influenzae*, *Pseudomonas aeruginosa* (Ochsner et al., 2000), *Serratia marcescens* (Letoffe et al., 1994). The apparent redundancy of heme-uptake systems in some of them has been explained by the fact that the heme sources recognized by the different systems are distinct. In *N. meningitidis,* heme from hemoglobin is transported by HmbR, whereas HpuA/HpuB can obtain heme from the hemoglobin–haptoglobin complex (Perkins-Balding et al., 2004). In *H. influenzae*, uptake of hemoglobin–haptoglobin is mediated by phase-variable Hgb-binding proteins (Cope et al., 2000), whereas a hemophore based transport system encoded by the huxCBA operon is employed for utilizing heme-hemopexin as a source (Morton et al., 2007). They may also require different levels of iron deprivation to be expressed. In *Serratia marcescens*, the hemophore-dependent system Has and the hemophore-independent system Hem are both required for optimal heme uptake but the role of HasA and the has system becomes more prominent when the concentration of available heme is less than 10^{-5} M (Benevides-matos & Biville, 2010).

Bacteria can also obtain ferric (Fe^{3+}) iron directly from Fe^{3+} chelating host proteins lactoferrin, transferrin, ferritin using membrane receptors that extract the metal (Cornelissen & Sparling, 1994). More common, however, are low-molecular weight Fe^{3+}-chelating compounds (typically <1kDa), the siderophores, which are secreted by microorganisms to the extracellular environment, bind Fe^{3+} with sub-nanomolar affinities

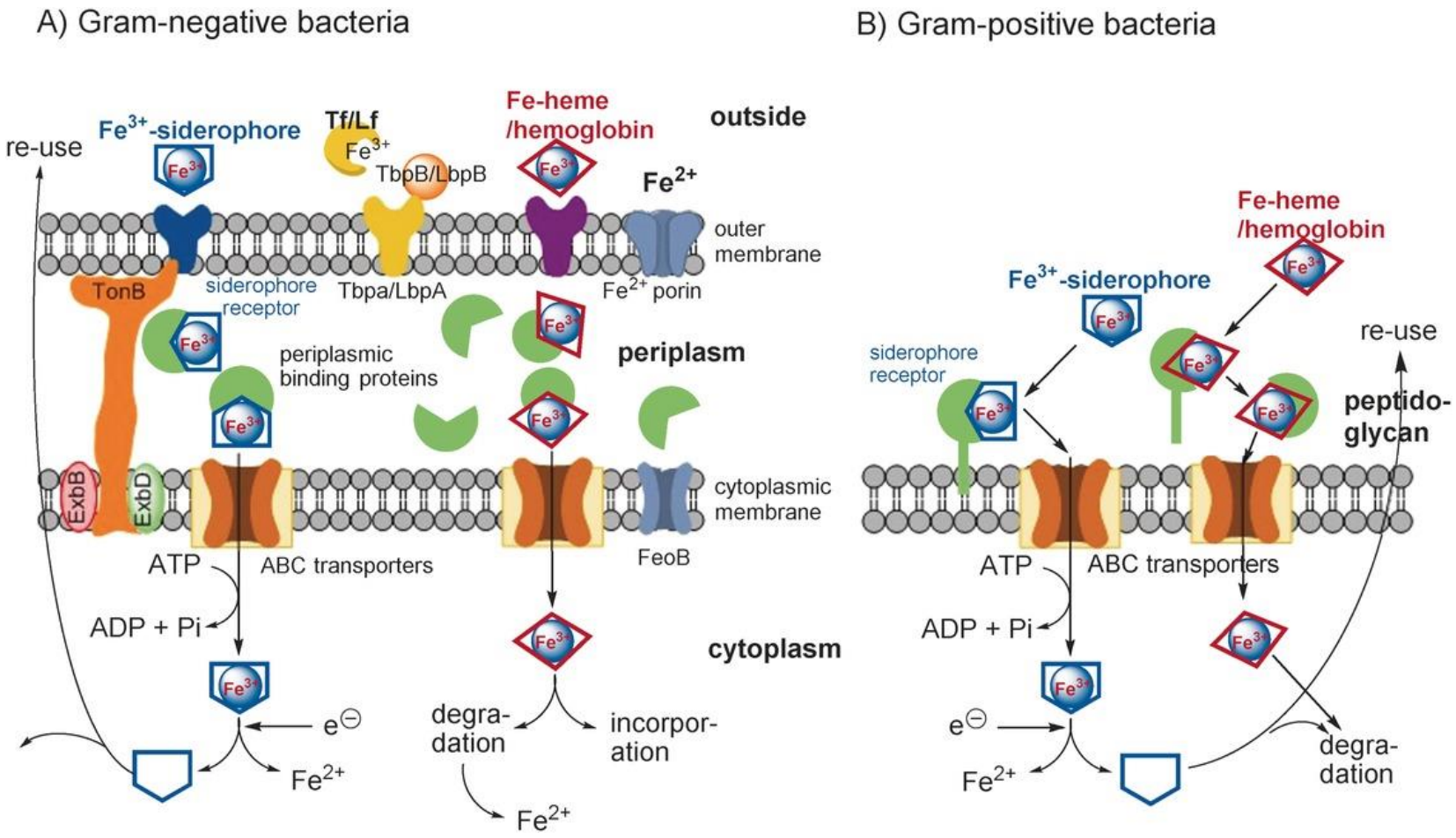

Fig. 1-1: Iron availability and uptake systems in Gram negative and Gram positive bacteria. U. Bilitewski, J. A. V. Blodgett, A.-K. Duhme-Klair, S. Dallavalle, S. Laschat, A. Routledge, R. Schobert, *Angew. Chem. Int. Ed.* **2017**, *56*, 14360. Reprinted with permission from John Wiley & Sons (License number 4437250601271).

and may even extract Fe^{3+} from the host iron chelating proteins (Neilands, 1995). To combat the Gram negative bacterial uptake systems, the host neutrophils and mucosal cells secrete Lipocalin-2 which can bind and de-activate the siderophore enterobactin. However, pathogens have evolved other siderophores like glycosylated enterobactin (salmochelin) or yersiniabactin which are not recognized by lipocalin-2 and hence escape the host immune system (Fischbach et al., 2006). A schematic showing different uptake systems in bacteria is shown in Fig. 1-1.

Thus, bacteria possess several and often at least partially redundant uptake systems to acquire iron from the environment and adjust in response to the available iron source. Because of the ubiquitous nature of these systems, these uptake and utilization systems are promising targets for novel therapeutic interventions. Majority of the focus till now has been on the Fe^{3+}-uptake systems. Antibiotics conjugated to siderophores, both natural (sideromycins) (Pramanik & Braun, 2006) and synthetic (Tillotson, 2016; Kohira et al., 2015) comprise the so-called “Trojan horse” strategy for attacking microbes. Ga^{3+} mimics of Fe^{3+}-siderophores (Ross-Gillespie et al., 2014) as well as small molecule inhibitors of siderophore transport systems have also been identified (Yep et al., 2014; Nairn et al., 2017).

1.1.3 Siderophores

Siderophores appear confined to the microbial world: plants and animals do not synthesize or utilize them for acquiring iron. While large number of fungi also produce siderophores, budding and fission yeast both do not (Neilands, 1987). To date more than 250 different siderophores are structurally characterized and grouped according to the functional groups which are involved in Fe^{3+}- coordination. The most common motifs are

catecholates, hydroxamates, α-hydroxycarboxylates and phenolates, which can also be combined in “mixed type” siderophores (Fig. 1-2). The most stable siderophores involve hexadentate coordination with octahedral binding geometry, which is ideal for binding iron (Abergel et al., 2008; Raymond et al., 2003).

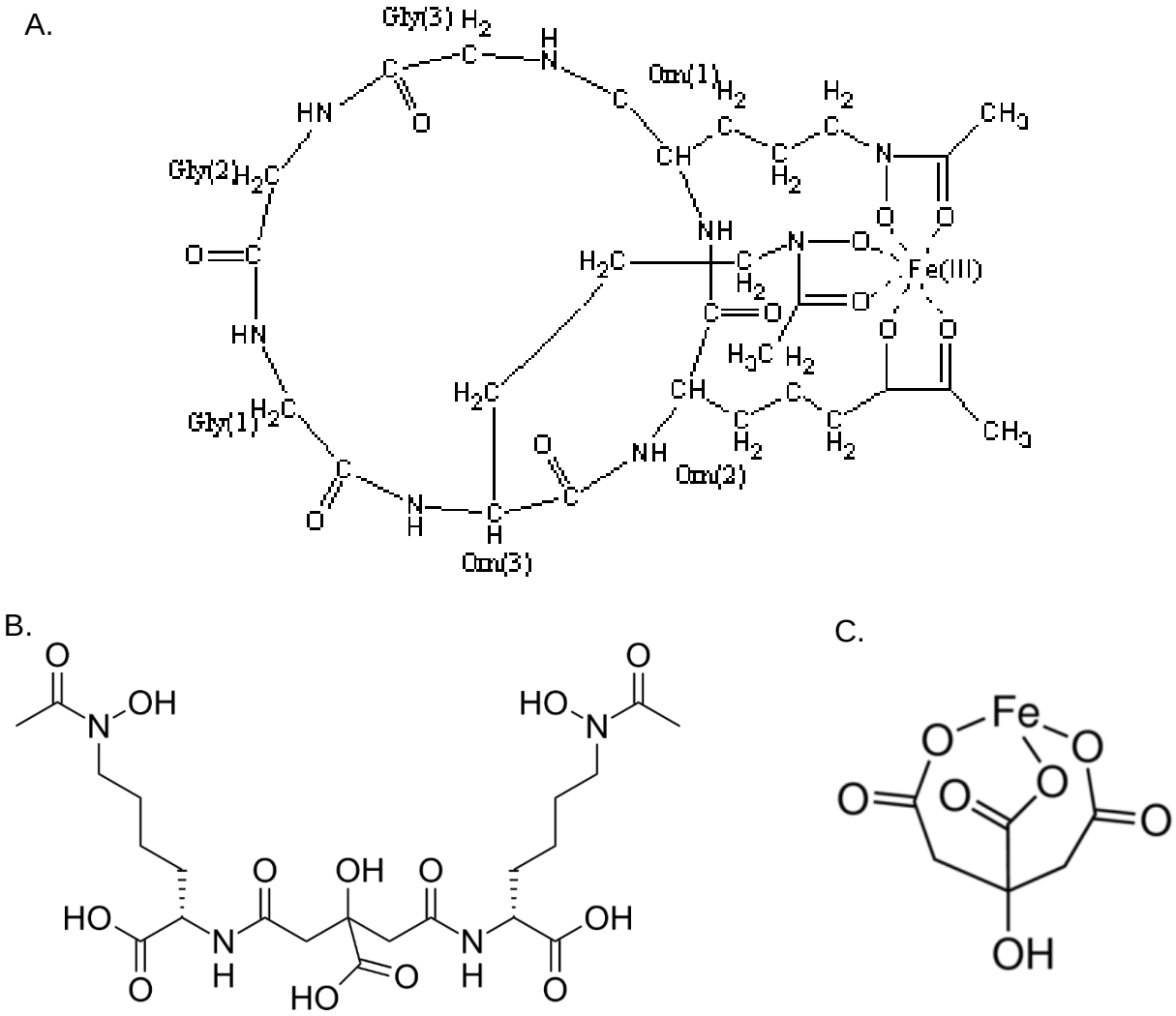

Fig. 1-2: Siderophores. A) The cyclic peptide hydroxamate siderophore Ferrichrome synthesized by fungi but utilized by several Gram negative bacteria B) The citrate-hydroxamate (mixed) siderophore Aerobactin in Fe^{3+}-free form C) Ferric citrate can also act as an iron source.

Siderophores are synthesized from common building blocks either by non-ribosomal peptide synthases (NRPS) or by NRPS-independent synthetases (NIS). The

formation constant (Ka) of typical siderophores with Fe^{3+} is 10^{30} M^{-1}, or greater with that of the catecholate siderophore of *Enterobacteriaceae,* enterobactin being of the order 10^{52} M^{-1}, the highest affinity measured for any biomolecule. Consequently, they can extract Fe^{3+} from host proteins such as transferrin, lactoferrin, ferritin, which have lower dissociation constants with ferric ion (10^{20} M for transferrin at pH 7.4) (Aisen et al., 1978). On the other hand, the attraction for Al^{3+} and all divalent cations are substantially less, making Fe^{2+} a far less preferred substrate for binding. This allows efficient release of the ligand by reduction to the lower oxidation state once the iron-bound siderophore is in the cytosol. The intact siderophore is then recycled for multiple rounds of chelation and transport. The siderophore may also be degraded to release the bound iron (Raymond et al. 2003). Bacteria often transport and utilize multiple xeno-siderophores to maximize their sources for iron acquisition.

Enterobactin (Ent) is formed from three catecholate or o-dihydroxybenzene units attached to a serine-trilactone scaffold through amide linkages (Fig. 1-3). Biosynthesis occurs from the aromatic amino acid precursor chorismic acid and L-serine with the help of several enzymes coded by the *ent* operon. The finished product is exported outside of the cell by the IM proteins EntS, AcrB, AcrD, MdtABC (Furrer et al., 2002; Horiyama and Nishino, 2014) in conjunction with the OM efflux pump TolC (Bleuel et al., 2005). Metal coordination at neutral pH occurs through the six catecholate oxygens. Coordination of the Fe^{3+} ion results in a net negative charge of 3 (Abergel et al., 2006). Concomitant with internalization into the cytoplasm, FeEnt esterase (Fes), hydrolyzes the siderophore to release the iron (Greenwood and Luke, 1978).

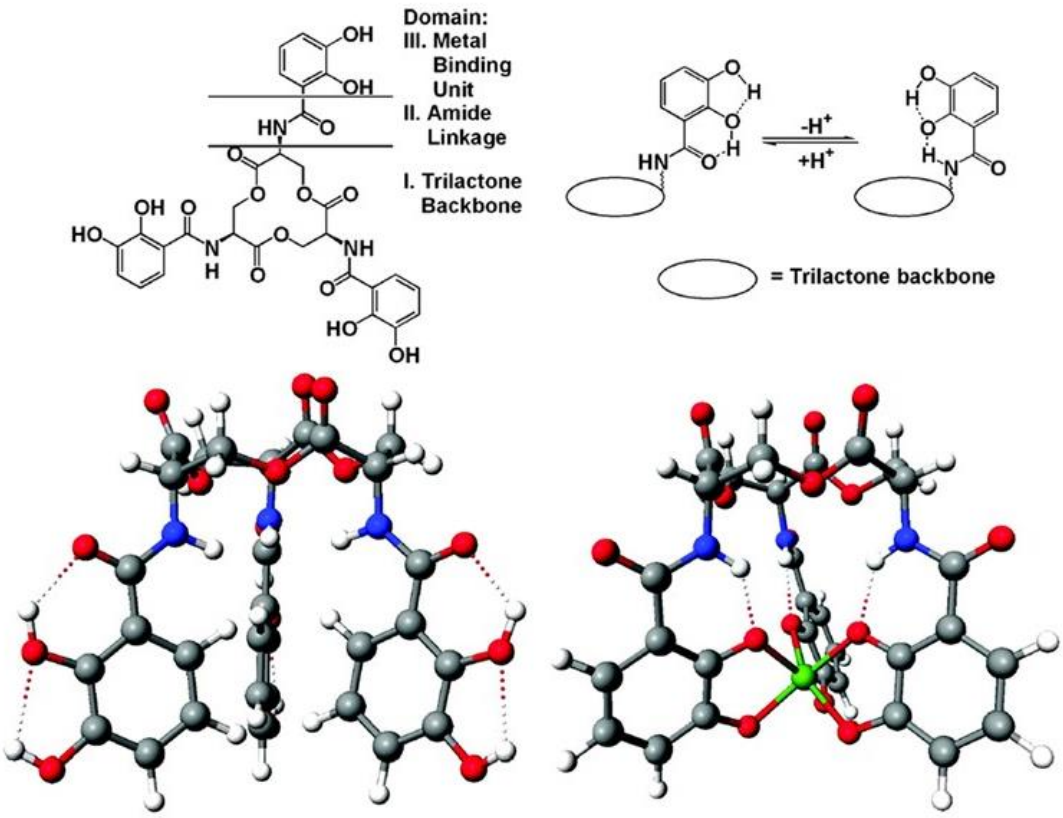

Fig. 1-3: Raymond KN, Dertz EA, Kim SS. Enterobactin: An Archetype for Microbial Iron Transport. PNAS April 1, 2003 100 (7) 3584-3588. Schematic (top) and space filling structures of enterobactin (bottom left) and its ferric complex (bottom right). Copyright © 2003, The National Academy of Sciences.

1.1.4 Regulation of Iron Uptake System

Expression of siderophore biosynthesis genes as well as majority of iron uptake proteins are highly regulated which effectively manages energy expenditure by the cell since the transport substrate is toxic in excess amounts. These genes are regulated in an iron-dependent manner by a protein called Fur (Ferric Uptake Regulator). Fur is a classical negative repressor of transcription, binding to and blocking expression of target genes in iron-replete conditions. Because Fe^{2+} transcriptionally controls expression of gene products that promote iron acquisition, Fe^{2+} was predicted to be a corepressor of Fur Mechanistically, Fe^{2+} binds the protein in iron-replete conditions and dimerizes it to

greatly increase its affinity for its DNA binding site, often called the “fur box” or “iron box” upstream of target genes. Although Mn^{2+} can also bind Fur, Fe^{2+} is thought to be its natural activator because of the relative abundance of iron (Neilands review 1995). The operator consensus sequence is 5’ GATAATGATAATCATTATC 3’, an array which occurs with some variation around the -10 and -35 regions of many iron-affected systems in many microbial species (Calderwood and Mekalanos, 1987). Although, this sequence appears to include a palindrome formed by 9 bp inverted repeats 5’ GATAATGAT 3’ with a gap, thereby suggesting a classical model of protein-DNA binding at palindromic

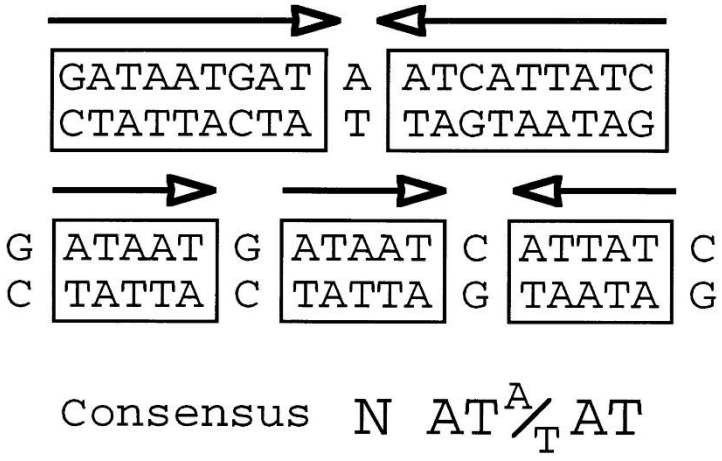

Fig. 1-4: Escolar L, Perez-Martin J, deLorenzo V. Opening the Iron Box: Transcriptional Metalloregulation by the Fur Protein. J Bacteriol. 1999 Oct;181(20):6223-9. Alternative interpretations of the Fur box; as a palindromic sequence of two 9-bp repeats (top) or an array of three 6-bp repeats of the consensus sequence. Re-printed with permission from American Society for Microbiology.

sequences, exemplified by, LacI, Cro, the actual interaction sites of Fur- operator appears to be different. From hydroxyl radical footprinting studies (deLorenzo et al., 1988) of the aerobactin promoter, it was deduced that the consensus sequence is more likely recognized by Fur as three repeats of 6 bp rather than as a 19-bp palindrome. The

hexamer NATA/TAT appears to be the unit of interaction with Fur in a target site (Escolar et al., 1998) with at least three units necessary to endow the complex with enough strength and specificity to be fully functional. (Fig. 1-4)

However, inspection of the genes found to be regulated by Fur has revealed that this protein also participates in functions not directly related to iron metabolism. These include cellular processes as varied as the acid shock response (Hall & Foster, 1996), super-oxide dismutases SodA and SodB (Neiderhoffer et al.,1990, Tardat & Touati, 1993), chemotaxis and flagellar expression (Karjalainen et al., 1991, Stojiljkovic et al., 1994), metabolic pathways (Karjalainen et al., 1991), bioluminescence (Makemson & Hastings, 1982), and production of virulence factors such as toxins (Litwin & Calderwood, 1993). So, despite having key regulatory roles in iron homeostasis, Fur mediated regulation appears to be more global and complex.

1.1.5 The Gram Negative Bacterial Cell Envelope

A discussion of the cell envelope architecture of bacteria and more specifically of Gram negatives is pertinent while talking about their iron uptake systems. The cell wall architecture of Gram negative (distinguished from Gram positive e.g. *Bacillus* spp. by the distinct pink or red color of the counter stain in Gram staining procedure) bacteria such as *Eschericia coli*, is more complex in that they possess two distinct layers instead of a thick (30-100 nm), murein (peptidoglycan or PG) covering the cytoplasmic phospholipid membrane. In *E. coli*, the inner (cytoplasmic) and outer membranes (IM and OM respectively) are separated by the aqueous periplasmic space which houses a much thinner (4-6 nm) murein sacculus just underlying the OM. The composition of the OM is complex and asymmetric, with the inner leaflet showing same lipid composition as the IM

and the outer leaflet consisting of lipopolysaccharides (LPS). This layer is highly immunogenic and the lipidA component often becomes the source of endotoxins. Both IM and OM include channel-forming transmembrane proteins that allow influx and efflux of hydrophilic molecules across the membranes. Transmembrane channels called Porins (discussed later) found in the OM of all Gram-negative bacteria (and also some Gram positives like *Mycobacteria sp*.), allow diffusion of small hydrophilic solutes, ions etc. Otherwise, the unique composition of the LPS tends to exclude lipophilic and molecules larger than 600 Da making Gram negative bacteria naturally resistant to a lot of naturally occurring antibiotics (Nikaido 1994). Many binding proteins in the periplasmic space allow transfer of substrates from the OM transporters to the IM receptors. Apart from receptor/transporter proteins, the IM also houses the electron transport chain (ETC) protein complexes which pump out protons from inside the cell into the periplasm. The low permeability of the IM creates a charge separation resulting in an electrochemical gradient across the IM (Chemiosmotic hypothesis, Peter Mitchell, 1961). The rapid downhill influx of protons through channel proteins generates a proton motive force (*pmf*) which is harnessed for ATP synthesis by F0F1 ATPases, flagellar motion by the Mot complex and facilitated transport of nutrients such as, lactose by the symporter LacY.

In comparison, the PG layer is much more porous, its major function being conformation of shape and stability to the cells. It associates with the OM via lipoprotein (Lpp), OmpA and peptidoglycan associated lipoprotein (Pal) which also interacts with the Tol system proteins (Sonntag 1978, Bouveret et al. 1995). Lack of this network turns cells into osmotically-fragile, spherical bodies called spheroplasts which require iso-osmolar medium to remain viable. PG is composed of a network of the polysaccharides N-acetyl

muramic acid (NAM) and N-acetylglucosamine (NAG) with oligopeptide chains attached to the lactyl group of NAM which in turn, are connected by pentapeptide bridges. Frequency of these peptide bridges are thought to influence the rigidity and permeability of the sacculus. Traditionally, the PG layer is considered as more of a planar network (PN model) with the glycan chains running perpendicular to the long axis of the cell and the peptide cross-links arranged in parallel (Weidel and Pelzer 1964). However, over the last four decades, accumulated evidences suggest a model what is called as a “vertical-scaffold” (VS). This model shows a vertical or perpendicular arrangement of the glycan chains with respect to the plasma membrane (Verwer et al., 1978; Koch 1998) (Fig. 1-5). The cross-linked peptide bridges form a continuous sponge-like matrix consisting of hexagonal cells rather than a simple layered structure. This arrangement makes it easier to fit number of basic facets of Gram negative bacterial cell physiology to the structure (Dmitriev et al., 2005). However, because the chemical parameters of the two models are closely related, direct experimental distinction of the models is not possible, and questions exist on the universality of the VS architecture in both Gram negative (Gumbart et al., 2014) and Gram positive cells (Beeby et al., 2013), none of the models can be completely disregarded at present. The arrangement of the murein sacculus may dictate critical aspects of the iron uptake systems of Gram negative bacteria. Hence, I will be discussing more about the cell wall architecture in the context of iron transport later.

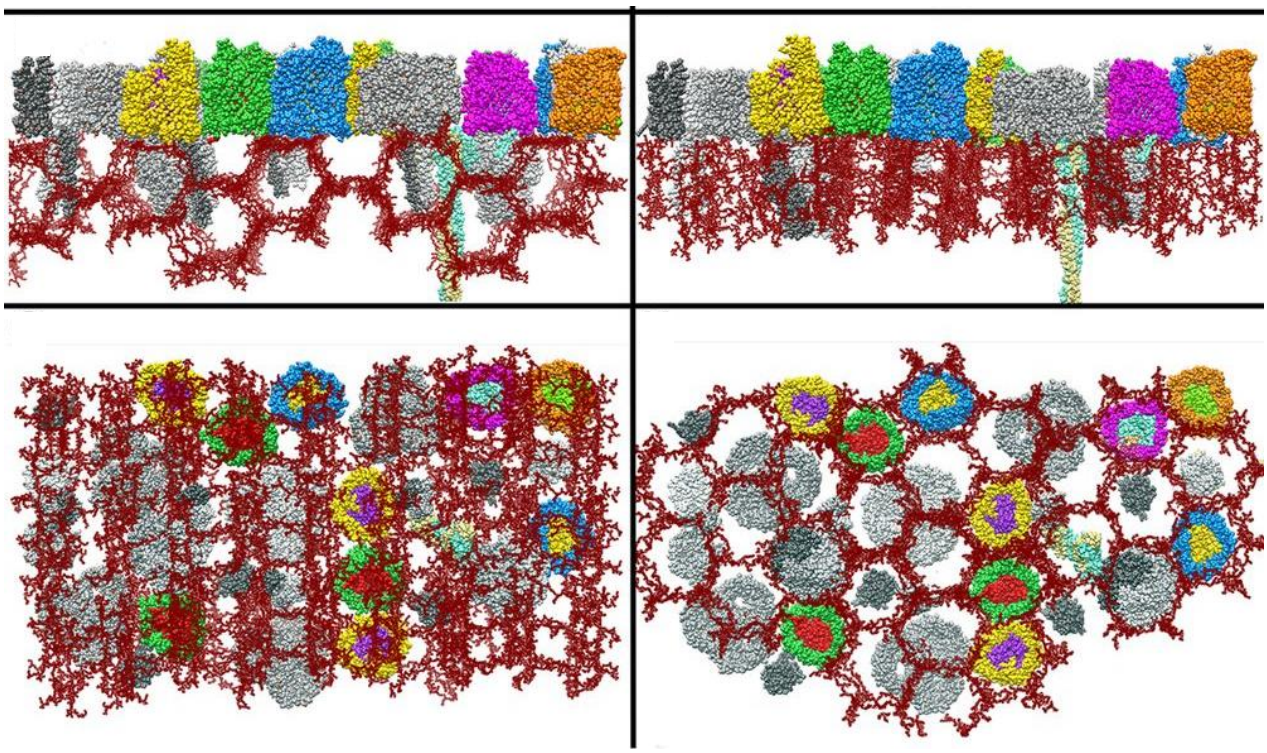

Fig. 1-5: Klebba PE. ROSET Model of TonB Action in Gram-Negative Bacterial Iron Acquisition. Margolin W, ed. *Journal of Bacteriology*. 2016;198(7):1013-1021. doi:10.1128/JB.00823-15. Arrangement of PG glycan strands (depicted as brown wireframe) in PN form (left top and bottom) or in VS model (right top and bottom) showing OM β-barrels and TonB (light blue and pale yellow). Re-printed with permission from American Society for Microbiology.

1.1.6 Outer membrane channel transporters

About 50% of the outer membrane mass is composed of proteins, which can be either integral membrane proteins or lipoproteins that are anchored to the membrane via N-terminally attached lipids. The integral membrane proteins with distinct β-barrel architecture, give rise to channels and transporters in the membrane. These channel-forming proteins can be distinguished into three categories:

(i) Porins/Classical Porins – Expressed at high levels, these are large, open water-filled channels that allow non-specific and spontaneous diffusion of small, hydrophilic nutrient

molecules and efflux of waste products. They are trimeric proteins with the subunits ranging between 36-38 KDa. Each monomer is composed of 16 β-strands that span the OM and are connected by short loops (1-4 residues) on the periplasmic side but long extracellular ones. Most importantly, the third external loop (L3) folds into the lumen of the β-barrel greatly influencing the size-selectivity of the channels (Weiss et al., 1991; Cowan et a., 1992). In *E. coli*, such proteins are exemplified by OmpF, OmpC and PhoE. The estimated pore size of these channels is about 11 Å which is similar to the diameter of most simple nutrients. As a result, rates of diffusion of molecules through them is grossly determined by the physiological properties of the solutes. They also show charge preference, OmpF and OmpC prefer neutral molecules and cations (Saint et al., 1996) whereas PhoE as well as major porins of *Neisseria* have general preference for anions. Although these non-specific porins are generally present in high concentrations, their expression is often dictated or regulated by the cellular environment such as osmotic conditions, temperature or presence or absence of certain metabolites or ions (Nikaido, Vara, 1985). For example, Phosphoporin or PhoE of *E. coli* is only produced under phosphate starvation and levels of OmpF are decreased and OmpC decreased when cells are in high osmolar conditions such as within the animal intestine. The smaller diameter of OmpC is thought to diminish the influx of bile salts into the cell (Stock JB et al., 1989).

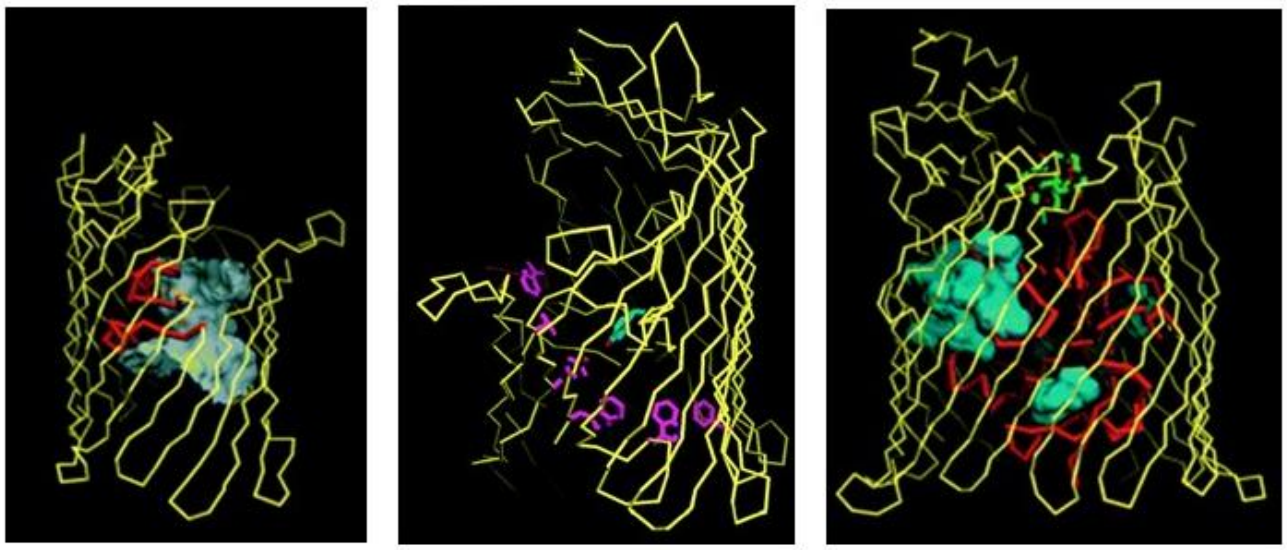

Fig. 1-6: Adapted from Koebnik, R., Locher, K. P. and Van Gelder, P. (2000), Structure and function of bacterial outer membrane proteins: barrels in a nutshell. Molecular Microbiology, 37: 239-253. Gram negative outer membrane β-barrel proteins A) OmpF B) LamB and C) FhuA as seen from the plane of the membrane. Protein segments that in-fold into the barrel interior (L3 in OmpF and N-domain in FhuA) are shown in red. Aromatic residues that constitute the “greasy slide” of LamB are shown in pink (C).

(ii) Specific Channels – These proteins are necessary for facilitated diffusion of nutrients or molecules which are either too large to enter the non-specific classical porins or too slow to pass through them and effectively serve as nutrient sources when available in micromolar concentrations. Examples of such specific channels are LamB, the transporter of maltose and maltosaccharides, Tsx (nucleoside channel) and sucrose transporter ScrY which is plasmid-borne in *E. coli* and in *Pseudomonas aeruginosa*, the glucose transporter OprB, basic amino acid channel OprD. Similar to the general porins, these channels are also trimeric with β-barrel subunits which comprise 18 antiparallel β-strands as opposed to 16 in the Omp proteins. L3 is also folded inwards but additionally L1 and L6 also fold in creating a constricted channel (Schrimer et al., 1995; Forst et al., 1998). However, the presence of a line of six successive aromatic amino acids called the ‘greasy slide’ allows

the interaction and easy passage of left-handed helices of non-reducing sugars (Dutzler et al., 1995; Meyer et al., 1997) (Fig 1-6). Thus, LamB can ultimately transport large number of sugar substrates like glucose, arabinose, lactose when they are present far below millimolar concentrations. ScrY is able to transport an even larger variety of sugars because of a slightly larger pore and a greasy slide that is suited to accommodate furanosyl rings. Thus, specific channels can be thought of as porins that include a ligand-binding site within.

(iii) Ligand-gated porins – The high-affinity siderophore receptors of the Gram negative bacterial OM belong to this class of transporters. Features of these transporters include, high specificity and affinity towards substrate (sub-micromolar or even nanomolar affinity), a channel that is blocked by an in-folded part of the protein and an absolute dependence on energy and an IM protein complex comprising of TonB-ExbB and ExbD for transport activity. The last feature confers them the title of TonB-dependent transporters (TBDTs). The substrates of these transporters are usually much larger and require wider channels which must be gated to maintain the permeability barrier. Apart from Fe^{3+}-siderophores, ligand-gated porins (LGPs) also transport metal complexes of Co^{2+} (Vit B12), Ni^{2+} as well as carbohydrate substrates in certain oligotrophic bacteria (Lohmiller et al., 2008; Dejean et al., 2013). Unlike the other two types of channel transporters, LGPs are monomeric β-barrels and consist of 22 antiparallel β-strands that comprise the C-terminal part of the protein and the N-terminal part encompassing 150-200 residues form the ‘plug’ or ‘cork’ within the channel. The β-strands are connected by 11 large extracellular loops and short periplasmic turns (Pawelek et al., 2006; Buchanan et al., 1999). The ligands bind to a site that is close to the external entrance of the barrel and is composed of both plug and barrel

sequences and binding of ligand induces conformational changes in the plug domain that moves a short motif near the end of the N-terminus called the TonB box from the side of the β-barrel to the center making it more exposed and capable of interacting with the C-terminal domain of the TonB protein. The extracellular loops of the proteins appear to play significant roles in ligand recognition and specificity (Annamalai et al., 2004), affinity as well as transport rates (Newton et al., 1999). Finally, interactions between TonB and the LGPs in energized cells somehow leads to energy-driven conformational changes in the N-domain that opens the channel to allow passage of bound ligands. The *E. coli* genome encodes 8 LGPs (Table 1-2) which are all either ferric-siderophore or Vit.B12 transporters and one gene for ton*B*gp and one each for exbB*gp* and exbD*gp* forming an operon.

Table 1-1: TonB-dependent receptors encoded by the *E. coli* K-12 genome.

Receptor	**Ligand**	**Reference**
FepA	Ferric enterobactin	Buchanan et al., 1999
FhuA	Ferrichrome	Pawelek et al., 2006
FhuE	Coprogen and Rhodotorulate	Sauer et al., 1987
FecA	Ferric citrate	Wagegg & Braun, 1981
Cir	Iron catecholate	Nikaido & Rosenberg, 1990
Fiu	Iron catecholate; degraded ferric enterobactin	Nikaido & Rosenberg, 1990; Yang, Klebba et al. (unpublished)
IutA	Aerobactin	DeLorenzo et al., 1986

BtuB	Vitamin B12	Shultis et al., 2006

Apart from solutes, the numerous channels and transporters of the bacterial membrane have been targeted by noxious elements like bacteriophages and colicins as ports of entry into the cell. Colicins are 30-70 KDa proteinaceous toxins, encoded by plasmids produced by and active against *E. coli* and closely related Gram negative bacteria. Both the passive diffusion pathway and the energy-dependent pathway have been parasitized by colicins. A list of OM proteins used by phages and colicins as receptors is provided in Table 1-2.

Table 1-2: OM receptors utilized by colicins and bacteriophages to colonize Gram negative bacteria

OM Receptor	**Colicins**	**Bacteriophages**	**References**
OmpA	K, L	K3, M1, Ox2	Pilsl et al. 1993, Koebnik et al. 2000
OmpF	N	K20	Bourdineaud et al. 1990, Koebnik et al. 2000
LamB		λ	Schwartz, M 1975
FhuA	M, microcin25	T1, T5, Φ80	Braun, V 1973
FepA	B, D	H8	Rabsch et al., 2007
BtuB	E1, A, E2E7E8E9, E3E6	BF23	Di Masi 1973
Tsx	K, 5,10	T6	Pilsl et. al. 1995, Hantke 1976
Cir	Ia, Ib		Konisky, J 1975

1.1.7 Ferric enterobactin permease A (FepA)

FepA is the OM transporter of the ferric iron-bound form of the sole siderophore synthesized by *E. coli*, enterobactin. Similar to the prototypic ligand-gated transporters of Ferrichrome (FhuA) and Vitamin B12 (BtuB), FepA is monomeric and composed of two domains: (i) C-domain comprising the β-barrel transmembrane channel (ii) N-domain formed by a globular plug that occludes the channel from free ligand passage (Fig. 1-7). It consists of 724 amino acid residues of which the first 153 comprise the N-domain. Forming the largest barrel known till date, the crystal structure (Buchanan et al., 1999) reveals 22 antiparallel β-strands which range in length from nine (β-22) to 24 (β-16) residues, connected by long extracellular loops (ranging from 12-37 residues), some of which extend 30-40 Å above the membrane bilayer. Majority of the aromatic residues of the protein are located in the barrel (only three in the N-domain) and the extracellular loops and their distribution is widespread. L7 includes the sole two Cysteines (487 and 494) of the protein which owing to their unavailability to modification by fluors, are thought to be disulfide bonded (Scott et al., 2002). The barrel is stabilized by hydrogen bonds between all the main chain polar amino acids and additionally by two salt bridges between strands 1 and 22. Phe724 at the end of the C-terminus is highly conserved and found to be important for correct folding and insertion into the OM (Stryuve et al., 1991). The N-domain is firmly anchored to the barrel. Four of the six β-strands form the core β-sheet of the N-domain. Seven single-turn α-helices are interspersed with the six β-strands. Two long loops are formed by connecting strand Nβ1 with Nβ4 (loop NL1) and strand Nβ4 with Nβ5 (loop NL2). These loops protrude into the extracellular space and suggests possible interactions with the ligand. The extreme N-terminal residues D12 to A19 extends into the periplasm

and comprise the TonB box. The N-domain is extensively engaged in interactions with the C-domain as well as several of the extracellular loops via hydrogen bonds.

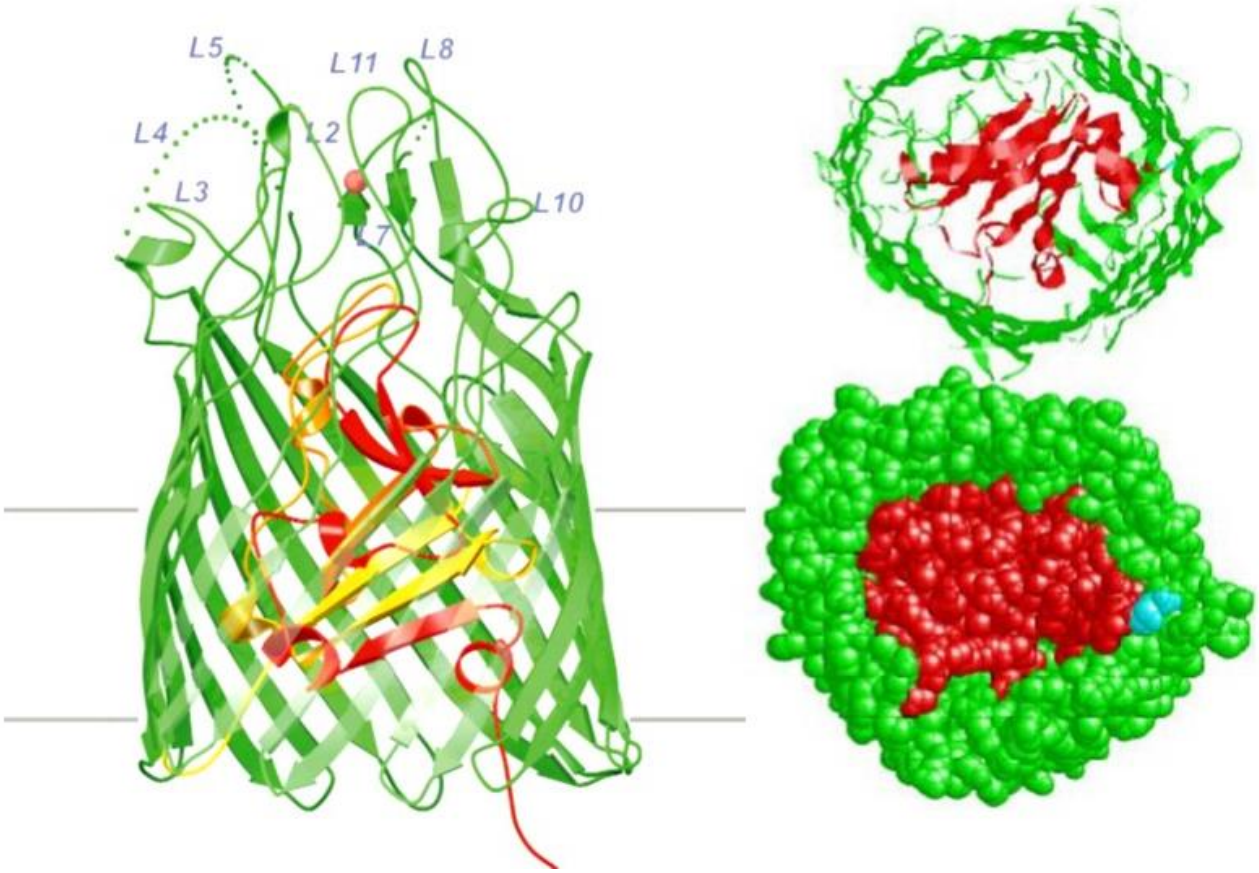

Fig. 1-7: Adapted in part from Buchanan SK, Smith BS, Venkatramani L, Xia D, Esser L, Palnitkar M, Chakraborty R, van der Helm D, Deisenhofer J. Crystal structure of the outer membrane active transporter FepA from Escherichia coli. Nat Struct Biol. 1999 Jan;6(1):56-63. Structure of FepA shown in ribbon format. The β-barrel is shown in green along with the extracellular loops and the N-domain is shown in red and gold (left). View from the top (right top) and bottom from the periplasmic side in space-filling format (right-bottom). The position of the TonB box is shown in cyan. Re-printed with permission from Springer Nature (License number 4437940261912).

Ligand binding studies of FeEnt and ColB and ColD to fluorosceinated FepA shows a biphasic kinetics suggesting an initial rapid step and a subsequent slower step

(Payne et al., 1997). This implies of two binding sites within the molecule, an initial site in the loop extremities (B1) and a secondary site deeper in the vestibule where the ligand sits on top of the N-domain. Both B1 and B2 are rich in aromatic and basic residues which interact with the aromatic, acidic residues of the FeEnt catechol groups. This results in high affinity binding (0.2 nM Kd), which also distinguishes between types of substrate. FepA loops can exclude ferric hydroxamates like ferrichrome, discriminate FeEnt from other catecholates by demonstrating much lower affinity (Annamalai et al., 2004). Nevertheless, specificity is not absolute. FepA transports two synthetic siderophores structurally related to FeEnt, Ferric MECAM (Heidinger et al., 1983) and Ferric TRENCAM (Thulasiraman et al., 1998) (but with 50- to 100-fold less affinity) apart from colicins and bacteriophage. Contrary to the crystal structure of FepA that shows the extracellular loops juxtaposed near the center, on top of the β-barrel, plenty of studies done in vivo as well as, crystallographic data of the FepA homolog FecA in ligand-free and bound forms (Ferguson et al., 2002) suggest that the loops undergo conformational motion to change from a ligand-free ‘open’ state to a ligand-bound ‘closed’ conformation, possibly driven by the avidity of the binding reaction (Scott et al., 2002; Bos et al.,1998; Locher et al., 1998; Jiang et al.,1997). Binding of the ligand is energy and TonB independent.

Mutagenesis of aromatic residues in the N-domain and deletion of part of N-domain loop NL1, or the entire N-domain showed that ligand binding and specificity are principally determined by the extracellular loops and the main role of N-domain is in ligand transport (Rutz et al.,1992; Scott et al., 2001; Annamalai et al., 2004). However, systematic deletions of all or part of nine loops (out of 11), showed that while some loops (L7 and L8)

were indispensable for specific recognition and transport (deletions turn FepA into an open channel), other loops affected ligand binding and transport parameters to variable extents

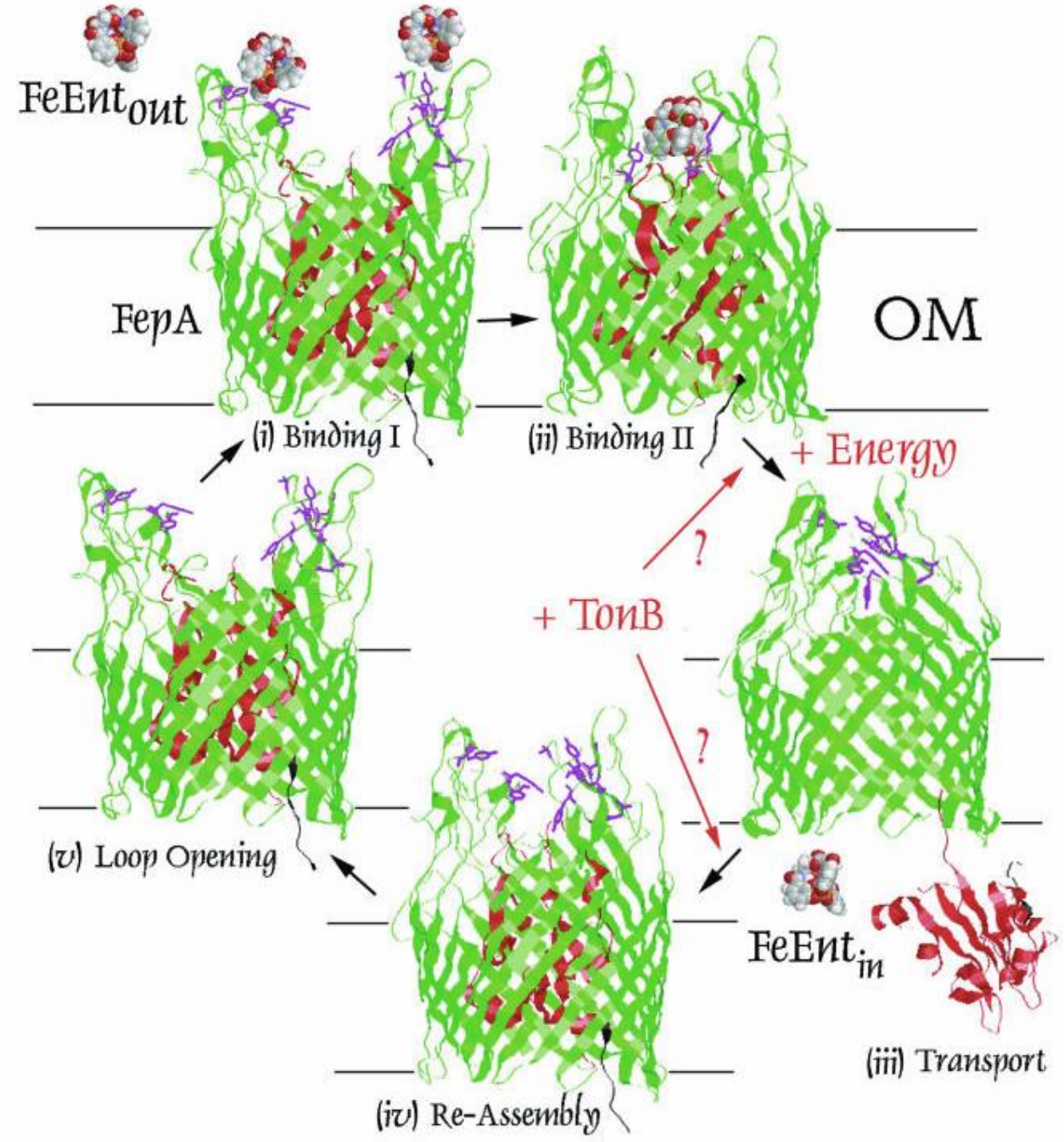

Fig. 1-8: Annamalai R, Jin B, Cao Z, Newton SMC, Klebba PE. Recognition of Ferric Catecholates by FepA. *Journal of Bacteriology*. 2004;186(11):3578-3589. doi:10.1128/JB.186.11.3578-

3589.2004. Conformational changes in FepA during Ferric enterobactin binding and transport. Re-printed with permission from American Society for Microbiology.

but not enough to abolish transport (Newton et al., 1999). Alanine scanning mutagenesis of aromatic and positively charged residues in the loops identified residues between residues 255 and 336 that are involved in FeEnt and colicin binding (Newton 1997, Cao 2000). Residues which affect FeEnt binding and transport are also found to be involved in either binding or transport of ColB and ColD which corroborates the observation that prior incubation of FepA with FeEnt blocks colicin killing and vice-versa (Murphy et al., 1990). Certain differences in binding and transport phenotype that are evident in the different mutants towards the two types of colicins and FeEnt highlights the differences between the types of substrates, their sizes and that all the target residues are not shared.

The presence of the N-terminal domain distinguishes the LGPs like FepA from other porins. Yet, the N-domain is found to be completely dispensable to the binding and transport process. In fact, as Scott et. al. showed by deleting the N-domain of FepA and replacing with that of FhuA, the N-termini of the proteins are exchangeable, and the process does not affect transport of the specific ligands (Scott et al., 2001). This suggests that this globular domain of the protein acts merely as a “gate” that protects the permeability barrier of the cell which would otherwise be compromised by the large pores of these transporters. This also implies some sort of movement or removal of the N-domain to allow opening of the channel and passage of the ligand. The conformational rearrangement involved in the process entails energy requirement reasonably making it a rate-limiting step of the transport process. Surprisingly, the exact nature of these conformational changes is still unclear despite years of research. Repeated observations made in this context include: (i) transport requires energy of the *pmf* as transport is

abolished in cells treated with energy poisons (ii) transport does not occur in absence of TonB as well as ExbB and ExbD (iii) interaction of TonB with the N-terminal periplasmic TonB box region (other periplasmic parts of the protein may also be involved) is necessary for transport as evidenced by mutations in both TonB box conserved residues and TonB that abolish transport (Gudmundsdottir et al., 1989; Cadieux et al., 2000) (iv) fluorophore accessibility to specific residues in the N-domain mutated to Cysteine suggest that the plug is dislodged into the periplasm either as a unit or by unfolding thereby opening the channel to allow ligand passage (Ma et al. 2007).

1.1.8 TonB-ExbBD complex

Central to the functioning of the OM ligand-gated transporters, the IM proteins TonB, ExbB and ExbD, are thought to act as an intermediary in the transduction of IM *pmf* to these transporters. TonB consists of 239 amino acids (36KDa) with three distinct domains or regions in its extended structure. These domains include, the cytoplasmic membrane-anchored N-terminal transmembrane domain (NTD), a rigid proline-rich central section in the periplasm and a C-terminal ββαβ domain (CTD) that interacts with the LGPs in the OM. There is currently no known structure for the entire TonB protein. Predicted structure has been assembled based on crystal structures of the CTD (Pawelek et al., 2006), NMR solution studies of the central region (Evan et al., 1986) and membrane topological determinations of the NTD (Klebba et al., 1993). Dimeric crystal structures of the TonB CTD and monomeric solution structure (Peacock et al., 2006) have raised controversies regarding the *in vivo* conformation of the protein. However, based on certain evidences, some groups believe the dimeric form to be more relevant *in vivo* and monomer-dimer transitions to be important for physiological function (Klebba, 2016). The

monomeric CTD (residues 155-239) consists of two α-helices positioned on the same face of a four-stranded antiparallel β-sheet. The central proline-rich region (residues 34-154) is characteristic in possessing a series of Pro-Glu and Pro-Lys repeats between residues 66 to 102 making it a rigid extended rod, as long as 10 nm spanning the periplasmic space (Evans et al., 1986; Skare et al., 2003). The NTD (residues 1-33) includes a small 11 residue periplasmic N-terminal region and a single helical hydrophobic transmembrane region (Roof et al., 1991). The ExbD protein possesses a single transmembrane N-terminal domain with the bulk of its sequences in the periplasm whereas, ExbB is predicted to contain three transmembrane spanning helices and a large cytoplasmic domain.

Several lines of evidence suggest that these three proteins exist as a complex in the IM such as, using formaldehyde cross-linking studies, TonB was found to contact both ExbB and ExbD through transmembrane domains (Skare et al., 2003; Higgs et al., 1998). Controversies existed on the oligomeric states of these proteins in the complex, till the recent crystallographic demonstration of ExbB as a stable pentamer, ExbD as a dimer and at least one TonB in the assembly (Celia et al., 2016; Higgs et al., 2002). Based on this structure, the five transmembrane domains of the ExbB pentamer forms a transmembrane pore while the cytoplasmic domains form a large enclosed cavity extending into the cytoplasm. This cytoplasmic cavity has five side fenestrations that may allow solvent or ion passage. The transmembrane pore is large enough to house only a monomer of ExbD and the second ExbD molecule is located on the outside of this transmembrane complex and TonB interacts with both ExbB and ExbD proteins (Fig. 1-9).

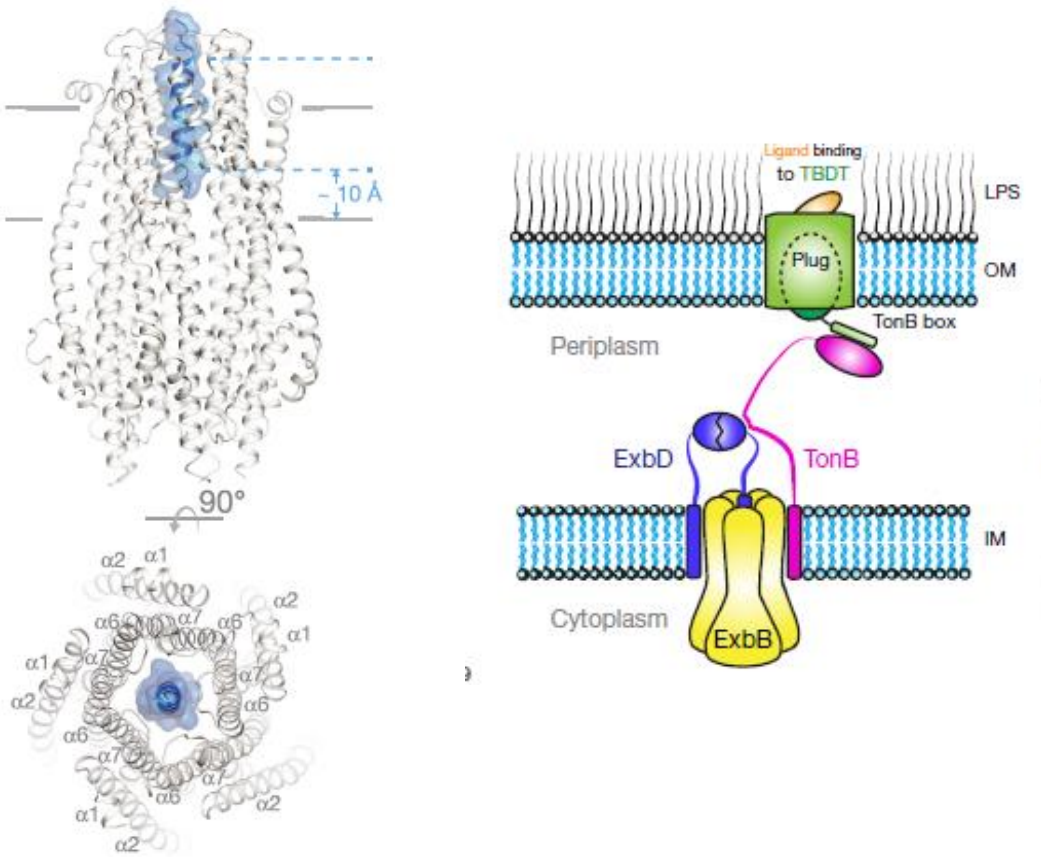

Fig. 1-9: Adapted from Celia H, Noinaj N, Zakharov SD, et al. Structural insight into the role of the Ton complex in energy transduction. *Nature*. 2016;538(7623):60-65. doi:10.1038/nature19757. Structure of the ExbB pentamer housing the transmembrane helix of ExbD monomer within its transmembrane pore (left). Structural model of the arrangement of the ExbB pentamer, ExbD dimer and at least one TonB in the IM TonB-ExbBD complex. Re-printed with permission from Springer Nature (License number 4438281035346).

1.1.9 Role of the TonB IM complex in energy-dependent iron uptake

Abolishment of uptake of siderophores and TonB-dependent colicins and bacteriophages in *tonB* deletion mutants, established the central role of TonB in the OM uptake processes of these ligands (Bassford et al. 1976). Similar phenotypes were observed in cells treated with reagents such a 2,4-dinitrophenol that uncouple oxidative phosphorylation from the electron transport chain (Bradbeer, 1993). In the absence of a

sustainable proton gradient across the OM and any other protein in the vicinity that can generate energy, TonB was tied to the role of transducing energy of the IM *pmf* to the OM where energy-dependent uptake of ligands takes place. However, the exact mechanism of how TonB achieves this is still not well understood. It is also known that TonB requires the ExbBD complex for efficient function. In *exbBD* mutants, 10% activity is retained which is substituted by the TolQR proteins (Bradbeer, 1993).

Sequence homologies of the TonB-ExbBD system with other proteins and biophysical evidences have provided ideas about mechanistic models. The N-terminal domains of the ExbBD proteins are homologous with the TolQR proteins of the Tol system which are involved in the assembly of the OM and undergo energy-dependent conformational motion (Noinaj et al., 2010). The membrane-spanning TolA portion can functionally replace the membrane-spanning TonB portion. TonB system is also evolutionarily related to the flagellar Mot protein complex. Both TolQRA and MotAB complexes depend on the *pmf* of the IM for dynamic function. TonB-ExbBD is proposed to undergo similar energized motion which is likely rotation, as suggested by the anisotropic measurements of GFP-TonB fusion proteins (Jordan et al., 2013). In these experiments, the motion of GFP-TonB in energized cells were slower than free GFP in the cytoplasm but much faster than lateral translation of proteins in the IM. Based on these experimental observations and sequence similarities with homologous proteins, TonB is presently believed to undergo rotational motion analogous to a rotor which turns opposite to the stator (ExbBD) in response to energization by the *pmf*. The kinetic energy of rotation can be transferred to molecules upon contact.

The CTD of TonB is found to possess affinity (micromolar) towards the PG layer. This affinity is rendered by the presence of LysM motifs in dimeric CTD (Kaserer et al., 2008). LysM motifs are lysin-rich sequences prevalent in PG-binding proteins, PG-degrading enzymes in bacteria apart from large number of other types of proteins across different species. This property possibly locates the TonB CTD to the vicinity of the PG just underlying the OM where the LGPs reside and TonB transiently associates with the PG. The PG layer with tight connections with the OM forms a stable enough structure capable of withstanding mechanical force. The OM porins are known to be tightly associated with the LPS with confined mobility in the membrane which is comparatively less than TonB in the IM (confined radius of FepA ~ 0.18 μm, TonB ~0.26 μm) (Lill et al., 2016). The LPS being a comparatively frozen structure under physiological conditions, the OM housing the LGPs (TonB box) upon contact with the TonB CTD (Shultis et al., 2006) can potentially convert the kinetic energy into mechanical force. These findings summarily disprove the “shuttle hypothesis” of physical dislodging of energized TonB to relocate at the OM, where its interaction with the OM proteins leads to dissemination of energy required for ligand uptake and subsequent return of TonB to the IM (Letain and Postle, 1997; Gresock et al., 2011).

The arrangement of the PG, as discussed earlier also has important implications on the mode of TonB action. Compared to the PN model, the diameter of the hexagonal cells in the VS model is ~60Å which is sufficiently large to precisely fit the β-barrels of majority of the OM proteins including the LGPs (Fig. 1-10). The VS model is also less restrictive to the lateral movement of the TonB CTD in the periplasm allowing it to interact with the ligand-occupied LGPs. Therefore, the PG layer possibly acts as a scaffold where

TonB undergoing rotational motion and lateral diffusion within its confined region in the IM, spans the periplasm and touches the LGPs to dissipate energy. It is possible to congregate these structural and biochemical considerations to describe a comprehensive model for the mechanism of TonB-dependent metal transport through LGPs (Klebba, 2016).

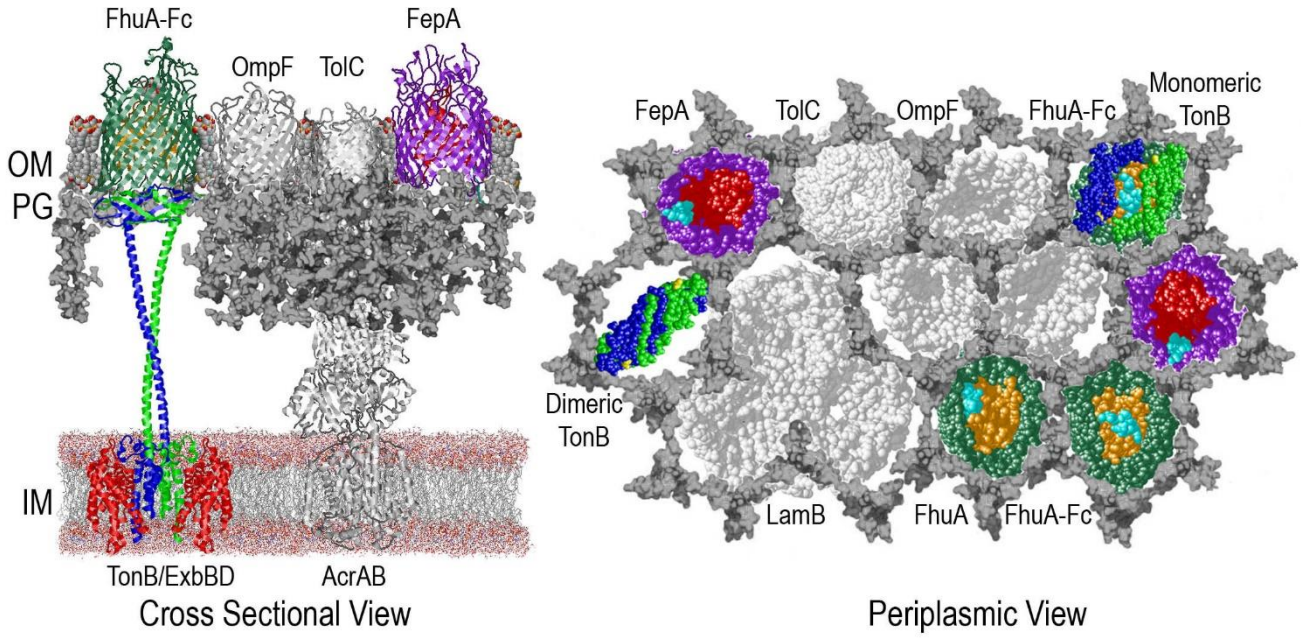

Fig. 1-10: Kaserer WA, Jiang X, Xiao Q, Scott DC, Bauler M, Copeland D, Newton SM, Klebba PE. 2008. Insight from TonB hybrid proteins into the mechanism of iron transport through the outer membrane. J Bacteriol 190:4001–4016. doi:10.1128/JB.00135-08. Schematic model of the arrangement of the PG-associated OM with OM proteins arranged in the honeycomb cells of PG represented in the VS model. Reprinted with permission from American Society of Microbiology.

1.1.10 ROSET model of TonB action

The Rotational Surveillance and Energy Transfer (ROSET) model suggests a mechanism for the transfer of the energy of the *pmf* from the IM to the OM via TonB-ExbBD to promote uptake of metal complexes through OM LGPs (Kaserer et al., 2008;

Klebba, 2016). According to this model (Fig. 1-11), driven by the downflow of protons across the electrochemical through the ExbBD channels, TonB undergoes rotational motion in the IM similar to the rotor (filament/TonB) within the stator (MotAB/ExbBD) in the flagellar motor complex. Spanning the periplasm via its central domain, the CTD of dimeric TonB transiently associates with the PG with weak affinity. Here, the OM proteins are positioned on the PG hexagonal cells to engage in interactions with TonB CTD. While, interactions with general porins are very weak and non-specific, the CTD monomer engages in specific, non-covalent interactions with the TonB-box of conformationally re-oriented, ligand-bound LGPs like FepA. Transient interactions of the rotating TonB-ExbBD complex with the PG impose frictional resistance on the complex forcing it to move laterally as well. Thus, the energized TonB dimer surveils the periplasmic face of the OM for LGPs. Upon encountering a TonB box peptide, the affinity of the monomeric CTD for it favors the switching of the TonB dimer to the monomeric form which recruits TonB box into the ternary β-strand interaction. This binding reaction transfers the kinetic energy of motion to the OM LGP triggering conformational change within its cork domain. If the cork domain of FepA and other OM metal transporters is likened to a rolled ball of wool, most recent evidence suggests that the interaction of TonB box and TonB is analogous to pulling of the free end (TonB box) of the ball to unroll the string. Single-molecule force microscopy using an atomic-force microscope shows that the non-covalent interaction between TonB-box of BtuB and TonB is sufficiently durable under force to allow unfolding of half of the plug domain before dissociation. This force-induced remodeling opens a channel within the barrel, whose dimensions are tailored to the siderophore ligand

allowing its passage into the periplasm, without compromise of membrane permeability (Hickman et al., 2017).

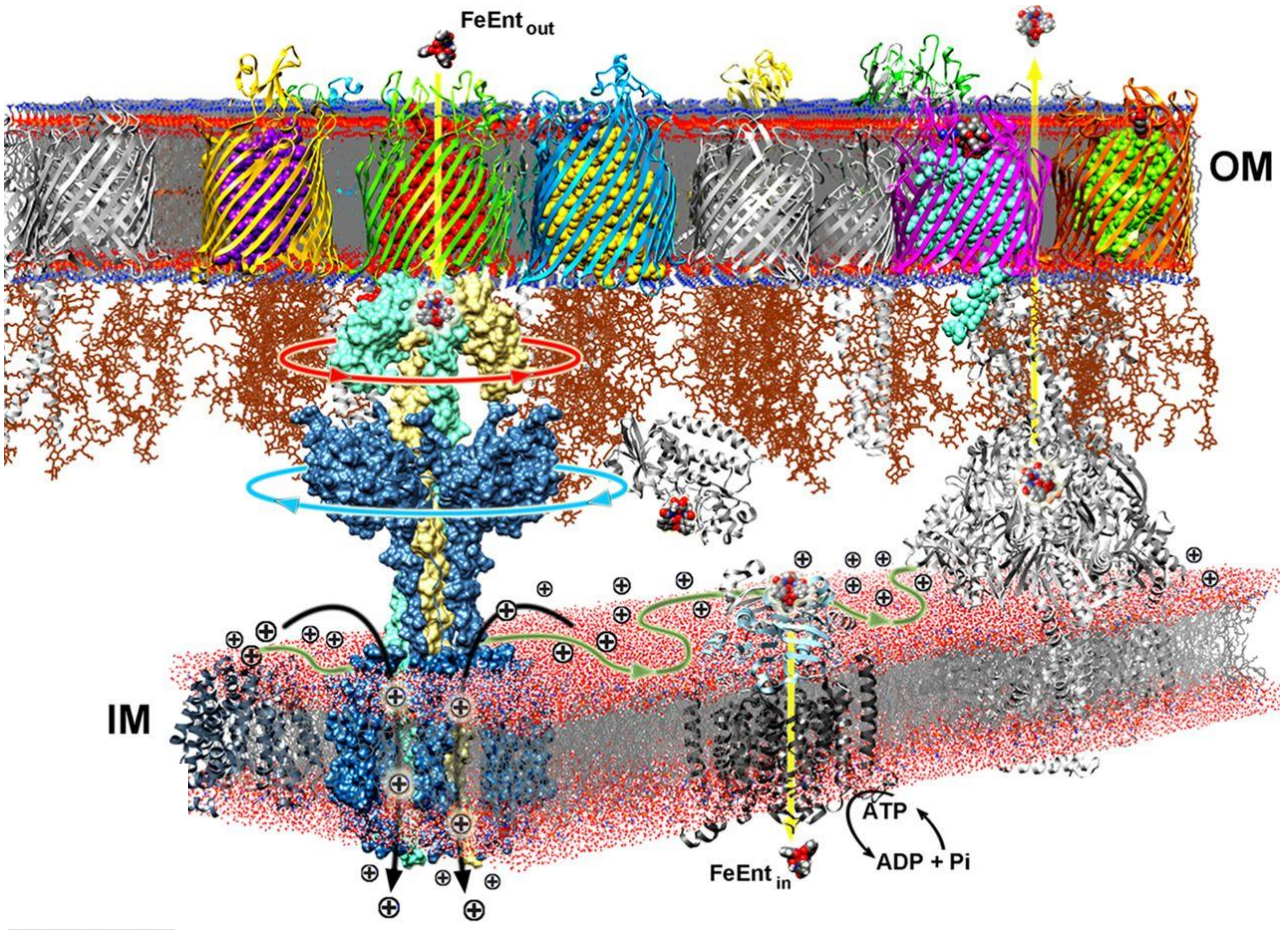

Fig. 1-11: Klebba PE. ROSET Model of TonB Action in Gram-Negative Bacterial Iron Acquisition. Margolin W, ed. *Journal of Bacteriology*. 2016;198(7):1013-1021. doi:10.1128/JB.00823-15. ROSET model of TonB action: Rotational motion of TonB-ExbBD (cyan and gold - blue) coupled to the downflow of protons across the IM surveilling the underside of OM, in association with PG. The LGPs in the OM are contacted by TonB when they are in ligand-bound forms and their TonB boxes are exposed. Transfer of energy from this interaction allows FeEnt to be internalized by FepA (green and red) into the periplasm, where it is bound by FepB (grey) and finally transported

into the cytosol by the ABC-type transporters FepCDG (black) in the IM. Re-printed with permission from American Society for Microbiology.

1.2 Significance of work

Transport of metals via TonB-dependent ligand-gated channels in the OM of Gram negative bacteria is one the most enigmatic phenomena in the biochemistry of membranes. Despite years of research and accumulation of observations regarding key features of the process, the exact mechanism of ligand uptake and the mode of energy transfer by TonB-ExbBD to facilitate this process, is unknown. Understanding these mechanisms will unravel one of the biggest biochemical mysteries of membrane transport systems. Not only that, TonB-dependent transport systems being a common feature in all Gram negative bacteria, including pathogens of the ESKAPE multi-drug resistant group, elucidation of the transport mechanism can pave the way for development of better drug targets. Since majority of transport systems depend on a common player, TonB, small molecules that target this protein, may have universal therapeutic potential across the spectrum of infectious diseases caused by Gram negative bacteria.

This work is an attempt to advance another step towards understanding the mechanism of TonB dependent transport of the Fe^{+3}-siderophore FeEnt through its cognate OM receptor FepA. The key focus is to determine the relationship of these proteins with the cell envelope architecture as this may hold important clues in deriving the mode of function of these proteins.

Chapter 2: Materials and Methods

The materials and methods described here are commonly employed techniques in the different studies. Methods unique to a study is described in the respective section.

2.1 Bacterial strains, plasmids and culture conditions

Overnight cultures of *E. coli* were grown in Luria-Bertani (LB) broth (BD Difco, USA) containing appropriate antibiotics at 37°C with shaking at 220 rpm. *C. crescentus* cells were grown in PYE or NB with 5 mM $CaCl_2$ at 30°C with shaking. Cells were sub-cultured into Nutrient Broth (NB) or iron-free Neidhardt MOPS minimal medium (Neidhardt et al., 1974) reconstituted with micronutrients and vitamins, as required. Antibiotics when used were always added as follows: Streptomycin – 100 µg/mL, Chloramphenicol – 20 µg/mL, Ampicillin – 100 µg/mL, Nalidixic acid – 20 µg/mL.

Table 2-1: List of strains used

Strain	**Relevant genotype**	**Reference**
Escherichia coli strains		
BN1071	F^- *thi entA pro trp rpsL*	Klebba 1982
OKN1	BN1071 *ΔtonB*	Ma 2007
OKN3	BN1071 *ΔfepA*	Ma 2007
OKN13	BN1071 *ΔtonB ΔfepA*	Ma 2007
NEB5α	K-12 *fhuA2 recA1 relA endA1 thi-1 hsdR17 Δ(lacZ)M15*	New England Biolabs
MG1655	F-, λ-, *rph-1*	Blattner 1997
KNK00	MG1655 *ΔentA*	This study

KNK05	MG1655 *ΔentA ΔlacZ*	This study
KNK056	MG1655 *ΔentA ΔlacZ-lacY*	This study
KNK013	MG1655 *ΔentA ΔfepA ΔtonB*	This study
T-184	*lacI*$^{+}$ *O*$^{+}$ *Z*$^{-}$ *Y*$^{-}$ (*A*) *rpsL* *met*$^{-}$ *thr*$^{-}$ *recA* *hsdM* *hsdR/F' lacI*^{q} O^{+} Z^{D118} (*Y*$^{+}$ *A*$^{+}$)	Tether 1980
Caulobacter crescentus strains		
NA1000	Synchronizable derivative of CB15	Marks 2010
Acinetobacter baumannii strains ATCC 17978		Baumann 1968

Table 2-2: List of Plasmids used

Plasmid	**Relevant genotype**	**Reference**
pHSG575	Cm^{R}	Hashimoto-Gotoh 1981
pITS47	*fepA*+ on pHSG575	Scott 2001
pITS23	*fepA*+ on pHSG575	Smallwood 2009
pITS767	*fepA*+ *tonB*+ on pHSG575	This study
pGT	eGFP-TonB under ptonB on pHSG575	Kaserer 2003
pGTFA698C	eGFP-TonB and FepAA698C on pHSG575	This study
pETFA698C	mEos3.2-TonB and FepAA698C on pHSG575	This study
pFLP2		Hoang, 1998
pWH1266	amp^{R}, tet^{R}	Hunger, 1990
P2682pro		Nairn, 2016

2.2 Preparation of plasmid DNA

Minipreps of plasmids were done using QIAquick Miniprep kit from QIAGEN following kit recommendations. For low copy derivatives of pHSH575, 10 mL LB cultures were used for minipreps using double volumes of buffers. Entire volume was passed through single QIAquick miniprep spin column and finally eluted in 30-50 µL of nuclease-free de-ionized water or resuspension buffer. Sometimes, Monarch Plasmid Miniprep kit from New England Biolabs was also used for plasmid isolation.

Purification of PCR products and extraction of DNA from agarose gels were done using QIAquick PCR purification kit and QIAquick Gel extraction kit respectively from QIAGEN following kit protocol.

2.3 Preparation of calcium chloride competent cells and heat shock transformation

A 5 mL LB culture of the host strain was grown overnight in the presence of appropriate antibiotics and sub-cultured next day 1:50 in 50 mL LB broth containing antibiotic. Cells were grown until mid-log with OD600nm 0.5 and then chilled on ice for 15 – 20 minutes. Cultures were transferred to 25 mL Corex tubes and centrifuged at 5000 rpm for 10 minutes at 4°C. After centrifugation, the supernatant was discarded and the pellet resuspended in 25 mL of ice-cold 0.1 M $CaCl_2$. Cells were handled gently while pipetting and resuspension and then kept on ice for 20 minutes. Next, cells were again centrifuged as before and supernatant discarded. Finally, the pellet was resuspended in 0.5 mL ice-cold 0.1M $CaCl_2$, 15% glycerol mix. 100 µL aliquots of cells were distributed in pre-chilled microfuge tubes and immediately stored in -70°C freezer.

For heat shock transformation of competent cells, 100 µL aliquot of cells were thawed on ice and 4-6 µL of plasmid DNA was gently added to the cells and incubated on ice for 30 minutes. Cells were then heat-shocked for exactly 2 minutes and placed back on ice for 2 minutes. Then 900 µL of super optimal broth with catabolite repression (SOC) media was added and the cells allowed to recuperate by incubating at 37°C with shaking for 1 hour. Then 100 µL of cells were plated on one LB plate containing antibiotic and the rest of the cells were spun down, resuspended in 100 µL of SOC broth and plated on another LB antibiotic plate. Single colonies were picked after 12-16 hours of incubation at 37°C.

2.4 Preparation of electrocompetent cells and electroporation

A 5 mL overnight culture of the strain was grown in LB with appropriate antibiotic. Then the strain was sub-cultured 1:50 in 50 mL LB broth containing antibiotic and grown to OD600nm 0.6-0.8. Cells were chilled on ice and then centrifuged in 25 mL Corex tubes at 7500 rpm for 8 minutes at 4°C. The supernatant was discarded and the cell pellet washed with 20 mL of ice-cold of sterile water and spun again as before. The wash step was repeated two times with 10 mL and then 5 mL of ice-cold water. After discarding the supernatant, the pellet was resuspended in 2 mL ice-cold sterile 10% glycerol water and centrifuged again at 7500 rpm for 5 minutes. The supernatant was discarded and finally cells were concentrated 100X by resuspending them in 500 µL of ice-cold 10% glycerol water. 40 µL aliquots of electrocompetent cells were frozen in -70°C freezer.

For electroporation, a *E. coli* gene pulser instrument (Bio-Rad) was used. Electrocompetent cells were first thawed on ice and 2-4 µL of salt-free plasmid or ligation mix was gently mixed with the cells. Then the cell-DNA mixture was transferred to a pre-

chilled 2 mm electroporation cuvette and cells were moved to the bottom of the cuvette by gently tapping. Then cells were pulsed at a set voltage of 2.5 kV for a few seconds. After pulse is complete, cells were immediately reconstituted with 1 mL of SOC broth and incubated for 45-60 minutes at 37°C with shaking. After incubation, 50 – 200 µL of cells were plated on LB agar plates containing antibiotics and incubated 12-16 hours at 37°C. Single colonies were picked or re-purified on antibiotic plate afterwards.

2.5 One-step gene replacement using PCR products

To perform one-step in-frame gene deletion in E. coli as described by Datsenko and Wanner (2000), PCR amplified fragments containing antibiotic resistance cassette and 36 nucleotide (nt) flanking sequence on both sides homologous to target gene, were used. Briefly, pKD46 encoding λ-Red recombinase was transformed into the host strain and selected on LB agar containing ampicillin at 30°C. Transformants were grown in 20 mL of SOB cultures with ampicillin and 2% L-(+) arabinose until A600nm of ~0.6 and then made electrocompetent by washing three times with ice-cold 10% glycerol water and then concentrated 100 times. 40 µL aliquots of cells were then electroporated with 2-4 µL of PCR fragments at 10-100 ng concentration. PCR products of ~1.1 Kb with 36 nt flanking homologous sequence were prepared by amplifying the Chloramphenicol cassette from pKD3 template plasmid, digested with DpnI for 2 hours and then gel purified. High fidelity 2X Q5 DNA Polymerase master mix (New England Biolabs) was used for PCR amplification. 200µL of transformed cells were plated on two LB agar containing chloramphenicol and incubated overnight at 30°C. If no colonies appeared, the rest of the cells left at room temperature were plated after 24 hours. Colonies obtained were re-

purified at 37°C and checked for deletion of target gene using C1, C2 and upstream check 5 and downstream check 3 primers.

To excise the chloramphenicol cassette, verified mutants were made competent and transformed with the pCP20 helper plasmid harboring FLP recombinase and selected at 30°C on ampicillin plates. A few colonies were purified non-selectively twice at 43°C for thermal activation of FLP as well as loss of all antibiotic resistance. Loss of antibiotic cassette was verified by PCR and sequencing afterwards.

2.6 Site-directed mutagenesis

For site-specific introduction of Cysteine substitutions, a two-stage PCR protocol based on QuikChange Site-directed Mutagenesis (Stratagene Cloning Systems, San Diego, CA) was employed. This involved running two separate PCR reactions with single primers for four amplification cycles and then mixing half of the contents of the two reactions to run another 18 cycles of amplification. Primers were prepared to meet specifications of QuikChange II Site-directed Mutagenesis kit (Agilent Technologies). For mutagenesis PCR, *Pfu*Turbo Cx Hot-Start DNA Polymerase (Agilent Technologies) was used. Two separate 50 µL reactions were set up using 10X *Pfu*Turbo Cx buffer, 0.1-0.2 ug DNA template, 0.2 mM dNTP mix, 100 ng/µL of Primer 1 or 2 and 0.5 µL DNA Polymerase. Thermal cycling was set up at 95°C for 2 minutes, 94°C for 30 seconds, 55°C for 1 minute and extension at 68°C for 2 minutes/Kb of template for four cycles. In the next step, 25 µL from each the two tubes were mixed together in a new tube and again cycled after addition of 1 µL of polymerase. 1-2 µL of DpnI (New England Biolabs) was directly added into the tube and digested for 2 hours at 37°C and correct sized band was purified from gel. 6-8 µL of digested DNA was used for transformation.

2.7 Siderophore nutrition assay

This is a modified qualitative assay of the ability of cells to transport FeEnt when a chelator is added to the media. Cells were subcultured in 5 mL NB media containing antibiotic, with 1% inoculum and grown till mid-log. Since, *E. coli* does not transport Apo-ferrichromeA, it was used as a specific chelator of Fe^{3+} in the media., added to a final concentration of 0.01 mM. Alternatively, 233 µM of 2,2'-Bipyridyl was used in some cases. First, chelator and antibiotic were placed in a 13X100 mm glass tube and then 3 mL of molten NB Top agar (0.7% agar) at ~42°C was placed on top of them. 50 µL of cells were next pipetted into the agar, swirl mixed and poured into a well of a 6-well cell culture plate. After the agar solidified, a sterile filter disc (6 mm in diameter) was placed aseptically at the center of the agar and 5 µL of 50 nM FeEnt added to it. The plate was incubated for 12-14 hours at 37°C and results photographed thereafter. When required, β-mercaptoethanol (βME) was added up to 1 mM to the mixture of agar and cells before plating. Extent of FeEnt transport occurring in cells was assessed from the diameter and intensity of the halo obtained around the discs.

2.8 Expression of FepA

Expression of FepA was studied by SDS-PAGE and immunoblot of whole cell lysates as well as cell envelope preparations. 1% overnight culture was sub-cultured into MOPS minimal media, grown for 5.5 hours till cells reached OD600nm ~1.0. 1 X 10^8 cells were lysed by boiling for 5 minutes with SDS-PAGE sample boiling buffer with or without 3% βME added, before loading on to a 10% SDS-PAGE gel. Following gel electrophoresis at room temperature, the proteins were transferred to nitrocellulose membrane using a semi-dry transfer apparatus. The membrane was blocked for 15 minutes with 1X TBS

with 1% gelatin and then incubated with a mouse anti-FepA monoclonal cocktail of mAb41 and mAb45 (Murphy et al., 1990) in TBS plus 1% gelatin overnight. A TBS plus 0.05% Tween 20 solution was used for three subsequent 5 minute washes. After washing, the blot was incubated with [^{125}I]-protein A conjugate for a minimum of 2 hours and exposed to an autoradiography imaging screen overnight. Radioactivity was quantitated by reading the screen on a STORMSCAN PhosphorImager (Molecular Dynamics).

2.9 Colicin sensitivity test

To determine sensitivity of a fepA^{+} strain to Colicin B, 100 µL of stationary phase cells were mixed into 5 mL of molten LB Top agar and poured onto LB agar plates containing appropriate antibiotic. Serial dilutions of purified ColB or a different colicin were prepared in one half of a 96-well plate. Starting at the top left well of the plate, 1:9 dilutions were prepared down the column and 1:1 across the row. After the top agar layer solidified, serially diluted ColB was spotted on the agar surface using a sterile Clonemaster previously dipped in the wells. The plates were incubated overnight and ColB titre was determined as the last ColB dilution able to clear the lawn of bacteria. When required, 1mM BMe was added to the Top agar.

2.10 Siderophore accumulation over time

Quantitative measurements of [^{59}Fe]Ent uptake in iron-starved cells were done to measure the amount of radioactivity accumulated in cells over time. 1% inoculum from overnight grown cells were introduced into MOPS media containing antibiotic and grown to late-log OD600nm ~1.0. If βME was to be used, cells were exposed to 5 mM βME (unless otherwise mentioned) for 0.5 hour. To assay the cells, [^{59}Fe]Ent was added to an

aliquot of the cells placed at 37°C, to a final concentration of 1 µM. Molar excess of FeEnt was used to prevent any considerable substrate depletion within the assay period. Then 100 µL aliquots of cells were filtered on 0.45 µm filters in triplicate after incubating the cells for 5, 15, 30 and 45 minutes and then quickly rinsed with 10 mL of ice-cold 0.9% LiCl to stop transport. Finally, amount of radioactivity collected in filters were measured in a Cobra-Packard Gamma counter in counts per minute (cpm) and converted to pmol/10^9 cells using number of cells and specific activity. Average of the triplicate values were plotted versus time using Grafit software 6.0.011 (Erithacus software Ltd.).

2.11 Siderophore binding assay

Concentration dependent ligand binding studies were done by placing cells on ice which allows FeEnt to bind FepA but is not transported. Overnight grown cells were subcultured with 1% in MOPS, grown for 5.5 hours and then chilled on ice. *C. crescentus* cells do not or grow very slowly in MOPS media. So, NB media containing 0.5 mM $CaCl_2$ and Nalidixic acid was used instead in which enterobactin (apo-siderophore) was added to 0.1 mM in early-log phase to induce iron deprivation. Cells were spun down, resuspended in NB and chilled on ice. To perform the assay, 5 X 10^7 aliquots of cells were placed in tubes on ice and in another set of tubes, 0.05 nM, 0.1 nM, 0.5 nM, 1 nM, 5 nM and 10 nM [^{59}Fe]Ent or [^{59}Fe]Fc in 10 mL ice-cold MOPS were taken. Then the FeEnt was mixed with the cells, allowed to incubate and filtered after 5 secs and the filters rinsed with 10 mL ice-cold 0.9% LiCl. This was done in triplicate for each concentration. Radioactivity collected was measured and pMol bound/10^9 cells was plotted versus concentration of [^{59}Fe]-siderophore. A binding curve was obtained by plotting the average

of the triplicate values into a non-linear fit to the “bound versus total” equation of Grafit 6.0.11 software. From the plot, K_d and binding capacity values were obtained.

Sometimes, instead of measuring binding at varying concentrations of [^{59}Fe]Ent, capacity were measured at 10 nM saturating concentration in wild-type and cystine disulfide mutants of FepA in cells pre-treated or untreated with 5 mM BMe. This technique, that we called ‘Capacity screening’, allowed comparative study of transport rates in FepA mutants when different parts of the protein are locked in conformation by disulfide bonds.

2.12 Siderophore transport

Concentration dependent transport assays were performed in a similar manner as binding except that the whole process was done at 37° to allow transport. Two aliquots of cells were mixed with [^{59}Fe]Ent and incubated for 5 and 65 seconds and then filtered with 0.45 µm nitrocellulose or HAWP filters and washed with LiCl. The 5 second time point measured the initial binding which when subtracted from the second time point, gave the amount of radioactivity transported over 1 minute. For *C. crescentus* [^{59}Fe]Fc transport studies a longer transport period of 3 minutes was considered. As before, for each concentration data was collected in triplicate, then averaged and plotted as pMol/min/10^9 cells versus concentration of radiolabeled ligand. K_M and Vmax values were obtained by plotting in a “enzyme kinetics” curve of Grafit 6.0.011 software.

Chapter 3: Mechanism of Ferric Enterobactin Internalization by FepA

3.1 Introduction

Metal transporters of Gram negative bacterial OM (FepA, FhuA, BtuB) consist of a transmembrane C-terminal 22-stranded β-barrel that places them in the porin superfamily. However, the ~150 residue N-terminal globular domain of the proteins fold into the channel blocking it (Pawelek et al., 2006; Buchanan et al., 1999). These proteins are highly selective and adsorb to the metal chelates with high affinity. Once, they bind to their specific ligands, small conformational changes occur within the N-domain of the proteins that presumably signals ligand-occupancy (Pawelek et al., 2006). The uptake of the ferric siderophore and Vitamin B12 through an occluded channel of the respective ligand-gated porins (LGPs) suggests structural changes in the N-terminal domains of these transporters which requires energy input. Since, the OM cannot sustain an ion gradient because of other porins, the IM protein TonB is tied to the transduction of energy from the IM to these proteins (Bassford et al., 1976).

No clear description of the nature of the conformational changes that open a channel or pore within the LGP β-barrel exists yet. Some models were proposed previously to describe possible methods of N-domain movement that might allow passage of Ferric enterobactin (FeEnt) through FepA. The ‘Ball and Chain’ model suggests that the N-domain dislodges into the periplasm as a unit by virtue of its hinge-region at residue 150, or by unfolding of its globular structure. In both cases, a large (~40Å) pore is potentially created allowing passage of the FeEnt molecule interacting with the large N-domain loops. Another model is the ‘Transient Pore’ which postulates conformational

motion of the N-domain without exiting the β-barrel and formation of a pore within the channel large enough (at least 20Å) to accommodate the FeEnt molecule. In this situation, the acidic FeEnt molecule can undergo step-wise interactions with basic residues near the top of the N-domain and those in the interior of the β-barrel according to their affinity, ultimately exiting the pore.

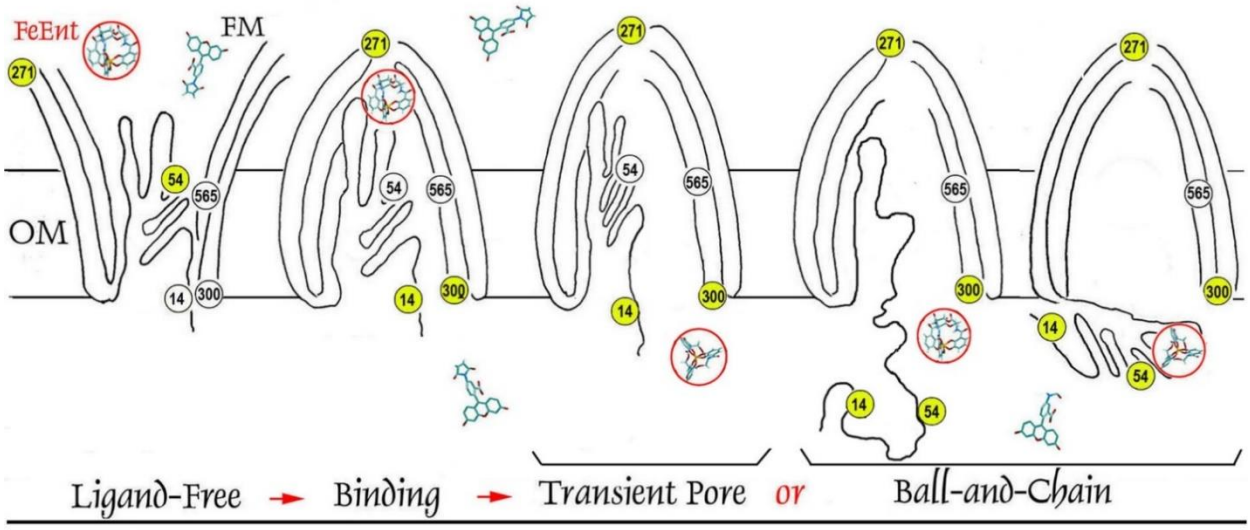

Fig. 3-1: Ma L, Kaserer W, Annamalai R, et al. Evidence of ball-and-chain transport of ferric enterobactin through FepA. J Biol Chem. 2006;282(1):397-406. Proposed models of FeEnt transport through FepA. Residues colored yellow or white represent important amino acids that showed differential accessibility to fluorophores upon cysteine substitution.

Ma et al. (2006) attempted to distinguish between these two models by testing the accessibility of strategically engineered 25 Cys sulfhydryls in FepA to modification by fluorescein maleimide (FM), *in vivo*. The single Cys substitutions were located either in the surface loops, occluded regions of the N-domain, or distributed near the periphery and the inside of the β-barrel. When subjected to fluorophore labeling, residues on surface loop and periplasmic face were labeled strongly. Labeling patterns of two N-

domain residues G54C and I14C turned out particularly informative. G54C which is located in the interior of the barrel on the surface of the N-domain, was weakly, nevertheless consistently labeled either in the absence of FeEnt or in *tonB*+ cells in energized state when FeEnt is present. This suggested that in the absence of FeEnt, an "open" conformation of the loops allows access of FM to G54C in the interior, which is blocked in *tonB* cells that bind FeEnt but cannot transport. In *tonB*+ cells in energized condition, labeling of G54C is most likely occurs from the inside, in the periplasm suggesting displacement of the N-domain into the periplasm. Residue I14C lies at the rim of the β-barrel. They found that labeling of I14C was greatly increased during transport which suggested that the residue became more accessible to FM labeling in the periplasm during transport. There was also a lack of labeling of residues which lie within the β-barrel and point towards the inside of the channel. These observations pointed toward a "Ball and Chain" mechanism of transport in which the N-domain is dislodged into the periplasm allowing residues G54C and I14C to be labeled by FM entering the periplasm by diffusion through OM porins.

In this study, we further investigate whether the N-domain dislocates into the periplasm as a unit or unfolds by conformational change to allow ligand entry. To distinguish between these two mechanisms, we engineered two classes of double Cys mutants of FepA expressed on a plasmid: (i) in close proximity that is, within cross-linking distance of no greater than 6Å within the N-domain, called N- to N-domain mutants (ii) with one residue in the N-domain and the second one in the interior of the β-barrel with the side-chain protruding into the channel, called N- to C-domain mutants. In this case, double-bonds may only be formed during transport of FeEnt when movement of the N-

domain brings its Cys residues within cross-linking distance of the β-barrel Cys residue. If the N-domain is expelled as a single unit, formation of Cys-Cys bonds in the first case, should not affect ligand uptake, but will be impaired if N- to C-domain disulfide bonds are formed or, the N-domain requires unfolding for transport. We created six pairs of double Cys mutants in the N-domain and three between the N- and C-domain by site-directed mutagenesis and tested the effect of disulfide bond formation on ligand binding and uptake by several methods in the absence and presence of reducing agents like β-mercaptoethanol (βME).

3.2 Methods

3.2.1 Creating double Cysteine mutants

We identified residues to be mutated by careful study of the crystal structure of FepA and picked residues in the N-domain with separations less than 6Å so that disulfide bonds may be formed in the native protein, or in the N-domain and the C-domain in which case disulfide bonds may be formed only during ligand transport. To make double Cys mutants, we first made a single Cys substitution in WT fepA cloned in pITS23 and then substituted the second Cys using QuikChange II Site-directed mutagenesis kit.

Previously, some double Cys mutants were made in WT *fepA* cloned in the plasmid pITS47 in OKN3 (*fepA*$^{-}$). However, some mutants in pITS47 showed reduced expression compared to mutants made in another plasmid pITS23 containing WT *fepA*. We found that an additional ~47 nucleotides in the terminator region of the cloned fepA gene in pITS47 was causing the reduced expression. To fix this problem, we performed allelic exchange between an end fragment of fepA in pITS23 with a fragment in pITS47 that

included the extra nucleotides. This got rid of the extra nucleotides at the end of the fepA gene in pITS47 and made it equivalent to fepA in pITS23. We also fixed some mutants by directly deleting the 47 nucleotides in pITS47 by site-directed mutagenesis. We verified mutations by sequencing and checked expression by SDS-PAGE and Immunoblots.

3.2.2. Siderophore nutrition tests

We performed siderophore nutrition assays on the single and double Cys mutants to check the effect of disulfide bonds on FeEnt transport. We added 1 mM β-mercaptoethanol (βME) or higher concentration into the agar to reduce the disulfide bonds when appropriate. We compared the diameter and nature of the halos obtained with the WT OKN3/pITS23 strain.

3.2.3. [^{59}Fe]Ent uptake assays

To check the effect of disulfide bond formation, we performed radioactive [^{59}Fe]Ent accumulation assays on double Cys mutants with and without βME and compared with WT. We grew cells in iron-deficient media for 5 hours or until they reached OD600 ~1.0, added 5 μM βME when required for another half hour. We then added [^{59}Fe]Ent to a final concentration of 1 μM, collected aliquots of cells in filters in triplicate, washed and counted them for radioactivity at particular timepoints for 45 minutes.

3.2.4 Binding capacity screening

We assessed the effect of disulfide bonds on the capacity of binding of the mutants with and without βME. Instead of performing traditional binding experiments over a range of radiolabeled substrate concentrations, we measured the binding capacity of all the mutants together at saturating concentrations. To perform Capacity screening, we added

[^{59}Fe]Ent to a final concentration of 10 nM to aliquots of ~5 X 10^7 cells kept on ice. This allows the ligand to bind but no transport occurs. We let the reaction to occur for 5 seconds, added 10 mL of ice-cold 0.9% LiCl to stop the reaction, filtered and washed the cells. Then we counted the amount of radioactivity bound in pmol/10^9 cells and plotted in bar graphs using Grafit software. Addition of 5 βME allowed us to assess the effect of disulfide bonds on binding capacities of the mutants.

3.2.5 Spectroscopic measurement of FeEnt uptake by universal assay

For each assay we used 50uL of a FM-labeled culture of OKN13/pITS23A698C at 5 x 10^8 cells/mL. We added the aliquot to 2mL PBS + 0.4% glucose at 37ºC in a fluorimeter cuvette with constant mixing and recorded the initial fluorescence intensity for 100 seconds. At that point, we added 5nM FeEnt to the cuvette and allowed it to incubate for 100 seconds. The maximum quenching with pITS23A698C was observed to be 60%. At 200 seconds, we added 50uL of the test strain (5 x 10^6 cells) that is OKN3/pITS23 or the different Cys mutants in OKN3. Fluorescence was continuously monitored. If there was no increase in fluorescence (indicating absence of uptake), we added βME at 800 seconds to a final concentration of 10mM. Several strains needed a second, similar addition of βME at 1,000 seconds.

3.3 Results

3.3.1 Construction of double Cys mutants in FepA

We constructed six double Cys mutants within the N-domain of WT FepA in the plasmid pITS23 by site-directed mutagenesis of residues that are least likely to affect the net charge and tertiary protein structure in those regions, such that disulfide bonds may

form in the native protein. These mutants were: G27C/R126C, A33C/E120C, N56C/D73C, I84C/T142C, D44C/T111C, L125C/ V141C (Fig. 3-2). Each of the Cysteines residues in the double Cys pairs are located one on each of the short β-strands within the N-domain such that if disulfide bonds are formed the strands may be locked in position preventing possible conformational changes within the plug.

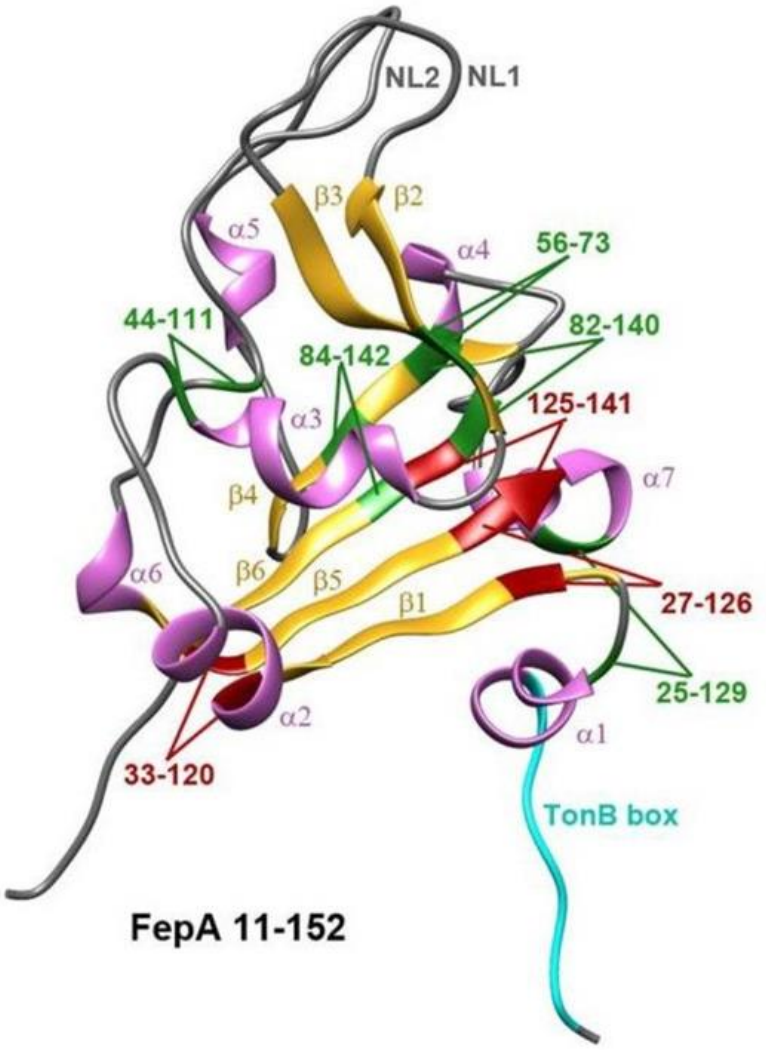

Fig. 3-2: Location of the Cys-Cys mutants in the N-domain of FepA. The β-sheeta are represented in gold and the helices in purple. The long loops are shown in grey and the N-terminal TonB box in cyan. The substituted Cys-Cys residues are marked in red in in the lower part of the protein

and green in the upper part. Mutants 25/129 and 82/140 are still under study. This schematic was prepared using Chimera software.

We also constructed three double Cys mutants with one Cys in the N-domain and the other one within the β-barrel with its side chain pointing inside the channel: M77C/T457C, A138C/T427C, A138C/A445C. These cysteines are located far apart to engage in disulfide bond formation unless they are brought in close proximity, if the N-domain attempts to dislodge into the periplasm during FeEnt transport. In either case, if disulfide bonds are formed, we expected to see its effect on ligand uptake in siderophore nutrition assays or quantitative radiolabeled ligand uptake measurements.

3.3.2 Siderophore Nutrition tests of double Cys mutants

Siderophore nutrition test is a simple assay often providing preliminary yet valuable information about the nature of ligand transport from the diameter and intensity of the halo of bacterial growth around the filter discs containing the ligand. If the Cys residues would engage in disulfide bonds, we expected transport to be affected and hence change the nature of the siderophore nutrition halos. We also tested the effect of the presence of a reducing agent like βME in the medium.

While single Cysteine mutants showed similar halos compared to WT pITS23/OKN3 cells (Fig. 3-3), several of the N-domain double Cys mutants showed no halos or absence of growth around discs. These included: G27C/R126C, A33C/E120C, N56C/D73C, L125C/V141C. Mutants I84C/T142C and D44C/T111C had positive siderophore nutrition tests although the halos were diffuse and bigger compared to WT. Addition of 1 mM βME to the top agar restored halos around discs comparable to WT

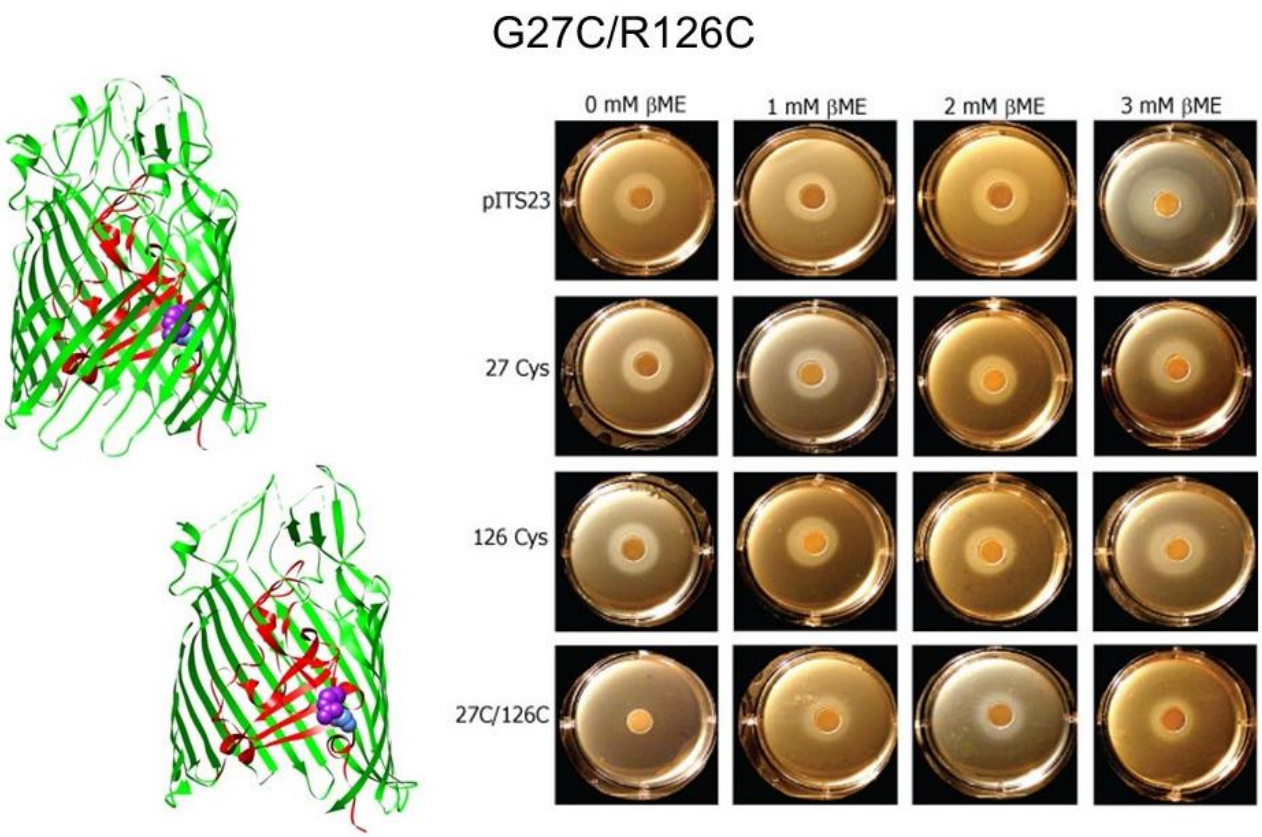

Fig. 3-3: Siderophore nutrition test for the N- to N-domain mutant G27C/R126C. The left shows a schematic of the location of the G27 (blue) and R126 (purple) residues within the N-domain (red) of FepA. Siderophore nutrition tests of WT pITS23, single mutants G27C and R126C and the double mutant in the absence or presence of 1 mM, 2 mM or 3 mM βME.

diameters in almost all the N-domain mutants except in N56C/D73C and L125C/V141C. In case of N56C/D73C, the halo obtained was comparatively bigger than pITS23 with 1 mM βME. This indicated that 1 mM βME was not sufficient to restore this double Cys mutant to full transport capacity. Even with treatment of L125C/V141C with 8 mM βME, the recovery of uptake in this mutant was quite poor (Fig. 3-4).

The siderophore nutrition of the N- to C-domain mutants were distinctively different. All three N- to C-domain mutants showed growth around discs comparable to

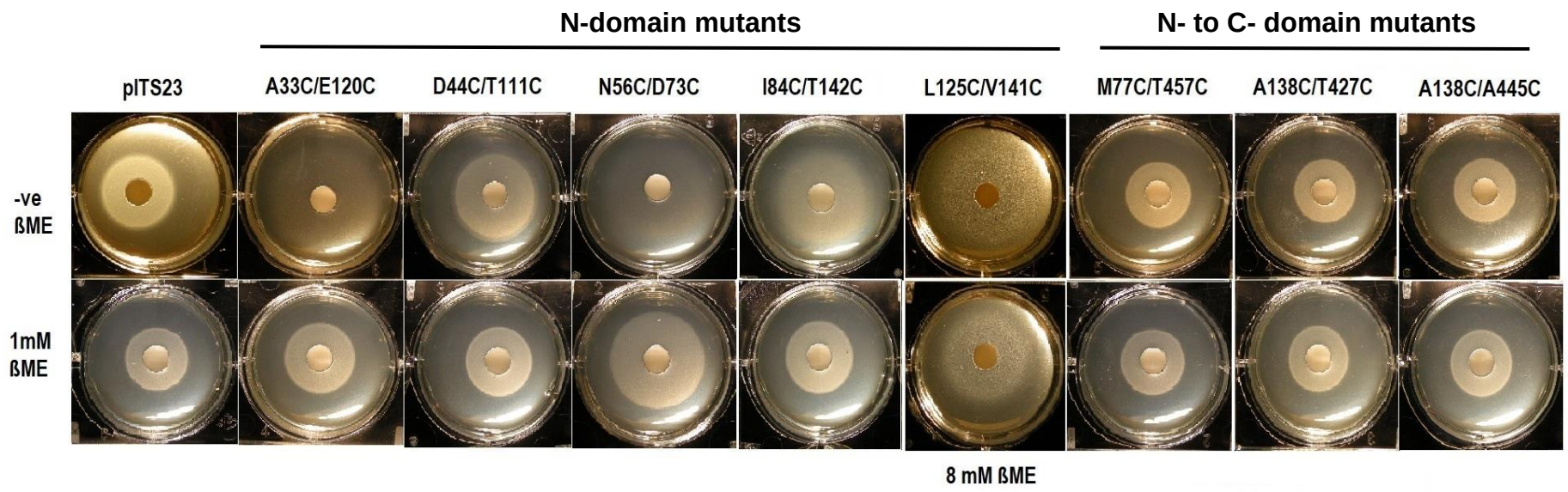

Fig. 3-4: Siderophore nutrition test in N-domain and N- to C-domain mutants. Except D44C/T111C, all N-domain mutants showed absence or poor growth of halos around discs which recovered with 1 mM βME. L125C/V141C hardly recovered even with 8 mM βME. N- to C-domain mutants showed no impairment in uptake in siderophore nutrition assay.

WT without the need for a reducing agent. We suspected that in these mutants, disulfide bonds were likely not formed.

3.3.3 [^{59}Fe]Ent accumulation studies

When we measured accumulation of radioactive [^{59}Fe]Ent over 45 minutes, mutants G27C/R126C, A33C/E120C, N56C/D73C and L125C/V141C showed impairment by at least 80% in uptake compared to WT OKN3/pITS23. When the cells were incubated with 5 μM βME for half hour prior to addition of [^{59}Fe]Ent, accumulation of the radioactive ligand was restored to WT levels. However, mutant N56C/D73C appeared to require higher levels of βME to uptake [^{59}Fe]Ent at WT levels closely matching the results of our siderophore nutrition tests. The two mutants I84C/T142C and D44C/T111C, which showed less effect on transport capabilities, again showed similar outcomes in the quantitative radioligand uptake experiments (Fig. 3-5A). In their cases, level of reduction in uptake was about 60% compared to WT which was restored to normal with 5 mM βME. On the other hand, the N- to C-domain mutants did not require the addition of βME to transport [^{59}Fe]Ent at levels identical to WT corroborating the findings of the siderophore nutrition tests (Fig. 3-5B). Hence, we excluded this class of mutants from further studies.

A.

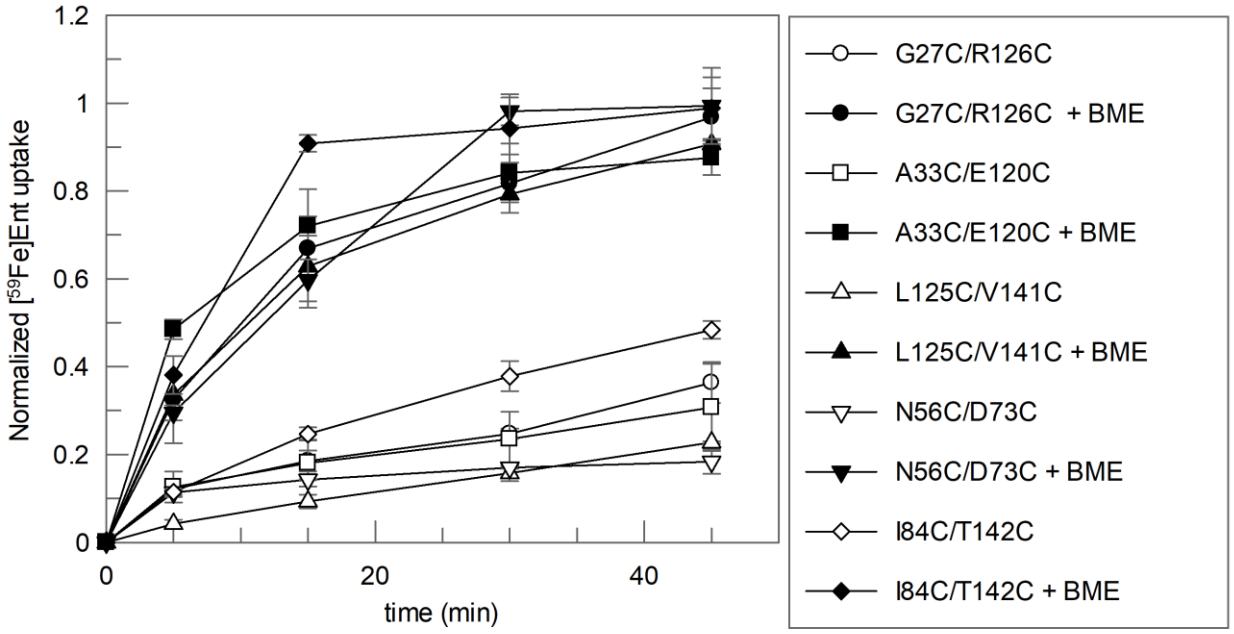

B.

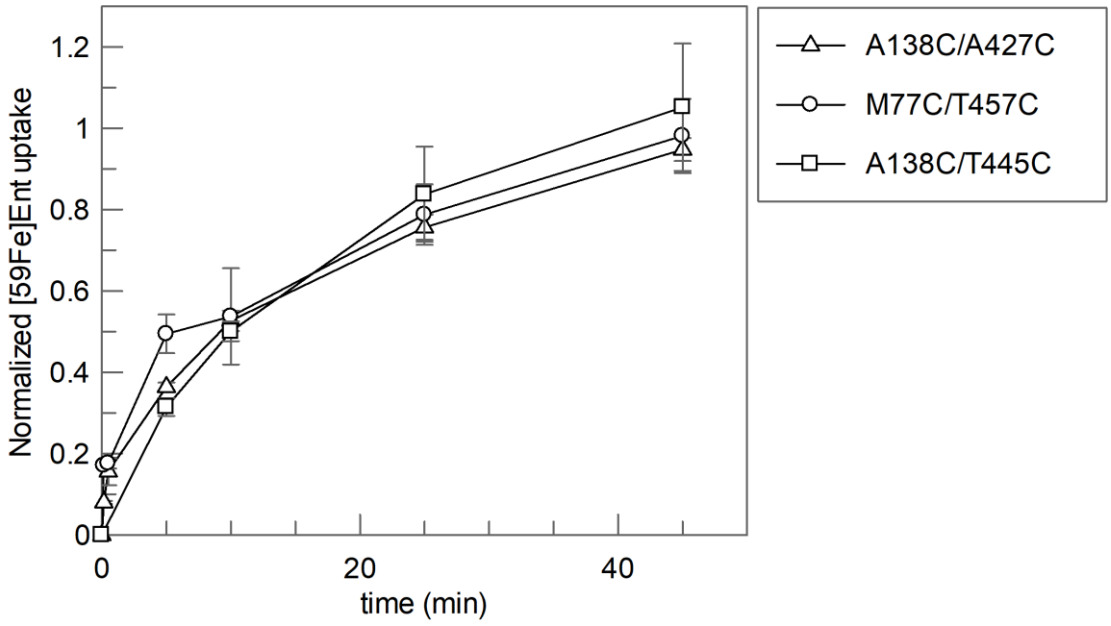

Fig. 3-5: Accumulation of [^{59}Fe]Ent over time in FepA Cys-Cys mutants. We grew WT pITS23 and all the Cys-Cys mutants in MOPS media and studied accumulation of [^{59}Fe]Ent over 45 minutes without and with treatment with 5 mM βME. Unfilled symbols represent uptake without βME and filled symbols represent uptake after addition of βME. A) Accumulation of [^{59}Fe]Ent in N-domain

mutants and B) Accumulation of [^{59}Fe]Ent in N- to C-domain mutants. All data is normalized with respect to WT accumulation levels. Each curve is an average of three experiments.

3.3.4 Expression of FepA in Cys-Cys mutants

To validate whether FepA was being expressed correctly in the OM of these mutants, we ran OM preparations of all the N-domain mutants as well as the WT on SDS-PAGE gels with the addition of 3% βME into the boiling buffer. Then we prepared an immunoblot with anti-FepA MAb and [^{125}I]-PrA conjugate to obtain quantitative levels of FepA expression. All the mutants expressed FepA at WT levels. As a control, we included a previously engineered double mutant I14C/G300C (Ma et al., 2007) that is known to express efficiently. Small amounts of degradation were apparent in the mutants I84C/T142C and L125C/V141C (Fig. 3-6). Nevertheless, this indicated that the impaired uptake in the N-domain Cys-Cys mutants was indeed an effect of disulfide bonds being formed with the globular domain of the protein.

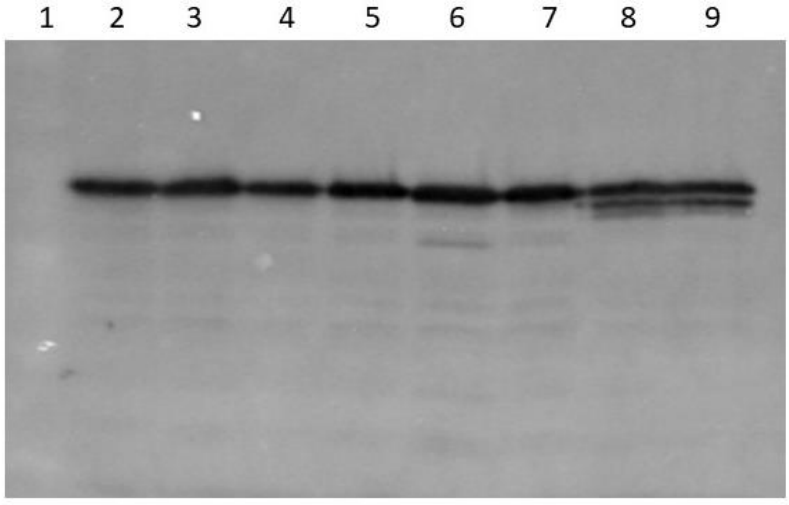

Fig. 3-6: [125I]-Protein A immunoblot of N-domain Cys-Cys mutants. Lanes: 1) MW marker 2) pITS23 3) I14C/G300C 4) G27C/R126C 5) A33C/E120C 6) D44C/T111C 7) N56C/D73C 8) I84C/T142C 9) L125C/V141C.

3.3.5 Effect of disulfide bond formation on binding capacity

Binding of FeEnt to FepA is thought to involve aromatic residues located in the upper extremities and loops of N-domain. Whether any of the β-sheet Cys disulfide pairs affected ligand binding, remained an important question. Although, we performed conventional binding kinetics experiments with several Cys-Cys mutants, to study all mutants in a convenient and stream-lined fashion, we modified the protocol for binding measurements to a simplified version called “Binding Capacity Screening”. Instead of measuring binding over a range of concentrations, we measured capacity at 10 nM saturating concentration for all the mutant pairs and compared the levels with that of WT (Fig. 3-7). The mutants fell in three categories: i) D44C/T111C and N56C/D73C showed no impairment in binding capacity ii) G27C/R126C, A33C/E120C showed slight impairment in binding which recovered to some extent upon treatment with 5 mM βME and, iii) mutants I84C/T142C and L125C/V141C showed only ~20% of WT binding. Addition of 5 mM βME was able to relieve this inhibition to >75% of WT levels in case of I84C/T142C but had no effect on the L125C/V141C pair. We tested L125C/V141C with higher concentrations of βME up to 30 mM which was still unable to restore binding beyond 30% of WT levels. However, due to observable effect of high concentration of βME on WT binding capacity, we could not test whether higher concentrations of βME could effectively break the disulfide bond in this mutant pair (Fig. 3-8). We performed these experiments three times to obtain standard deviations in the data.

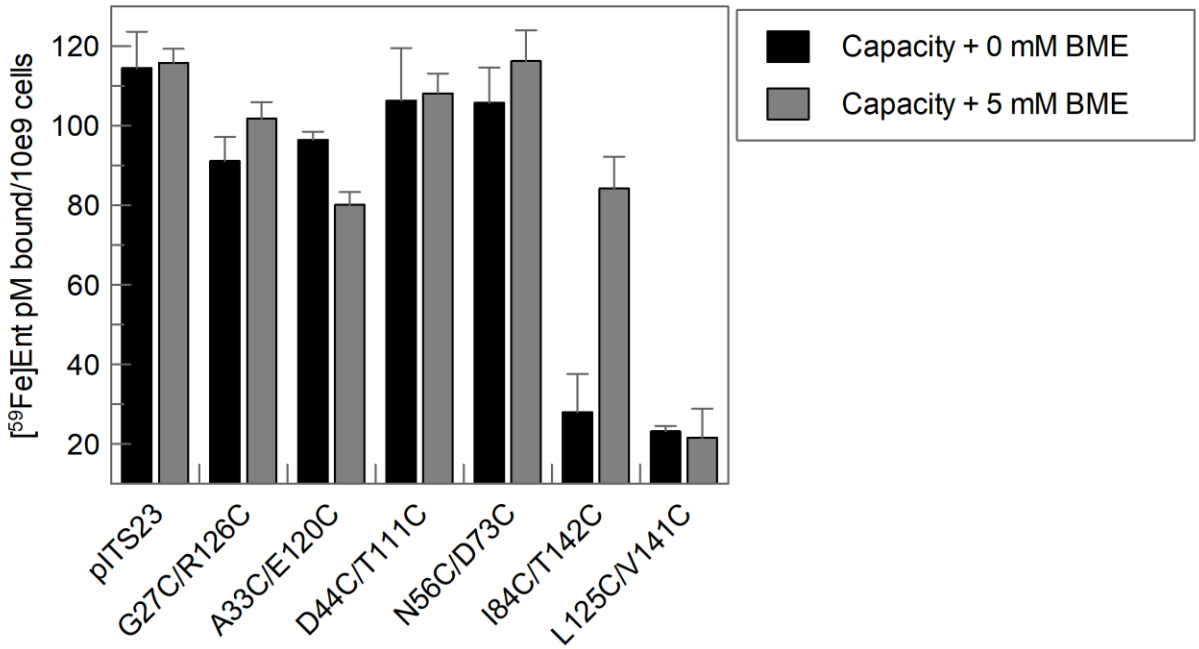

Fig. 3-7: Capacity screening of N-domain Cys-Cys mutants. We tested binding capacity of the mutant pairs and compared with WT pITS23 binding at 10 nM concentration of [^{59}Fe]Ent in the absence or presence of 5 mM βME.

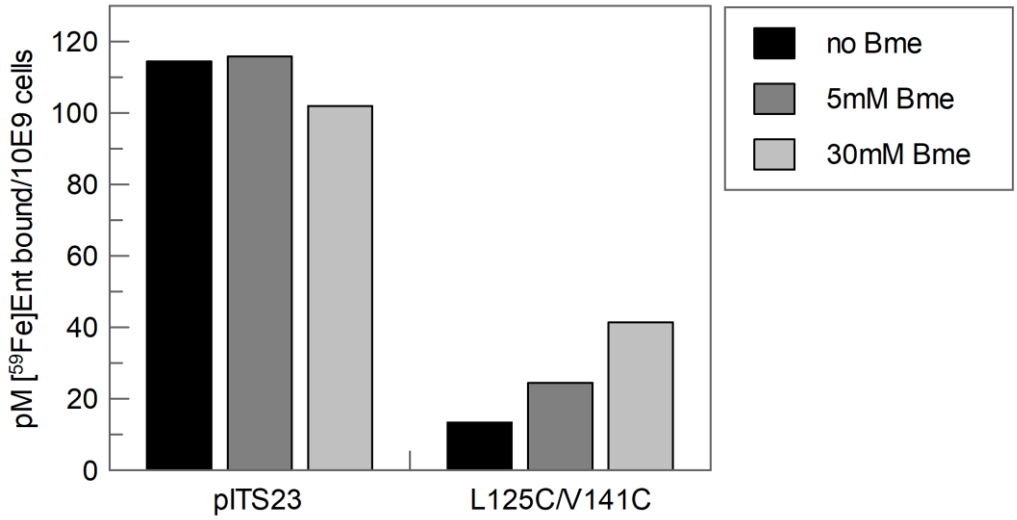

Fig. 3-8: Binding capacity at higher concentration of βME. We tested whether the inhibition of binding in L125C/V141C is relieved by adding higher concentrations of the reducing agent.

We attempted to check the effect of disulfide bond formation on transport rates with similarly designed experiments as ‘Capacity Screening’ but the pitfall in these assays was

that the experiments were extremely labor and resource intensive. It was impossible to study all the mutants in a single day's experiment. Although, we sometimes obtained satisfactory results, it was difficult to repeat these experiments efficiently to obtain statistical validation. Hence, we embraced a spectrofluorimetric assay to measure the uptake of FeEnt in the double Cysteine mutants.

3.3.6 Spectroscopic measurement of FeEnt uptake by Universal Assay

The assay is based on the ability of FeEnt to bind to and quench the fluorescence of fluorescently labeled FepA in live bacterial cells that are unable to transport the FeEnt due to the lack of TonB. If *fepA*$^{+}$ *tonB*$^{+}$ live bacteria are added to the system, the quenched fluorescence recovers back to the initial intensity due to the removal of FeEnt from the solution by the cells (Chakravorty et al., Unpublished data). For each assay we used Fluorescein maleimide labeled culture of OKN13/pITS23A698C as the "sensor" strain, which gives the initial fluorescence intensity. Upon addition of FeEnt, the fluorescence quenches and stays quenched until the addition of test strains which in our case were either OKN3/pITS23 or the different N-domain double Cys mutants. Mutants with impaired transport capabilities would require the addition of the reducing agent βME to recover the fluorescence.

When subjected to this assay the mutants fell in one of four groups. i) The first group showed no difference from the OKN3/pITS23 control strain. Mutant D44C/T111C fell into this group and did not require the addition of any βME to transport the FeEnt from solution, with uptake rates close to WT. ii) This group was able to transport the FeEnt only when 10mM βME was added at 800 seconds. Mutant A33C/E120C behaved in this fashion. As soon as we added the reducing agent, uptake resumed at rates similar to WT.

iii) This group included the mutant N56C/D73C. Initial addition of 10 mM βME showed some uptake but the addition of another 10 mM restored the uptake and the kinetics of fluorescence recovery was very similar to cells expressing WT FepA. iv) The final group included all the other double mutants constructed, i.e. G27C/R126C, I84C/T142C and L125C/V141C. All of these mutants required 20 mM βME to function but transported at much slower rates compared to WT FepA as indicated by the slopes of the recovery curves. Fig. 3-8 shows normalized fluorescence from the sensor strain, subsequent quenching from addition of FeEnt and the concomitant recovery of fluorescence upon uptake of the siderophore by the test strains with or without addition of βME. Each curve is an average of three experiments.

3.4 Discussion

With very little or no role in ligand selectivity, the contribution of the N-domain of the LGPs appears to be solely in “gating” an otherwise a large pore within the β-barrel. Strains lacking the N-domain of FhuA, evidently have greater outer membrane permeability (Braun et al, 2002). However, exact nature of the conformational changes leading to channel opening are still not clearly understood. Observations made by Ma et al., (2008) pointed towards a ‘ball and chain’ mode of N-domain movement, but it did not elaborate whether the globular domain unfolds or dislodges as a unit in to the periplasm. Nevertheless, multiple evidences suggest the interaction between the N-terminal TonB box of the LGPs and the TonB CTD potentially plays a role in the mechanical gating of the channel

A.

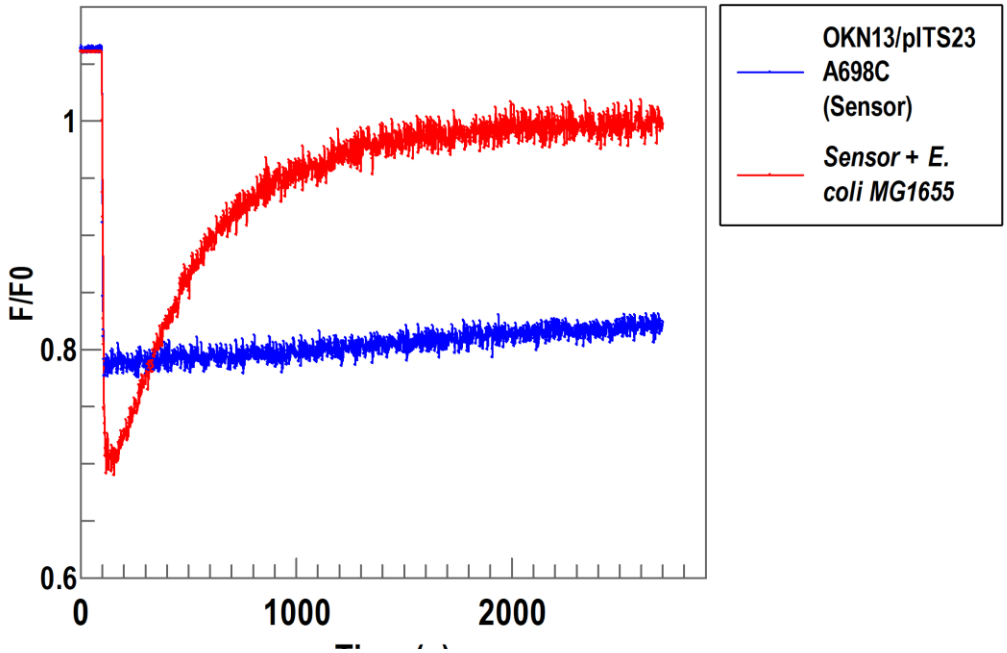

B.

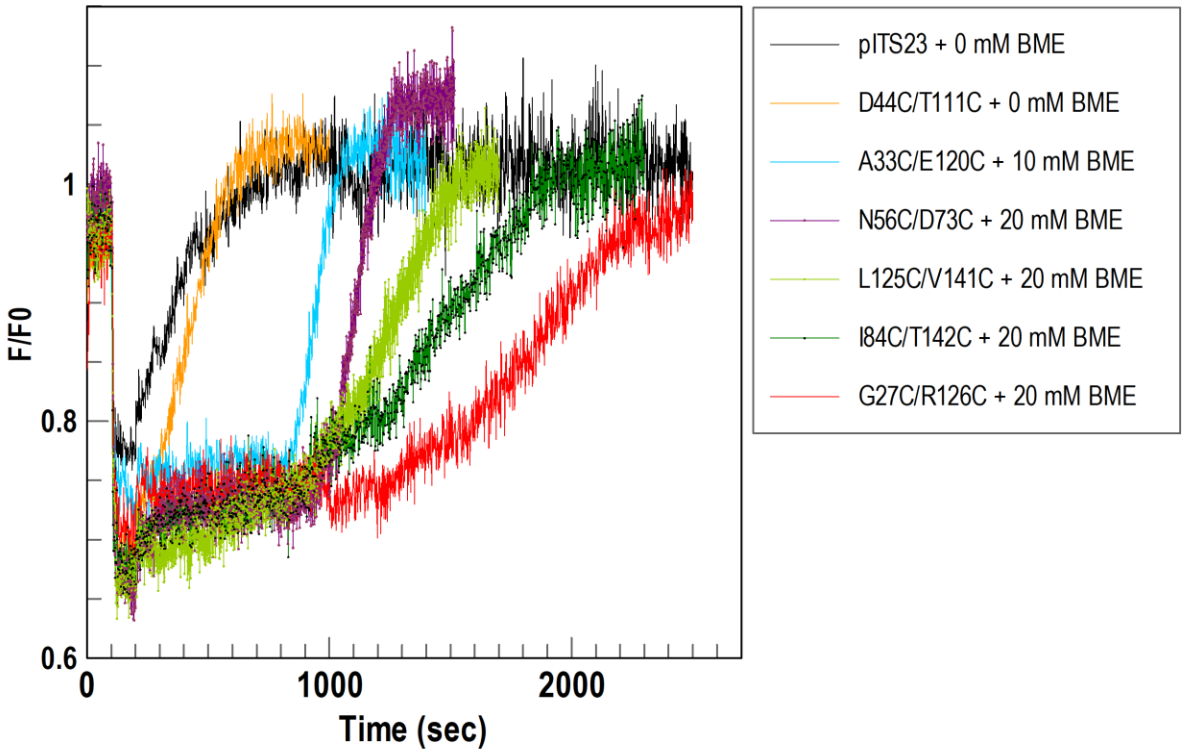

Fig. 3-9: Spectroscopic observation of effect of disulfide bonds on FeEnt transport. (A) Behavior of sensor and test strain in Universal assay for FeEnt transport. (B) Normalized fluorescence showing response of pITS23 and the different N-domain Cys mutants upon addition of varying concentrations of βME. Each curve is a result of 3 separate experiments.

(Pawelek et al., 2006; Klebba 2016; Gumbart et al., 2007; Hickman et al., 2016). The aim of this work is to determine the intricacies of the conformational changes occurring in the globular domain, presumably in response to energy transfer by TonB upon interaction with the TonB box.

Disulfide locking have previously been used to restrict intra-molecular mobility and probe conformational changes in bacterial proteins such as rhodopsin (Yu et al., 1999), aspartate receptor (Falke & Koshland Jr. 1987). By strategically substituting residues which were least likely to affect the normal functioning of the protein, in different parts of FepA in to Cys, we were able to track conformational changes in the N-domain of FepA in response to ligand binding and entry. We engineered Cys pairs throughout the N-domain such that the β -sheets and helical turns were prevented from separating when such conformational changes were necessary for ligand entry. On the other hand, the Cys pairs we created in the N- and C-domains substituted residues in the C-domain that stick inside the β-barrel and in the N-domain face the barrel walls. In the ligand unbound state, these disulfide bonds are too far apart to form naturally in the protein, unless they are brought together by ligand passage. In either case, reduction of the disulfide bonds, if formed, would be necessary to observe ligand uptake. Precise observation of the crystal structure of FepA allowed us to cherry-pick suitable residues for Cys modification.

Preliminary siderophore nutrition tests already began to demonstrate a clear distinction between the functionality of the two classes of mutants. While none of the N- to C-domain mutants showed any impairment in ligand uptake capabilities, as indicated by the development of halos around discs without any need for βME addition, several of the N-domain Cys pairs showed lack of halos in the untreated form. Addition of βME

restored activity to wildtype levels which indicated the necessity for conformational changes within the N-domain for ligand internalization. Except N56C/D73C, all the Cys pairs that showed lack of transport, are located closer to the lower half of the N-domain, facing the periplasm. Wildtype level transport by the single Cys mutants suggested that the mutations by themselves did not affect the normal functioning of the protein. Radioactive immunoblots confirmed expression of the N-domain disulfide mutant at wildtype levels underscoring the effect of disulfide bond formation on ligand uptake in these mutants.

[^{59}Fe]Ent uptake studies offered quantitative measurements of the effect of disulfide bonds on the two classes of mutants. Similar to the siderophore nutrition tests, the N- to C-domain mutants appeared to transport at wildtype levels without any requirement for βME addition, suggesting that the Cys residues are not brought in close enough vicinity to engage in disulfide bond formation during transport of the siderophore. On the other hand, all of the N-domain mutants were clearly affected to variable extents in their uptake capabilities unless the reducing agent was present (Table 3-1, Fig. 3-5A). The different extent of impairment of the different mutants reflected which residues were critically affected by the disulfide bond formation, thereby locking the occluding domain of FepA in particular conformations. Cys pairs I84C/T142C and D44C/T111C located near the central part of the N-domain appeared to be less involved in the conformational changes required for ligand transport. Ligand binding to FepA is thought to be biphasic with two sites within the protein where FeEnt consecutively interact with aromatic and basic amino acids leading to specific and tight binding (Payne et al.,1997). The first site is located in the loop extremities whereas, the second site is deeper in the vestibule on

top of the N-domain. Presumably, the two cysteine mutant pairs and their surrounding residues interact with the ligand when avid binding occurs, and such interactions are hampered by the presence of the disulfide bonded cysteines. Additionally, low temperature of the binding experiments might be inducing changes in the protein conformation within the disulfide bonded regions. To measure only the binding step of the transport process, we performed experiments on ice. This could potentially affect binding capacity. In the case of L125C/V141C, the inability of high concentration of βME to relieve the inhibition suggests this possibility of alteration of protein conformation and also that the reducing agent might not be reaching protein interior in sufficient concentrations.

The Universal fluorescence assay is based on the previously described observation that, when an appropriate concentration of FeEnt is added to a solution containing live E. coli cells expressing FM-labeled FepA, the initial fluorescence quenches and subsequently recovers to the original or near original intensity as the FeEnt is gradually transported and thus depleted from solution (Smallwood et al., 2014). The precision and sensitivity of the Universal assay helped verify the finding of our radioactive ligand uptake and binding experiments. The assay is so designed that once the ligand is added to the TonB deficient ‘sensor’ strain in solution, quenching of fluorescence occurs due to binding of all labeled FepA molecules, but the fluorescence intensity does not recover unless there is transport. Since, the sensor strain is incapable of transporting the ferric siderophore, recovery occurs only when the added test strain is transport competent. Hence, the effect of the disulfide mutations in OKN3 harboring the different mutant versions of pITS23, were clearly evident when we mixed them with the OKN13/pITS23A698C-FM sensor. While wildtype pITS23 and D44C/T111C recovered

without the need for adding any reducing agent, all the other mutants required either 10 or 20mM βME to recover transport capabilities with concomitant fluorescence unquenching. The requirement for varying concentrations of βME to break the disulfide bonds provides some idea about the extent of disulfide bond formation in these mutants, with mutants requiring more βME possibly being more tightly and extensively bonded. We attempted multiple ways to observe the extent of disulfide bond formation in SDS-PAGE gels. However, the results turned out to be inconsistent and inconclusive. The nature of the recovery curves suggests that the mutant pairs that required more βME and longer time periods of recovery are located in regions of the protein where the reducing agent reaches less efficiently. Since, the accumulation and binding assays are biochemical in nature, they are less precise compared to the Universal assay as in the latter we observe the real time transport of ferric siderophore by live bacterial cells. Taking this in to account, we can infer that the mutation N56C/D73C which requires ~6X more time to recover (Table 3-1) even in presence of 10 or 20 mM βME is either strongly disulfide bonded or the bound FeEnt is preventing enough concentration of the reducing agent from breaking the disulfide bond. Hence, the localization of the cysteine pairs seems to be governing how βME interacts with each of these pairs.

Table 3-1: Summary of results from different assays for FeEnt transport due to the formation of the disulfide bonds in the N-domain of FepA. For the Universal assay, we chose an arbitrarily normalized fluorescence value of 0.97 before addition of FeEnt and recorded the time of recovery up to that level for the WT and each mutant. The time of recovery in WT was set as 1. We then recorded the recovery time in the different mutants to the normalized fluorescence of 0.97 as multiples of the time taken by the WT to recover to the same level.

Assay	**βME (mM)**	**Levels with respect to WT**					
		G27C/R126C	A33C/E120C	L125C/V141C	N56C/D73C	I84C/T142C	D44C/T111C
^{59}FeEnt Accumulation	0	30	25	18	18	40	50
	5	80	80	80	100	100	100
^{59}FeEnt Binding Capacity	0	67	70	17	95	25	100
	5	83.3	60	17	100	67	100
Universal Assay	**Multiple of recovery time with respect to WT**						
	0	NA	NA	NA	NA	NA	1.1
	20	4.1	1.83 (10mM)	2.64	5.56	3.26	NA

Based on this data we deduce a model for ligand internalization through FepA which appears to involve partial unfolding of the N-domain in to the periplasm. The requirement of disulfide bond reduction for transport in majority of the engineered disulfide pairs in the globular domain indicates that it does not exit the channel as a unit. The residues located near the bottom and central part of the N-domain appear to be most affected in different assays. These residues include G27/R126, A33/R120, V125/L141, I84/V142 and N56/D73. Thus, the β-strands undergo unfolding, potentially in a hierarchical fashion involving β1, β5, β6 and β4 (Fig. 3-2). The crystal structure of the TonB box of FhuA (Pawelek et al., 2007) engaged in interactions with the TonB CTD is suggestive of the idea that this kind of interaction may also give rise to a “mechanical pulling” of the gating N-domain in the LGPs. Our model reconciliates with this idea by suggesting that following ligand occupancy, FepA and its homologs undergo small conformational changes in the interior of the protein exposing the TonB box. Following recognition by the energized TonB, the monomeric TonB CTD binds the TonB box transferring the kinetic energy of rotation (Klebba, 2016) that potentially catalyzes the partial unfolding of the N-domain of LGPs. These conformational changes within the N-domain must be able to open a channel within the β-barrel allowing tight ligand passage.

Chapter 4: Role of peptidoglycan in TonB-dependent transport of Ferric enterobactin by FepA

4.1 Introduction

Originally described in the context of resistance of *E. coli B* towards phage T1, the TonB (T-one resistance) protein is concomitantly tied to the transport kinetics of metals (Fe^{3+}, Co^{2+}, Mn^{2+}, Zn^{2+}) in Gram negative bacteria. In 1971, it was shown that attachment of T1 phage to *E. coli* is dependent on TonA (FhuA) and TonB and occurs only in energized cells (Wang and Newton, 1971). This suggested a functional relationship between FhuA and TonB (Luckey et al., 1975). Later, the source of the energy was shown to be the electrochemical potential of the cytoplasmic membrane thereby, tying TonB to the energized cytoplasmic membrane (Bassford et al., 1976; Bradbeer 1993). Since the OM lacks an energy source, TonB is implicated in the flux of energy from the IM to the OM required for the irreversible adsorption of phage T1 or transport of Ferrichrome through FhuA. Subsequently, ExbB and ExbD proteins were also shown to be required by TonB to harness the *pmf* of the cytoplasmic membrane (Bradbeer, 1993) for transport of various ferric-siderophores, Vitamin B12, infection by phages T1 and Φ80, and transport of some toxic bacterial colicins (Cao & Klebba, 2002).

The structure of the 239 amino acid TonB protein, constructed from NMR descriptions of its rigid central domain (Evans et al., 1986), bioinformatic predictions about its helical N-terminal domain (NTD) (Klebba et al., 1993) and crystal structure of its C-terminal domain (CTD) (Pawelek et al. 2006), reveal a periplasm spanning, tripartite arrangement. Combined with other findings, the TonB NTD is thought to associate with oligomeric ExbB

and ExbD proteins within the IM. The rigid central pro-lys rich rod like part bridges the Gram-negative periplasm to place the CTD at the underside of the OM bilayer. When metal transporters (LGPs) in the OM bind ferric-siderophores, large conformational changes occur in the proteins that lead to high affinity receptor-ligand interactions and also relocate the N-terminal TonB box sequence of the proteins to the interior of their C-terminal β-barrel structure. X-ray crystallographic studies as well as solution structures demonstrated interaction of the TonB box of LGPs with CTD of TonB (Pawelek et al., 2006; Peacock et al., 2005). However, the mechanism by which TonB transduces the energy derived from *pmf* in the IM to the LGPs in the OM to bring about siderophore transport is not clearly understood.

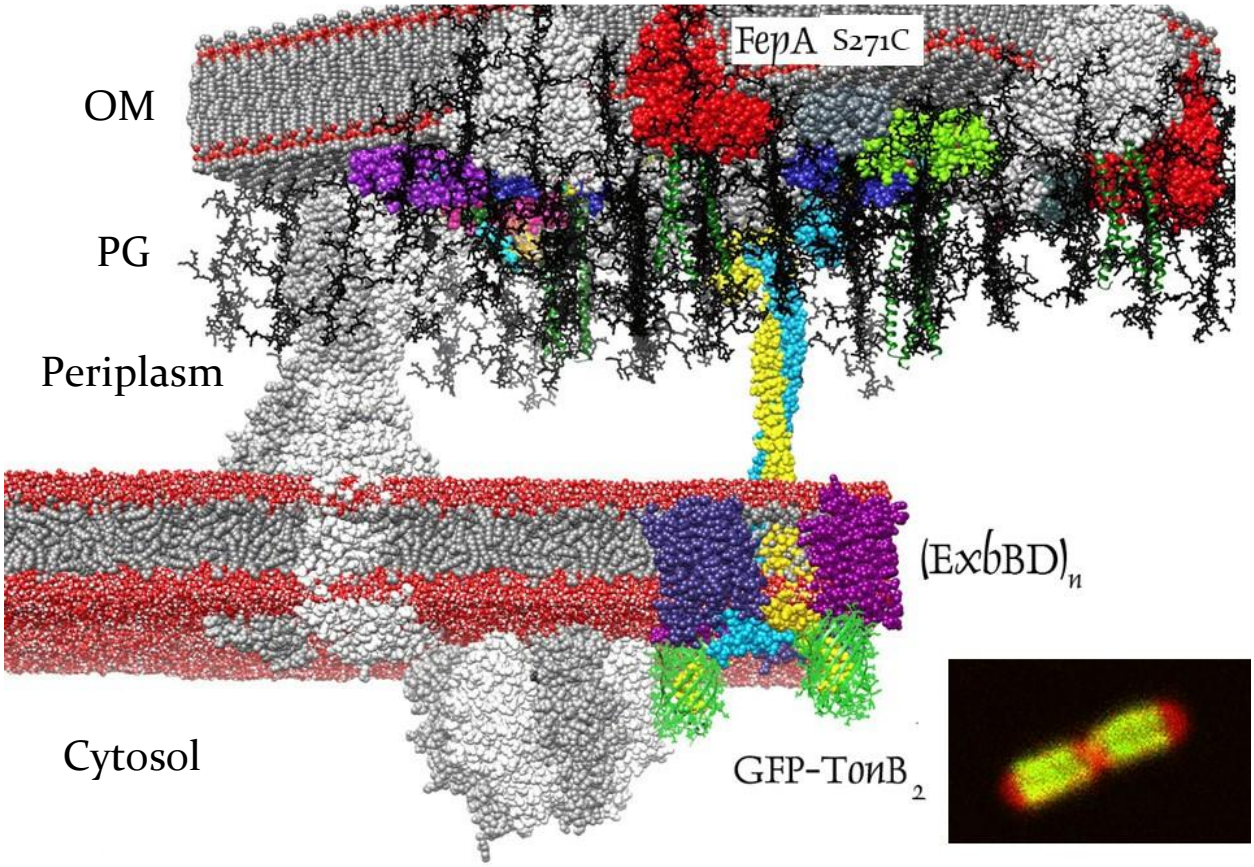

Fig. 4-1: Schematic representation of the Gram negative cell envelope depicting the outer membrane (OM), periplasm, inner membrane (IM) and cytosol. The OM and IM are represented in the frozen bilayer format. The peptidoglycan (PG) network (black) underlies the OM. Different OM β-barrels including FepA (green) are etched in the OM in red, green, gray. The N-terminal domain of the TonB dimer (yellow and cyan) are embedded in the multimeric ExbBD complex (purple and blue) whereas the flexible central domain spans the periplasm and the C-terminal domain associates with PG. The GFP β-barrels of the GFP-TonB fusion (Kaserer et al., 2008) are attached to the N-terminus of TonB. The inset shows the microscopic localization of FepAS271C labeled with A546M throughout the *E. coli* cell and GFP-TonB restricted to the center. Molecular graphics were created by the UCSF Chimera package.

The fractionation pattern of TonB in sucrose-gradient centrifugation led to the postulation of the primary “shuttle hypothesis”. It suggested that TonB shuttles between the IM and the OM upon energization by the *pmf* harnessed by ExbBD. The NTD extricates from the IM when the CTD contacts the OM proteins like Lpp, OmpA. Once it encounters ligand bound LGPs, the conformationally stored energy is discharged, and TonB returns to the IM (Letin and Postle, 1987). However, the thermodynamic feasibility of the postulated extrication of TonB from IM is questionable and ultimately led to the death of the hypothesis. Recent observations of GFP-TonB fusion proteins, the general affinity of TonB for peptidoglycan, and the rapid physical motion of TonB driven by pmf led to the proposition of the Rotational Surveillance and Energy Transfer (ROSET) model of TonB action (Kaserer et al., 2008; Klebba 2016).

Experiments with purified TonB CTD showed a general affinity of the C-terminal 69 residues for OM proteins such as OmpA, lysozyme, but also specific affinity for OM LGPs like FepA (Kaserer et al., 2008). However, this specific affinity was not dependent on the

TonB box residues. The TonB CTD showed sequence similarity to a class of periplasmic proteins, typified by LdtC (previously YcsF), containing PG binding domains. Like TonB, these proteins are potentially IM-anchored and have a central Pro-rich region and a Lys-rich motif (LysM) that confers them affinity towards PG (Leo et al., 2015; Maxwell et al., 2013). TonB CTD also contains LysM domains and particularly the dimer superimposes with 4 LysM polypeptides containing two potential PG binding sites on each monomer. Pull-down experiments of the TonB CTD with increasing concentrations of purified murine sacculus confirmed the affinity of the TonB CTD for the PG layer. By virtue of this affinity, TonB assumes an extended structure and is potentially positioned underneath the OM while interacting with the OM proteins. The PG layer possibly acts as a matrix where the IM and OM proteins can interact (Klebba, 2016). Interestingly, the VS model of PG architecture makes such interactions theoretically easier. In this model, the PG layer forms ~60Å honey-comb like cells which is roughly the size of the β-barrels of many OM porins including LGPs as well as TonB CTD dimer (Meroueh et al., 2006, Artola-Recolons et al. 2011; Park et al.,2012).

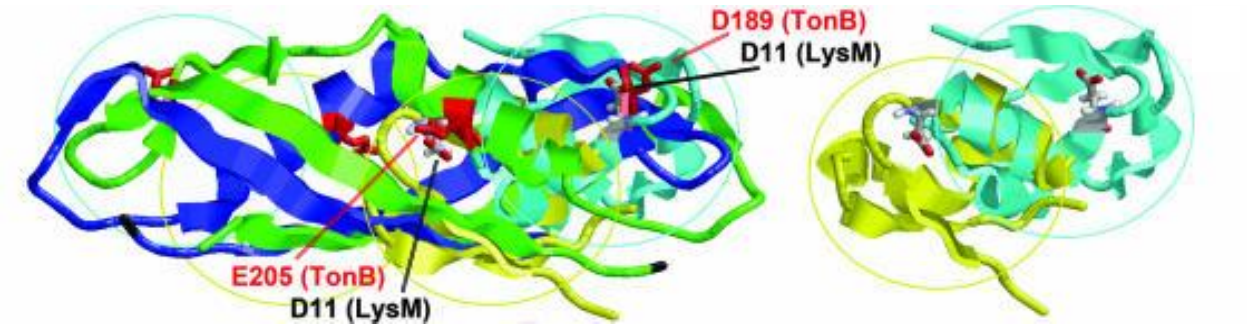

Fig. 4-2: Kaserer WA, Jiang X, Xiao Q, Scott DC, Bauler M, Copeland D, Newton SM, Klebba PE. 2008. Insight from TonB hybrid proteins into the mechanism of iron transport through the outer

membrane. J Bacteriol 190:4001–4016. doi:10.1128/JB.00135-08. Four LysM motifs in the TonB dimer. Reprinted in part with permission from American Society of Microbiology.

Fusion constructs of TonB downstream of GFP under control of the Fur-regulated TonB promoter (pGT) expressed both proteins in OKN3 ($fepA^+$ $tonB^-$) and were fluorescent with WT levels of TonB activity. The fusion protein showed membrane-bound fluorescence compared to cytosolic GFP, disproving the idea of TonB dislodging from the membrane (Kaserer et al, 2003). FepA with Cys substitution of S271, labeled with Alexa Fluor maleimides and co-expressed with the pGT plasmid, revealed far less number of TonBs per cell compared to FepAs which corresponded with biochemical findings. Surprisingly, it also showed restrictions on TonB localization close to the poles of cells (Jordan et al., 2013). Although, this raises questions on how physical interactions occur between FepA and TonB molecules in all parts of the cell, cell morphology and variable density of the PG layer at the poles seem to be playing a role on distribution of TonB.

Anisotropic measurements of GFP-TonB fusion protein, suggested that TonB undergoes motion coupled to the electrochemical proton flow across ExbBD (Jordan et al, 2013). The time-frame of transition of the fluorescent GFP-TonB molecule in the anisotropic experiments, indicated that the motion is likely rotation. Primary structural homology of ExbBD to the MotAB complex also suggests analogous movement of the TonB-ExbBD complex. In the flagellar assembly, the MotAB proteins and the filament behave like a stator and rotor of a motor assembly in response to downflow of protons by MotAB, such that the two elements rotate in opposite directions upon energization (Kojima and Blair, 2001). In the context of TonB-ExbBD, this rotational motion will also bring about lateral movement of the complex within the fluid bilayer at rates determined by the frictional

resistance with the murein layer from the transient interactions of TonB as well as ExbB and ExbD with PG (Lill et al.,2016). This may allow TonB-ExbBD to survey the underside of the PG layer for ligand bound OM proteins docked on the honeycomb cells of the murein sacculus. Taken together, these findings suggest a mechanism for TonB action. By virtue of the affinity for PG, the TonB C-terminal dimer localizes at the periplasmic interface of the OM, where driven by the *pmf*, TonB-ExbBD undergoes rotational motion and also moves laterally while surveilling the underside of the OM bilayer until it encounters the exposed TonB-box of the LGPs. High- affinity of the CTD monomers for TonB box allows interaction of the LGP and TonB and the kinetic energy of TonB rotation is transferred to the OM protein, triggering conformational changes in the protein interior that allows internalization of the bound ligand. Germane to this concept is the structure and organization of the PG in the cell envelope since, the TonB-EXbBD proteins physically associate with it. Although the VS array of PG is less restrictive than PN for movement of TonB, both models potentially accommodate TonB's rotation in association with PG. Hence, irrespective of its arrangement fashion, the murein layer is proposedly an essential component of the ROSET model. The PG layer may also be responsible for the localized distribution of TonB.

This work investigates the relationship of the TonB CTD with the PG layer in the context of uptake of metal ligands through OM proteins. By strategically degrading the *E. coli* murein sacculus *in vivo*, we observe its effect on cell morphology, uptake of the *E. coli* siderophore FeEnt by its cognate receptor FepA, as well as study the distribution of FepA and TonB in live cells devoid of PG. These novel experiments will potentially characterize the periplasmic biochemistry in living cells, which is crucial for TonB-dependent systems.

4.2 Methods

4.2.1 Transformation and expression of SAR Endolysins in *E. coli*

To degrade PG in live cells of *E. coli*, we used SAR endolysins from three different phages (Table 4-1, Fig.), encoded in plasmids to transform the prototype *E. coli* K-12 strain MG1655 or its derivatives and the lab strain BN1071. The plasmids as well as the vectors were gifted by Dr. Ryland Young of Texas A&M University.

Table 4-1: SAR endolysin plasmids used in the study.

Plasmid	Vector	Gene and Source Phage	Reference
pJFLyz	pJF118EH high-copy, amp^+, ColE1, p_{tac}	P1Lyz; phage P1	Xu et al., Science 2005
pZE-R21	pZE12 medium copy, amp^+, ColE1, $p_{Ltac\ 0\text{-}1}$	R21; phage 21	Sun et al., Nat Struct Mol Biol 2009
$pLyz_{103}$	pJF118EH	Lyz_{103}; Erwinia phage ERA 103	Kuty et al., J. Bacteriol 2010.

We used cells treated with CaCl2 for transformation using standard heat shock procedure. We selected transformants on LB plates containing Ampicillin and Streptomycin. Sometimes, we added 0.2% Glucose to the agar to arrest leaky expression from pJFLyz plasmids. We harvested colonies between 12-14 hours and purified them by re-streaking on to fresh plates. To prepare frozen stocks, we scrapped cells from the plates with a sterile spatula, resuspended cells in a small volume of LB with 10% glycerol making sure that the cell turbidity reached that of fully-grown cultures. We froze small aliquots of this resuspension and used one aliquot for each experiment. We thereby avoided repeated freeze-thaw cycles of the frozen stock and mimicked use of fresh

transformant for each experiment. We grew overnight cultures in LB broth (Amp^+, $Strep^+$ and 30mM $MgSO_4$) at 37ºC with shaking.

4.2.2 Preparation of Spheroplasts

To induce iron starvation conditions, we sub-cultured in either 1X MOPS minimal medium supplemented with 0.4% Sodium succinate and micronutrients or Nutrient Broth with addition of 0.1 mM apo-FerrichromeA once cells reached an OD600nm of 0.1. We inoculated with 3% overnight cultures in media containing appropriate antibiotics and 30mM $MgSO_4$ and grew them until they reached an OD600nm of 0.5. At this point, we added IPTG to a final concentration of 0.1-0.5mM and continued to grow with shaking. Spheroplast formation initiated around 1.5-2 hours after the addition of IPTG which we followed microscopically by visible transitioning of cells from rods to round morphology. Spectroscopically, spheroplast formation was indicated by a drop in OD600 values which stayed stable over time unless lysis of spheroplasts occurred. By 4-5 hours we obtained greater than 90% spheroplast formation.

For iron and lactose uptake experiments, we harvested the spheroplasts by centrifugation at 4,500 rpm for 12 minutes and discarded the supernatant carefully. Then we gently resuspended the pelleted spheroplasts in 0.1M Potassium phosphate buffer (KPi) [K_2HPO_4/KH_2PO_4] at pH 7.4 with 8% polyethylene glycol 6000 (PEG-6000) and 30mM $MgSO_4$. This recipe provides iso-osmolar conditions for spheroplasts which remain viable upto 8 hours as determined by spectroscopic measurements.

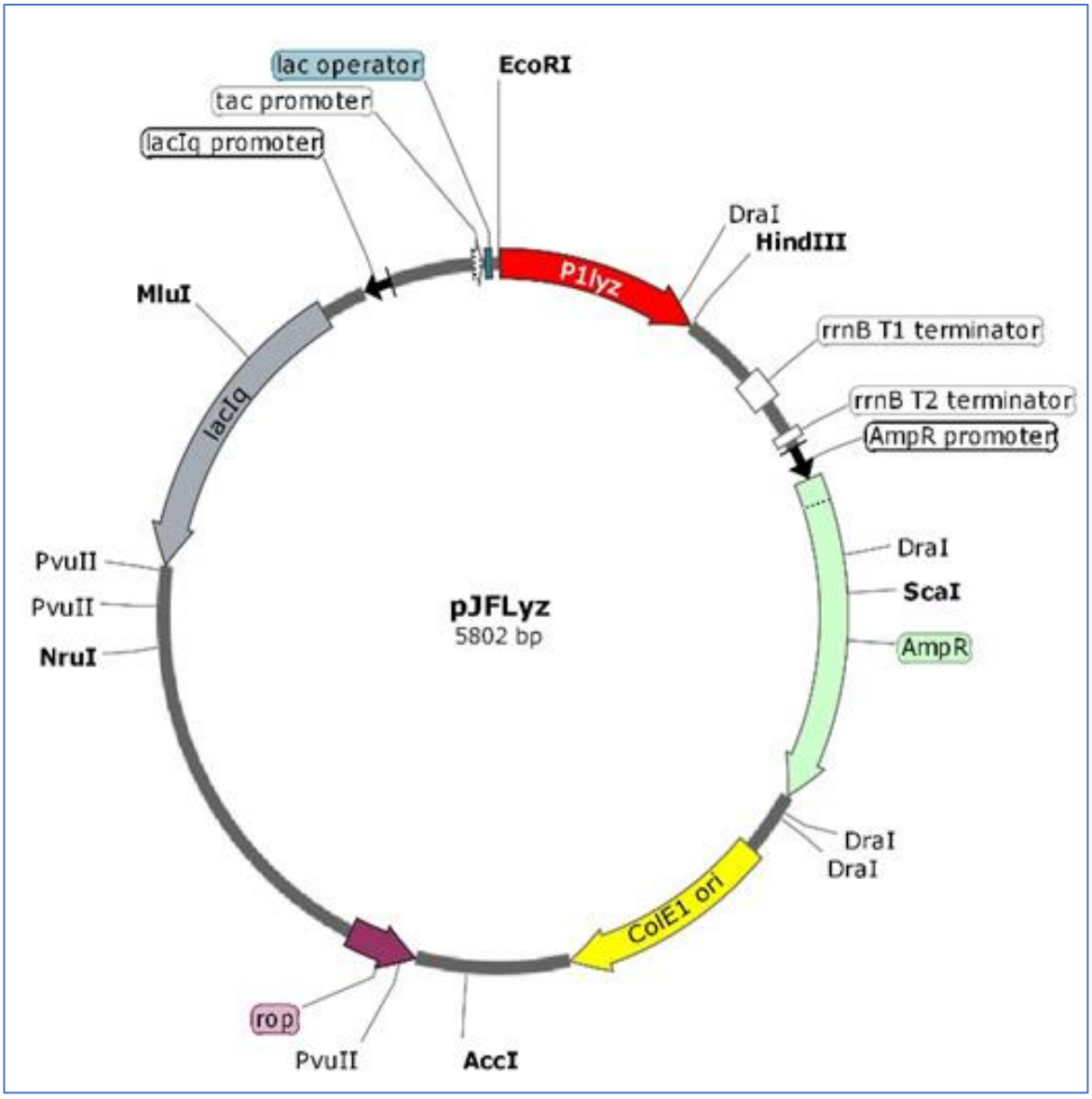

Fig. 4-3: Plasmid map of pJFLyz (P1Lyz endolysin cloned into pJF118EH using EcoRI and HindIII restriction sites) under control of p_{tac}, created by SnapGene Viewer.

4.2.3 Expression of FepA in spheroplasts

We compared the expression of FepA in spheroplasts with that of whole cells by performing [^{125}I]-PrA immunoblots with anti-FepA Mab 41+45 after running SDS-PAGE gels prepared by the Laemmli recipe of OM vesicles. We spectrophotometrically assessed the amount of protein in each sample and loaded equivalent concentrations in each well.

4.2.4 Siderophore Nutrition tests

We performed Siderophore nutrition tests as described before (Materials and methods), after subculturing strains in NB with appropriate antibiotic and $MgSO_4$. We induced spheroplast formation with addition of 0.5mM IPTG at around an OD600nm of 0.6 and directly added 50µL of the cultures in 3mL molten NB top agar containing apo-FcA, 30mM $MgSO_4$ and antibiotics. In certain cases, we added 0.1mM IPTG to the agar. We observed formation of halo around discs after 12-14 hours.

4.2.5 Uptake of [^{59}Fe]Ent and [^{14}C]lactose

To perform radionucleide uptake assays, we sub-cultured strains in 15mL MOPS or NB media with apo-FcA, grew them to OD600 of 0.5, and then added 0.1mM IPTG to induce spheroplast formation. We harvested the cells by centrifugation and resuspended them in appropriate volume of 0.1mM KPi buffer with 8% PEG-6000 and 30mM $MgSO_4$ to concentrate all strains to OD_6 of 10. For [^{59}Fe]Ent accumulation assay, we diluted the strains by 1/10 and measured accumulation of [^{59}Fe]Ent over 30 minutes at different time points in triplicate, as described previously. We counted the radioactivity accumulated by cells and spheroplasts and plotted pmol of ^{59}FeEnt/10^9 cells vs time using GraFit 6.0.

For [^{14}C]lactose accumulation assay, we added the radio-labeled substrate to a final concentration of 10mM at time 0 seconds to aliquots of OD600nm 10.0 cells in tubes maintained at 37ºC in a water bath. We filtered 50µL aliquots of the cells in triplicate at 5 seconds and washed the filters with 3mL of ice-cold mixture of 0.1M KPi buffer (pH 5.5) and 0.1M LiCl. Similarly, we collected cells at 60, 120 and 300 seconds. After drying of filters, we added scintillation fluid and counted the radioactivity accumulated in a Perkin Elmer Scintillation Counter. We converted the counts/minute (CPM) into pmoles of [^{14}C]lactose/10^9 cells and plotted them vs time using GraFit 6.0.

4.2.6 Live cell count assay

We performed modified plate count assay to determine the number of live spheroplasts over time. Since, spheroplasts do not thrive well on hard agar, we used 0.7% soft LB agar. To perform the assay, we serially diluted the strains in the KPi iso-osmolar buffer and mixed 300µL of cells in 3mL of molten LB top agar cooled to 40ºC, containing 30mM $MgSO_4$. We plated the mixture in 6 well plates and incubated overnight at 37ºC. We counted the number of colonies appearing on the surface and within the agar and obtained the approximate number of live cells in the stock by multiplying with the dilution factor.

4.2.7 MacConkey lactose utilization assay

To identify whether spheroplasts are capable of normal lactose utilization, we serially diluted them and mixed appropriate dilutions with 15mL molten MacConkey 0.7% top agar with $MgSO_4$ and grew overnight at 37ºC. After incubation we observed the color of the colonies under a colony counter inverted microscope (Nikon Inc. USA) under 40X magnification.

4.2.8 Epifluorescence microscopy

In order to make FepA and TonB fluorescent, we needed to co-express both proteins from a single plasmid that can be co-transformed with the pJF118EH plasmids. Hence, we PCR amplified *fepA* gene along with its native promoter from the plasmid pITS23A698C and cloned the fragment downstream of the amplified pGT plasmid (containing EGFP and TonB expressed as a fusion protein under the iron regulated TonB promoter). We used the Gibson assembly method to fuse both fragments to create the plasmid, pGTFA698C (Fig. 4-4A). After sequence verification, we expressed pGTFA698C along with pJF118EH or pJFLyz in the strain KNK013 (Δ*entA*, Δ*fepA*, Δ*tonB*).

To label FepAA698C with Alexa Fluor maleimides (Thermo Fischer Scientific, USA), we used a scaled down version of the labeling protocol discussed before. We started with small volume (1-2mL) cultures for labeling and adjusted buffer volumes accordingly. For whole cells, we used fully grown MOPS or NB cultures but, for spheroplasts, we labeled before induction with IPTG as they are too delicate multiple centrifugation steps of the labeling protocol. Labeling and washing buffers for spheroplasts additionally contained 30mM $MgSO_4$. After washing of the uninduced labeled pJFLyz strains, we resuspended them in NB/MOPS supplemented with antibiotics and Mg^{2+}. We allowed the strain to recuperate for 10-15 minutes at 37ºC and then added IPTG to allow induction of endolysin.

4.2.9 iPALM/dSTORM

Interferometric Photoactivatable Localization Microscopy/Stochastic Optical Reconstruction Microscopy (iPALM/dSTORM) offers super resolution of molecules down to 1-2nm. The principle is based on the use of photoactivatable or photoconvertible

fluorophores that allows resolution of spatial differences in dense population of molecules (http://zeiss-campus.magnet.fsu.edu/). Therefore, to observe FepA and TonB molecules at single molecule resolutions, we used the photoactivatable fluorophore Alexa Fluor-647 maleimide to FepAA698C expressed from the plasmid pETFA698C (Fig. 4-4B). The plasmid also contains TonB fused at its N-terminal to the photoconvertible protein mEos 3.2 (Zhang et al., 2012). To construct pETFA698C, we amplified the *mEos 3.2* gene from the plasmid mEos 3.2-N1 (gift from Michael Davidson [ADDGENE plasmid #54525]) and cloned it with the amplified pTF (TonB and FepA under natural promoters in vector pHSG575) plasmid.

We subcultured KNK013/pETFA698C in MOPS grew the cultures for 12-14 hours at 37ºC with shaking. We harvested 2 mL culture and prepared for labeling in labeling buffer with 10 μM A647M at 37ºC in water bath for 15 minutes. Following labeling we quenched any unbound fluorophore with 1.3 mM βME then spun down and washed with 1X PBS. We finally resuspended the cells in ~1.8 mL 1X PBS with 0.4% Glucose. For KNK013/pETFA698C/pJFLyz we grew the cells in MOPS up to OD600 0.6 and labeled 2 mL of the culture in the same manner as whole cells and resuspended back in MOPS supplemented with requisite antibiotics and other nutrients. Then we induced the cells with 0.1 mM IPTG and allowed them to form spheroplasts.

We carefully took the iPALM coverslips and put each in a well of a 6 well plate in a fashion that the gold fiduciary beads were facing upwards. We then washed the coverslips with 1N KOH for 2 minutes. We washed the coverslips thoroughly with double distilled water and let them dry as much as possible. From a 1/100 dilution in double distilled water of poly-L-Lysine hydrochloride (Thermo Scientific, USA) from a stock of 10

mg/mL, we added requisite amounts of the poly-L-Lys to the air-dried coverslip to completely submerge it and incubated for 20 minutes. Following incubation, we drained out the poly-L-Lys, washed with 1X PBS and allowed it to air-dry. Next, we added 40 µL of labelled cells (either whole or spheroplast) and incubated at 37ºC for 5 minutes. We secured the lid of the plate and spun it down at 2500 rpm for 10 minutes. For fixation, we flooded the well with freshly prepared 2% para-formaldehyde and let it stand for 10 minutes, following which, we thoroughly washed the coverslip twice with 1X PBS. After the wash, we put the STORM buffer and mounted a smaller coverslip on top of it and sealed the edges with Vaseline. In case of experiments in presence of FeEnt, we added FeEnt to a final concentration of 5 µM to the cultures and incubated for 10 minutes prior to addition to the coverslip and the rest was as described previously.

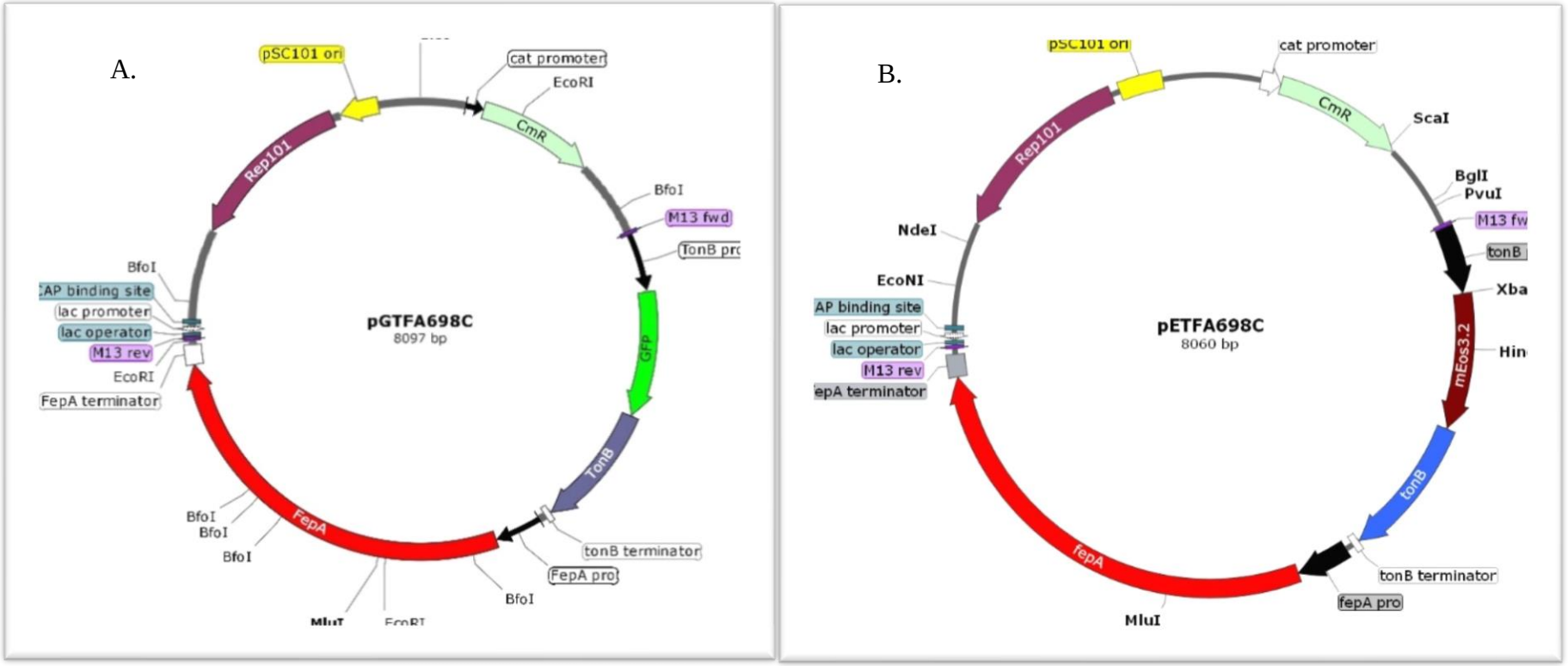

Fig. 4-4: A) pGTFA698C plasmid (8097 bp) containing GFP-TonB fusion under native *E. coli* TonB promoter and FepA with A698C substitution under native FepA promoter. B) pETFA698C plasmid (8060 bp) encoding mEos3.2-TonB fusion and FepAA698C.

4.3 Results

4.3.1 Siderophore nutrition test with cells expressing SAR endolysins

We expressed the plasmids encoding the three SAR endolysin genes that selectively degrade the bacterial murein sacculus in two *E. coli* strains KNK00 and BN1071. We tested the effect of the degradation of PG on uptake of FeEnt by FepA and Fc by FhuA in preliminary siderophore nutrition tests. We subcultured the cells in NB and induced the plasmids with 0.5mM IPTG. We also prepared IPTG negative controls. Once induced, we performed siderophore nutrition test with variation in test conditions such as: 0 mM IPTG (no induction; control), 0.5 mM IPTG and 0.5 mM IPTG along with 0.1 mM IPTG in agar. After overnight incubation, for both FeEnt and Fc utilization some induced strains showed diffuse halos with larger diameter than uninduced controls. In KNK00 strain, less intense halos indicating reduced siderophore transport appeared in the case of the endolysins P1Lyz and R21. In BN1071 derivatives, changes in the nature of the halos were observed only with plasmid pZE-R21. The effect appeared to be more pronounced when the inducing agent was added in the agar as well. The results seen with KNK00/pJFLyz in Fc uptake were replicated in tests with FeEnt (Fig: 4-5). The least or no effect was seen with Lyz_{103}.

Assay with Ferrichrome **Assay with Ferric enterobactin**

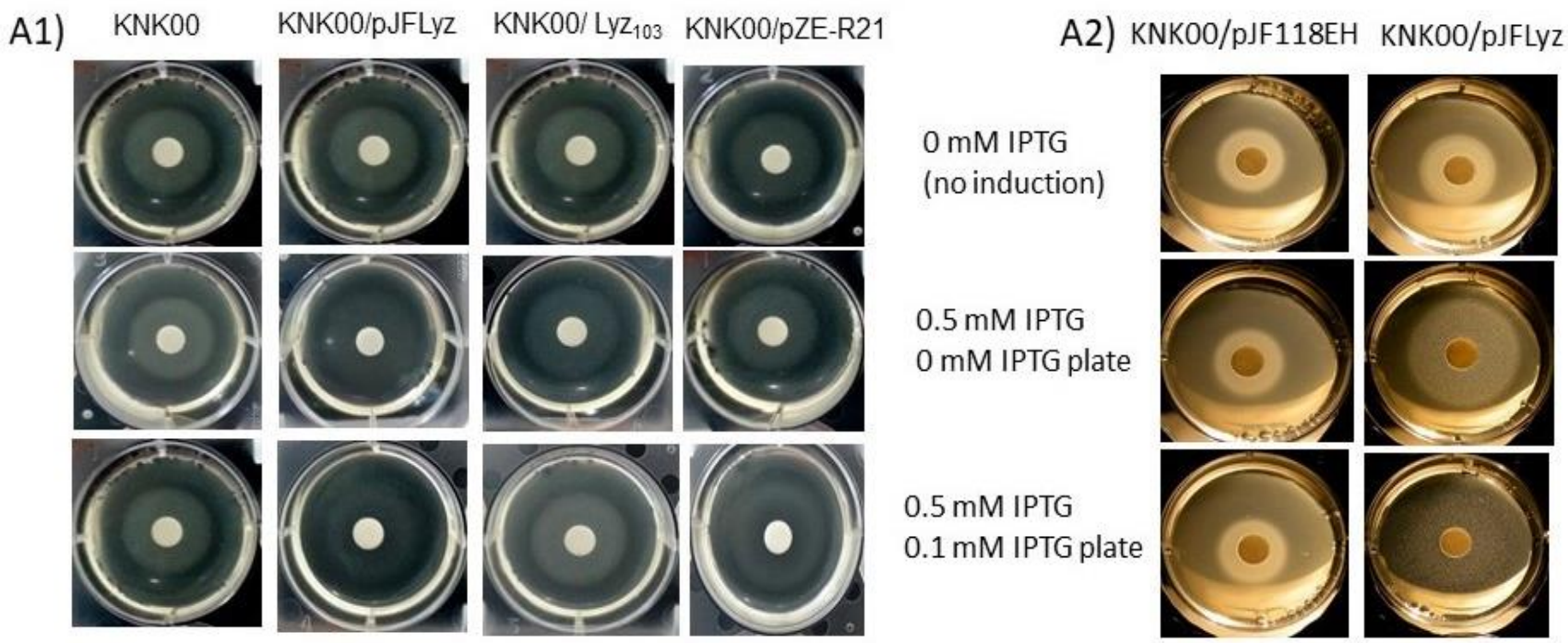

Fig. 4-5

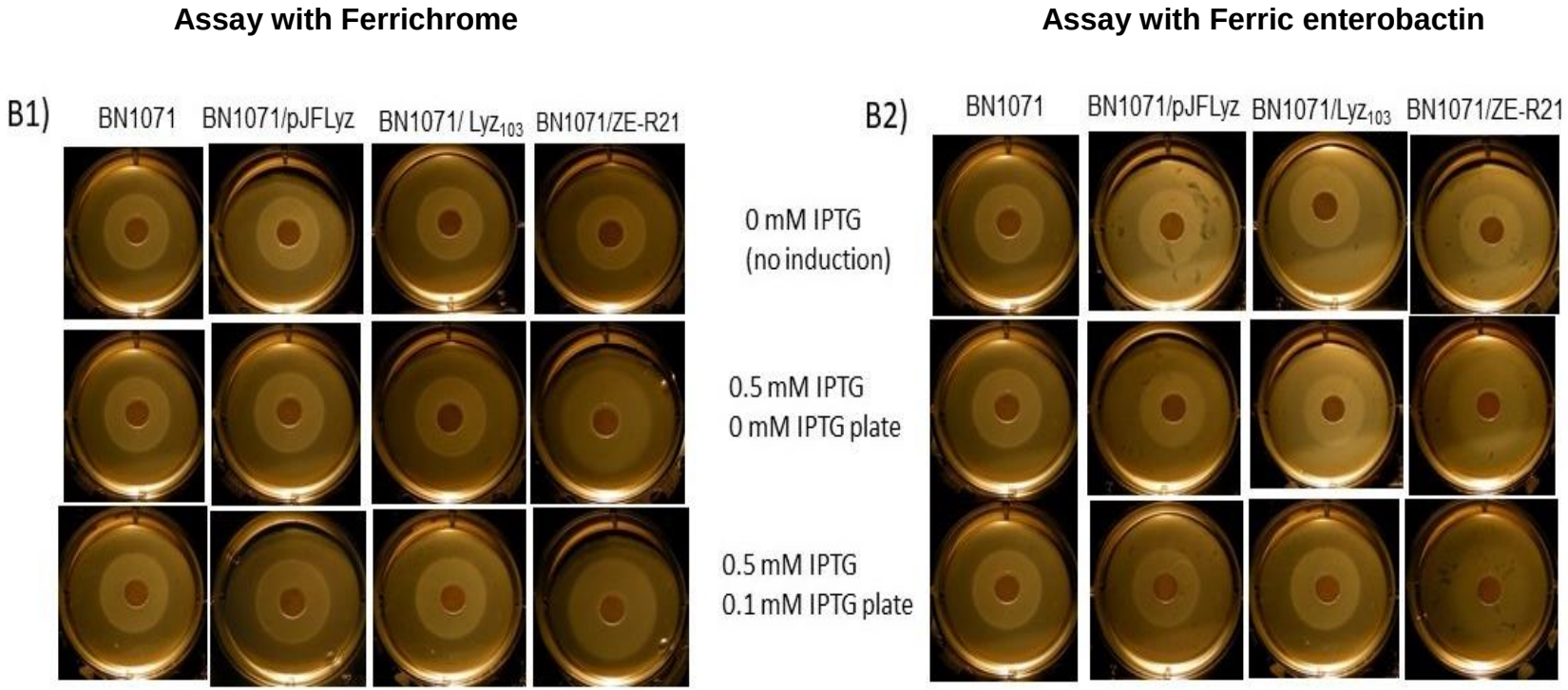

Fig. 4-5: Siderophore nutrition tests with Ferric ferrichrome (A1 & B1) and Ferric enterobactin (A2 & B2). KNK00 and BN1071 host strains harboring different SAR endolysin plasmids were subcultured in NB and induced with 0.5 mM IPTG at mid-log. 50 µL of cells were then mixed with molten top agar containing apo-ferrichromeA as the iron-chelating agent and plated. 0.1 mM IPTG was added to the agar in some cases. Siderophores at final concentration of 50 µM were then placed on the filter discs on the solidified agar surface. Panel A1 shows halos obtained for KNK00 strains alone (control) or containing the three different plasmids; A2 shows KNK00 containing the empty vector pJF118EH and the P1Lyz expressing plasmid pJFLyz. Panel B1 and B2 show the BN1071 strain alone or harboring the three plasmids.

4.3.2 Survival and stability of spheroplasts

Isotonicity of the suspension medium is critical for maintaining stable spheroplasts since they lack the structural framework and stability provided by the murein network. We attempted to record the stability and survival of the spheroplasts over time. We studied the growth of KNK05/pJFLyz in NB constituted with antibiotics, Mg^{2+} and apo-FcA without IPTG and with 0.1 mM and 0.5 mM IPTG. We also compared the growth with KNK05/pJF118EH as well as the KNK05 strain. The growth curve showed the time course of spheroplast formation (Fig. 4-6A). We also counted the number of bacilli vs cocci in the induced cultures at the same time points as collecting OD600 values (Fig. 4-6B). Transition of rods into round spheroplasts occurred around 2 hours after induction which also reflected in the OD600 values by drop in the turbidity of the culture. Once spheroplast formation commenced the culture barely grew further, whereas the uninduced controls grew normally. Number of live cells/mL calculated from the colonies obtained on soft agar was always 40-60% of the cell number calculated from absorption measurements at 600 nm. It showed some variability over the two repeats of the experiment, especially at approximately 3.5 hours, but had similar trends on both days. This variability led to the large SD as seen in Fig. 4-6C. In general, the cultures stayed viable for long periods, even after spheroplast formation was complete, with greater stability in the culture induced with 0.1 mM IPTG. Although, lower concentration of IPTG appears to produce a longer half time of spheroplast formation, it probably allows a gentler transition leading to larger number of viable colonies.

A

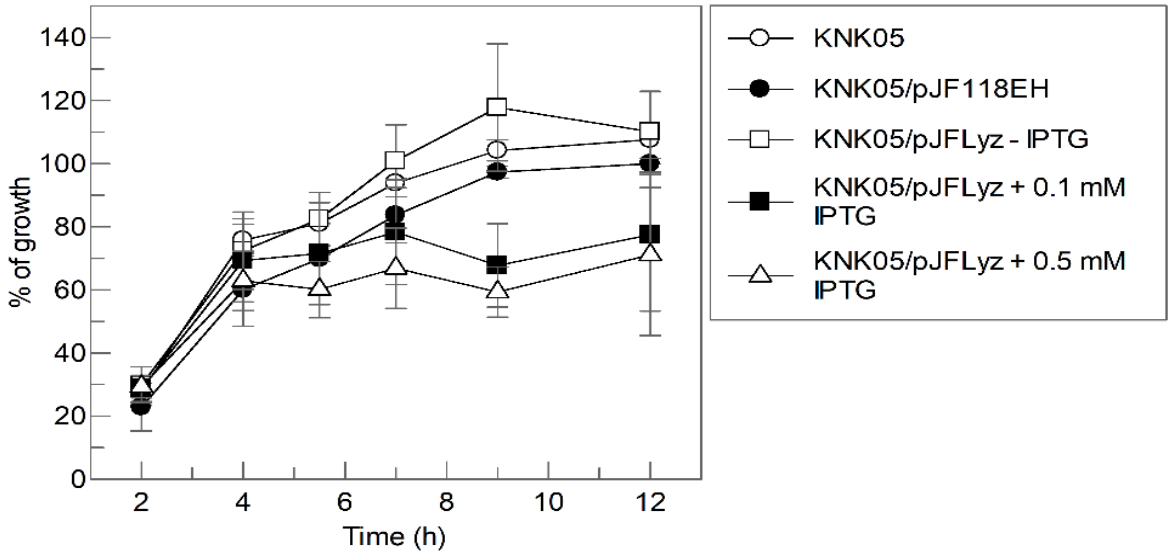
% of growth
140
120
100
80
60
40
20
0
2
4
6
8
10
12
Time (h)
KNK05
KNK05/pJF118EH
KNK05/pJFLyz - IPTG
KNK05/pJFLyz + 0.1 mM IPTG
KNK05/pJFLyz + 0.5 mM IPTG

B

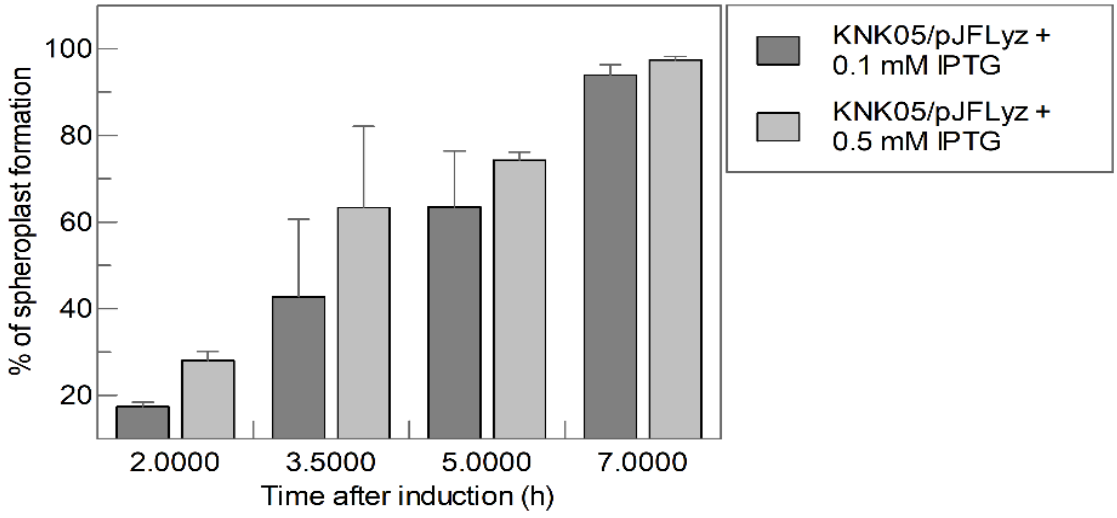
% of spheroplast formation
100
80
60
40
20
2.0000
3.5000
5.0000
7.0000
Time after induction (h)
KNK05/pJFLyz + 0.1 mM IPTG
KNK05/pJFLyz + 0.5 mM IPTG

C

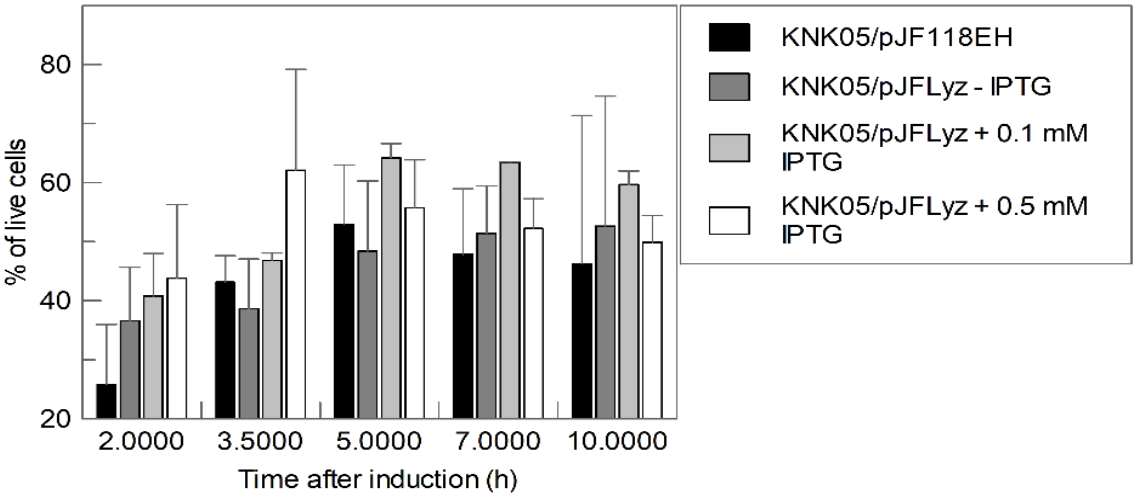
% of live cells
80
60
40
20
2.0000
3.5000
5.0000
7.0000
10.0000
Time after induction (h)
KNK05/pJF118EH
KNK05/pJFLyz - IPTG
KNK05/pJFLyz + 0.1 mM IPTG
KNK05/pJFLyz + 0.5 mM IPTG

Fig. 4-6: Growth, percentage of spheroplast formation and survival of spheroplasts. A) OD600 values obtained spectrophotometrically for the different strains at different time intervals were converted into percentage of growth occurring with respect to the KNK05 host strain. Arrow mark indicates the time point of IPTG addition. B) Percentage of spheroplast formation starting from 2 hours after addition of 0.1 or 0.5 mM IPTG were calculated by counting the number of round spheroplasts vs. rod cells at different time points. To calculate percentage, number of spheroplasts were divided by the total number of rod and round cells and multiplied by 100. A minimum of 6 fields were counted for each time point. C) Number of colonies obtained were divided by the number of cells predicted by OD600 values to calculate percentage of live cells at different time points 2 hours after induction with IPTG. All data are average of results obtained from 2 experiments.

We prepared OM vesicles of KNK00 cells expressing either pJF118EH or pJFLyz grown in NB with apo-FcA or in MOPS minimal medium. We harvested cells and spheroplasts, lysed them in French Press and extracted OM using 0.5% Sarkosyl. We loaded equivalent concentrations in SDS-PAGE gel and prepared an [^{125}I] immunoblot with anti-FepA to check the FepA expression in cells devoid of PG. The spheroplasts showed comparable expression levels to the KNK00/pJF118EH strain as well as KNK00 alone in both media (Fig. 4-7). This showed that the spheropalsts obtained by degradation of PG were not only stable, protein expression and transport to OM were unaffected in such conditions.

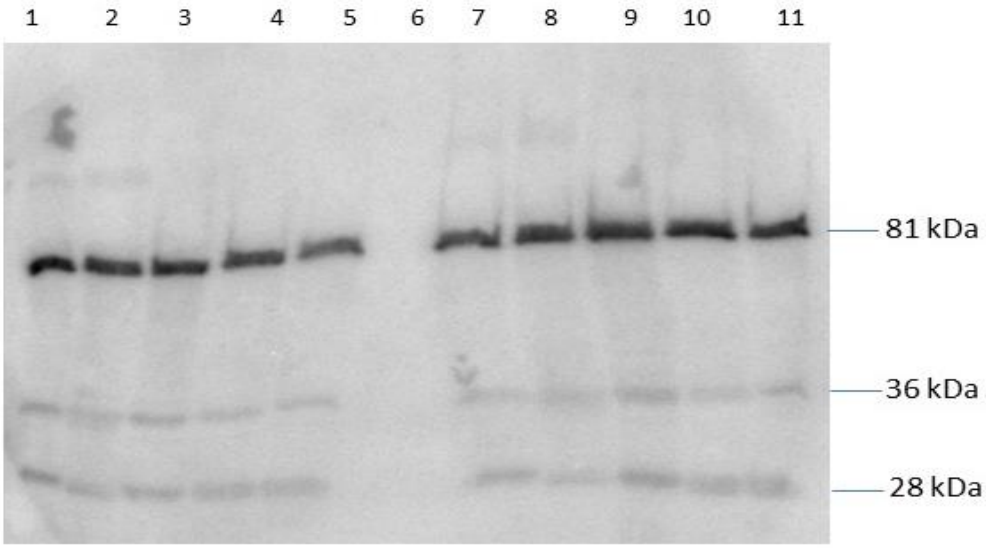

Fig. 4-7: [^{125}I]-ProteinA immunoblot showing expression of FepA in whole cells and spheroplasts of P1Lyz. Lanes 1-5 were from cells grown in NB with apo-FcA and lanes 7-11 were from cells grown in MOPS. Lane 6 contained the MW marker. Lanes 1&7 – KNK00, lanes 2&8 – KNK00/pJF118EH, lanes 3&9 – KNK00/pJFLyz – IPTG (no induction) lanes 4, 5 & 10, 11 – sample 1 and sample 2 of KNK00/pJFLyz + 0.5 mM IPTG respectively, prepared on 2 days.

Proper execution of the radionucleide uptake experiments required washing of the cells and spheroplasts out of the growth media containing the inducing agent and resuspension in an isotonic buffer. We studied the stability of the spheroplasts in three different buffers: a) 20 mM Tris-Cl (pH 5.5) with 0.1 M NaCl, b) 20 mM Tris-Cl (pH 8.0) with 0.3 M sucrose and c) 0.1 M KPi (pH 7.4) with 8% PEG-6000. All three buffers additionally contained 30 mM MgSO4. From the study of the OD600 values obtained over time, in the three different buffers tested, the buffer with NaCl as well as the KPi buffer with 8% PEG-6000 appeared to yield spheroplasts that remained stable over long periods . The sucrose containing buffer at pH:8.0 appeared to be less suitable. However, the low pH of the NaCl containing

buffer made it unsuitable for the [^{14}C]-lactose uptake assays. Hence, the KPi buffer was the best candidate which we named "Spheroplast Maintenance" (SM) buffer.

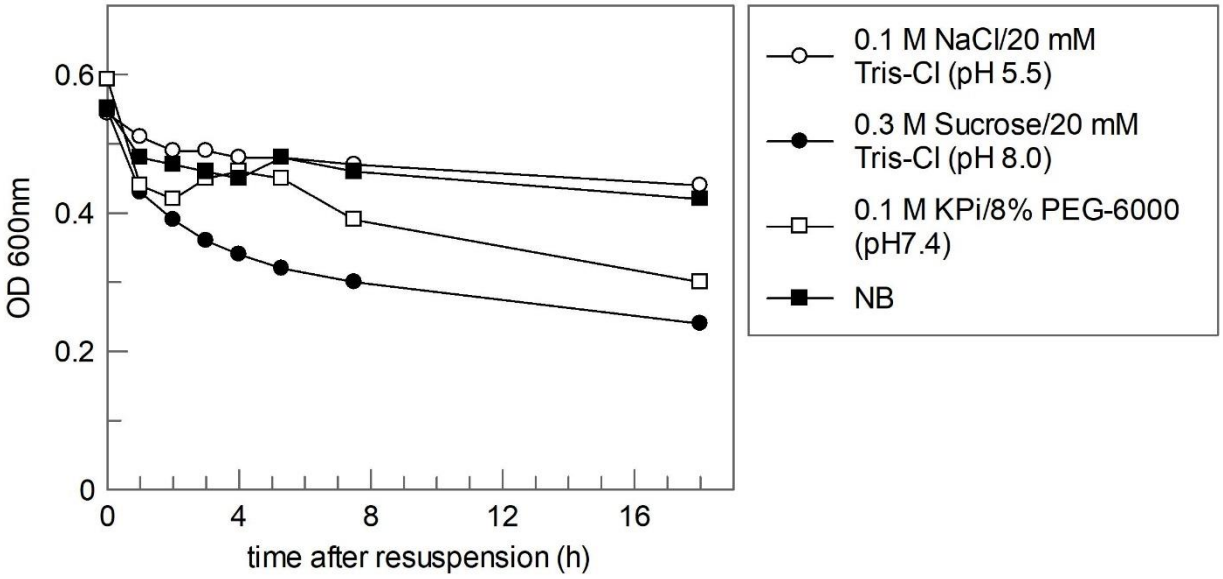

Fig. 4-8: Spectrophotometric observation of stability of spheroplasts of KNK05/pJFLyz in different resuspension medium. KNK05/pJFLyz cells subcultured in NB in different flasks were induced with 0.1 mM IPTG. Once >90% spheroplasts formed, cultures were spun down and resuspended gently in either NB or three different buffers a) 20 mM Tris-Cl (pH 5.5) with 0.1 M NaCl, b) 20 mM Tris-Cl (pH 8.0) with 0.3 M sucrose and c) 0.1 M KPi (pH 7.4) with 8% PEG-6000. OD600 values were obtained at regular time intervals over an 18-hour time-period.

4.3.3 Epifluorescence observation of FepA and TonB in spheroplasts

Previously, we had observed FepA S271C and GFP-TonB fusion proteins in intact *E. coli* cells by expressing them from two separate plasmids (pUC18/FepAS271C and pGT) (Jordan et al., 2013). Epifluorescence observation of the cells revealed, FepA molecules distributed throughout the OM, but GFP-TonB was mostly absent from the poles. We wanted to observe the localization of the proteins and the state of the membranes, once

the cells were depleted of the PG. First, we needed a plasmid that co-expresses the two proteins FepAA698C (A698C residue has greater fluorophore quantum yield than S271C) (Smallwood et al, 2014) and GFP-TonB. We engineered the plasmid pGTFA698C by Gibson cloning in the pHSG575 vector and co-transformed it with the pJFLyz plasmid into strain KNK013. Uninduced cells with intact PG, showed uniform distribution of FepA molecules throughout the cells after labeling with A546M, whereas, GFP-TonB were present only at the center of the cells, in agreement with what we had observed before. Once we induced the same strain to express P1Lyz by adding 0.1 mM IPTG, the cells gradually transitioned into spheroplasts. When we resuspended them in Kpi buffer with 30 mM MgSO4, the spheroplasts were round entities with FepA molecules lining the outer periphery and the IM colored green from the membrane-bound GFP-TonB encompassing the cytoplasm, were pushed to a side. Resuspension in SM buffer led to re-distribution of the cytoplasm throughout the cell and GFP-TonB was no longer restricted to the center of the cells. The juxta-position of the IM and OM suggested isotonic conditions of the medium (Fig. 4-9). The stability of the spheroplasts in this medium over a time-period suitable for further experiments enabled us to perform radionucleide uptake assays with these cells.

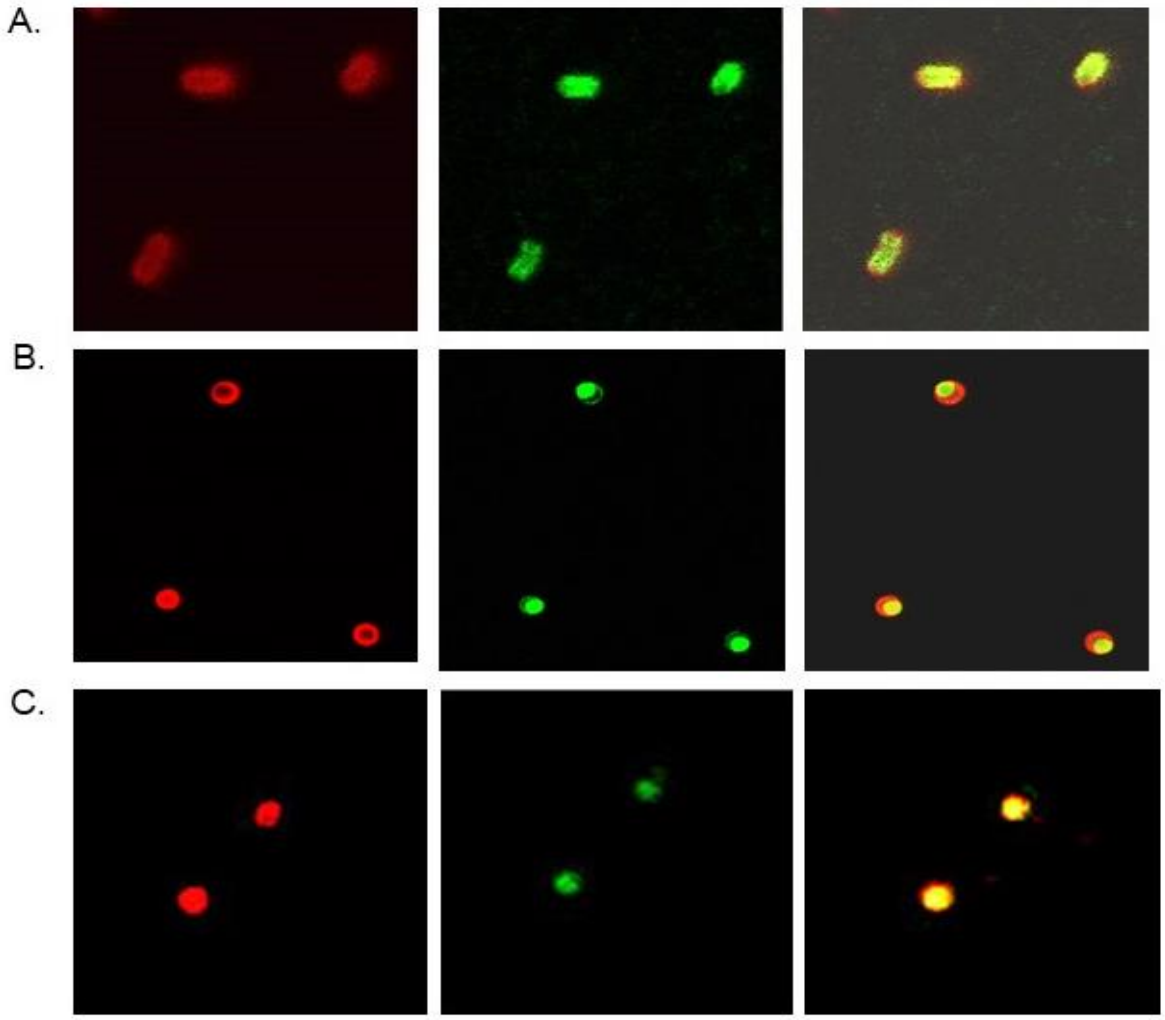

Fig. 4-9: Epifluorescence observation of FepAA698C-A546M and GFP-TonB in cells and spheroplasts. KNK013/pGTFA698C/pJF118EH or KNK013/pJF118EH/pJFLyz cells were grown in NB with apo-FcA and FepAA698C was labeled with A546M. Whole cells and spheroplasts were spun down and resuspended in KPi with 30 mM MgSO4 (A, B). Alternatively, spheroplasts were resuspended in SM buffer consisting of KPi, 30 mM MgSO4 and 8% PEG-6000 (C). A) Whole cells show much less or no GFP-TonB at the poles whereas FepA is located throughout the outer periphery. B) Spheroplasts suspended in KPi buffer alone have material-dense cytoplasm and the IM containing GFP-TonB pushed to a side of the cell. C) Addition of 8% PEG-6000 re-distributes the cytoplasm throughout the cell, juxta-posing the IM and OM.

4.3.4 [^{59}Fe]Ent uptake by spheroplasts

Prompted by the reduced uptake of FeEnt and Fe-apoFc by KNK00 and BN1071, harboring certain plasmid encoded SAR endolysins, we attempted to study the amount of radiolabeled [^{59}Fe]Ent accumulated by these strains over time and compared that with the levels in non-spheroplast control cells. We grew cells in either MOPS plus Na-succinate minimal medium or NB with apo-FcA added, induced the strain KNK00/pJFLyz with IPTG and prepared spheroplasts. As controls we kept strains KNK00, KNK00/pJF118EH and KNK00/pJFLyz without induction. We added [^{59}Fe]Ent to 1 µM to each of these strains at time point “0” and followed the uptake over a period of 30 minutes by filtering aliquots of cells at different intervals of time. For [^{59}Fe]Ent uptake experiments, we could directly filter the cells without spinning down from the growth medium, as done previously (Ma et al., 2007). Alternatively, we spun down the cells and spheroplasts and resuspended them in SM buffer which is free of any carbon source that might interfere with the [^{14}C]-lactose uptake assays in our studies of LacY-mediated lactose transport. Spheroplasts of KNK00/pJFLyz showed at least 60% reduction in [^{59}Fe]Ent accumulation compared to uninduced cells and the empty vector controls (KNK00/pJF118EH). We saw similar reduction in the strain KNK05/pJFLyz which we later used for studying lactose uptake. Cells cultured in MOPS with succinate or NB displayed equivalent impairment in uptake of the radiolabeled Fe^{3+}-siderophore (Fig. 4-10). We repeated the experiments multiple times to statistically validate the results.

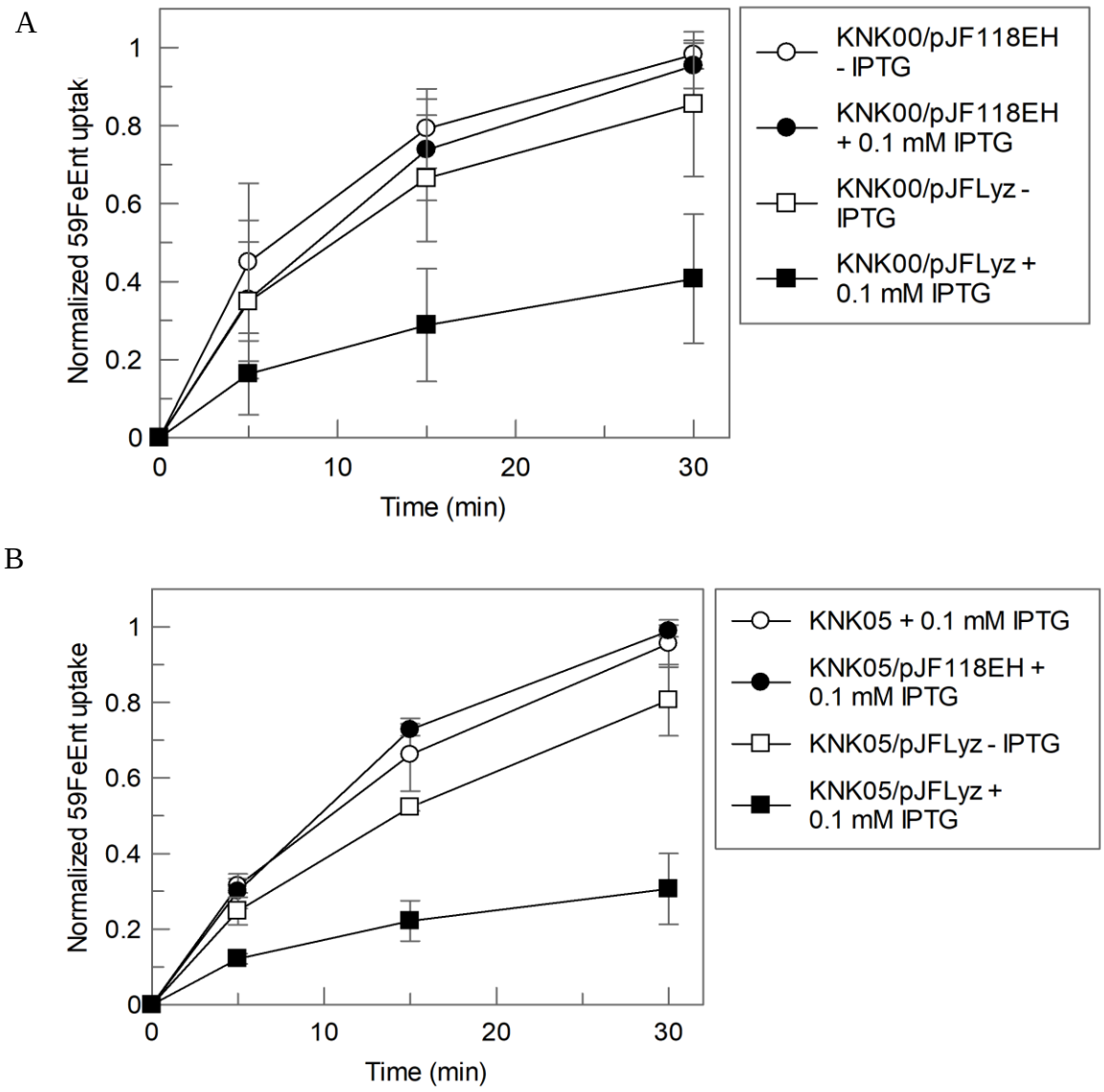

Fig. 4-10: Accumulation of [^{59}Fe]Ent by KNK00 (A) and KNK05 strains (B) harboring plasmids pJF11EH (empty vector) or pJFLyz. Cells were grown in iron-deficient MOPS medium (A) or NB with apo-FcA (B), induced with IPTG and then cells and spheroplasts were exposed to 1 µM [^{59}Fe]Ent. At time points 5, 15 and 30 minutes, aliquots of cells were filtered in triplicate and washed with LiCl. Accumulated radioactivity in cells was normalized with respect to control strain that accumulated ○maximum for each day of experiment. A) KNK00/pJF118EH without (○) or with (●) IPTG addition show identical accumulation whereas, KNK00/pJFLyz induced (■) to form

spheroplasts transport only 40% of KNK00/pJF118EH uninduced (□). B) KNK05/pJFLyz spheroplasts (■) showed >60% reduction in [^{59}Fe]Ent transport compared to uninduced KNK05/pJFLyz (□) as well as KNK05/pJF118EH (●) control and KNK05 (○) alone.

Our preliminary siderophore nutrition tests showed reduced uptake of Fe^{3+}-siderophore by BN1071/pZE-R21. We attempted to verify this observation in radioactive [^{59}Fe]Ent accumulation studies. Surprisingly, following similar protocols to induce spheroplast formation by adding IPTG to BN1071/pZE-R21 in either MOPS with succinate or NB, yielded very little success in obtaining spheroplasts. Following prolonged periods of induction of up to 7 hours, we observed only 20-30% spheroplast formation (data not shown). [^{59}Fe]Ent accumulation over time with induced BN1071/pZE-R21 cells did not show any impairment in uptake of the radiolabeled siderophore when compared to the uninduced strain as well BN1071 control (Fig. 4-11).

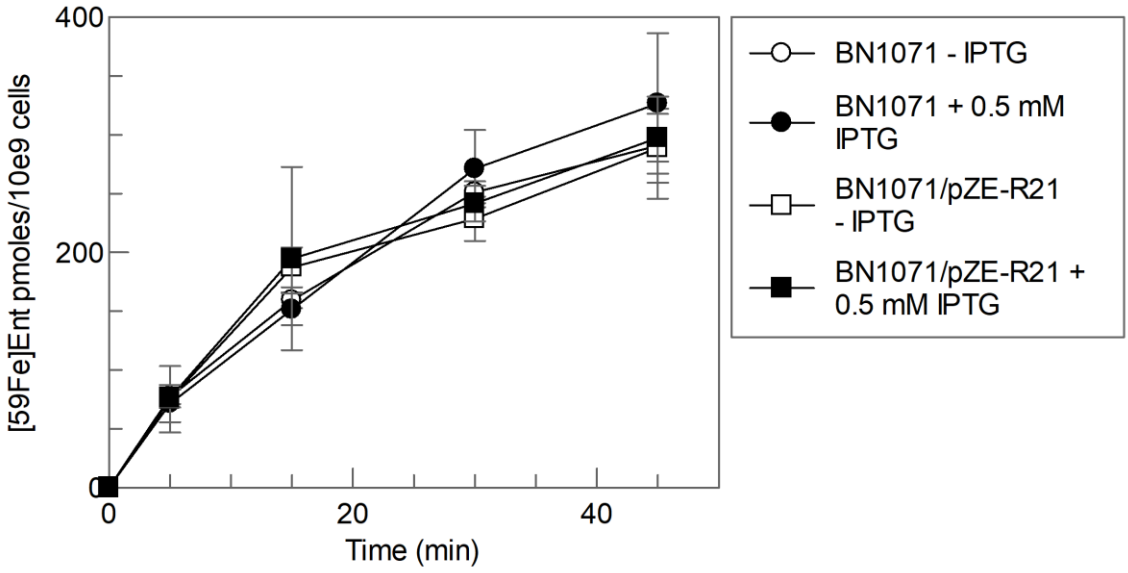

Fig. 4-11: Accumulation of [^{59}Fe]Ent by BN1071 cells harboring pZE-R21. BN1071 and BN1071/pZE-R21 cells were treated with 0.5 mM IPTG (●, ■) and exposed to 1 μM [^{59}Fe]Ent in the same way as uninduced cells (○,□). Radioactivity accumulated over 45 minutes by the

different strains were identical and did not show any impairment of iron uptake capacity in IPTG treated BN1071/pZE-R21, which did not produce substantial amount of spheroplasts.

It is possible that the cell envelope of the BN1071 host strain is more resilient than MG1655. This may be attributed to the several genetic manipulations previously made on the strain before it was adopted as a host strain by the Klebba lab for iron uptake studies in *E. coli*. We therefore continued further experiments with the KNK00 and KNK05 host strains only.

4.3.5 Proton motive force dependent transport via LacY

LacY (Lactose permease) in *E. coli*, specifically binds and transports D-galactose and disaccharides such as lactose, containing a D-galactopyranosyl ring with a H^+ (galactoside/H^+ symport) and does not recognize D-glucose or D-glucopyranosides, which differ in the orientation of the C4-OH group only (Jiang et al., 2014). Since, the process is *pmf*-dependent, we attempted to investigate the fate of lactose uptake mediated by LacY in cells devoid of PG.

MacConkey agar is a common microbiological differential medium used to selectively isolate lactose-fermenting Gram negative bacteria. We used MacConkey Top agar (with 0.7% agar) to determine whether spheroplasts are capable of fermenting lactose. We serially diluted lactose-utilizing control cells (KNK00), lactose non-utilizing whole cells (KNK00 ΔlacZ::CmR) and spheroplasts (KNK00/pJFLyz) in appropriate media, mixed higher dilutions with molten MacConkey Top agar and incubated them at 37ºC to obtain isolated colonies. When observed under 40X magnification in an inverted colony-counter, KNK00 and KNK00/pJFLyz colonies appeared red or pink whereas the ΔlacZ deleted strain showed white colonies (Fig. 4-12). Thus, our preliminary investigation suggested

that degradation of PG in cells with functional lactose-utilization genes, did not affect their lactose transport capabilities.

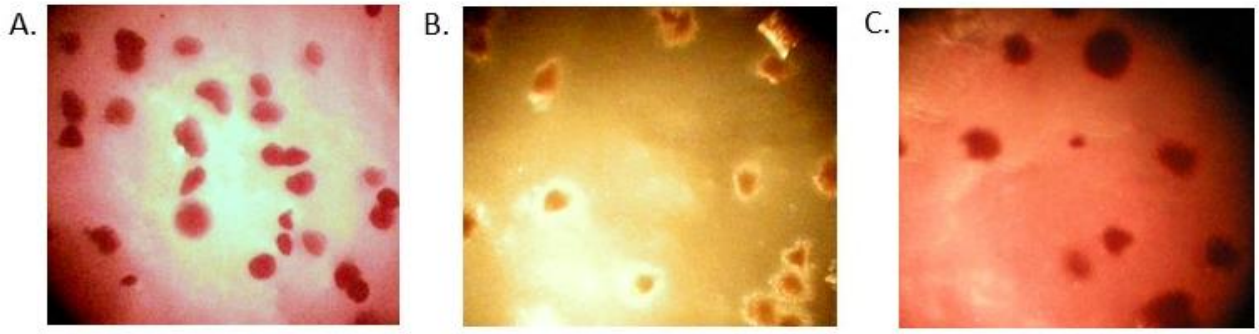

Fig. 4-12: MacConkey lactose utilization assay by whole cells and spheroplasts. A) KNK00/pJF118EH B) KNK00 *ΔlacZ::CmR* C) KNK00/pJFLyz. Cells capable of fermenting lactose give rise to pink or red colonies whereas, cells with disrupted lac operon genes cannot. Spheroplasts of KNK00/pJFLyz showed red colonies on soft agar suggesting unimpaired lactose transport capabilities.

To follow-up this preliminary finding with quantitative experiments, we attempted to measure transport and accumulation of radiolabeled substrate in the KNK00 strains. However, since KNK00 ($lacZ^+$) has a functional β-galactosidase, we chose a non-utilizable tritiated homolog of lactose, [$^3H_1$]-methyl-β-D-thiogalactoside ([^{3}H]TMG) as the radioactive substrate for the uptake experiments. We grew cells in MOPS with Na-succinate, added IPTG to induce the chromosomal lac-operon genes as well as expression of P1Lyz. Once spheroplasts of KNK00/pJFLyz formed, we spun down all the strains and resuspended them in the SM buffer to wash out the inducing agent. We added [^{3}H]TMG to a final concentration of 0.4 mM to aliquots of the strains and measured transport rates in pmol/min/10^9 cells. The data showed comparable transport rates of KNK00/pJFLyz spheroplasts with the KNK00/pJF118EH strain whole cells, but both

strains seemed to transport much slower than the KNK00 host. In comparison, the negative control T-184 (lacY$^-$) strain manifested very little transport of [^{3}H]TMG as expected. Disappointingly, the strains showed large variation in the transport rates when the experiment was repeated multiple times (Fig. 4-13). This day-to-day variability of the data prompted us to look at accumulation of the radionucleide at several time points rather than measuring Vmax transport rates. Also, because of relatively high cost and scarce availability of [^{3}H]TMG, we decided to use [^{14}C]lactose for further experiments. But, this necessitated experimentation in a lacZ- background strain. Hence, we constructed strains KNK05 (KNK00 ΔlacZ) and KNK056 (KNK00 ΔlacZlacY) by precise deletion of the chromosomal lac operon genes in the KNK00 strain. We followed the accumulation of [^{14}C]lactose in induced cells and spheroplasts over 5 minutes by filtering aliquots of cells exposed to the radiolabeled substrate at different intervals and compared the levels with cells incapable of transporting lactose. Cells containing the empty plasmid pJF118EH as well as spheroplasts with compromised PG showed differential uptake of [^{14}C]lactose compared to the negative control. Levels of uptake by whole cells and spheroplasts were very similar and the observations repeated in multiple experiments. However, when compared to the accumulation by the KNK05 host strain alone, the pJF118EH and pJFLyz harboring strains showed less transport into cells (Fig. 4-14). Nevertheless, comparable levels of uptake in the plasmid containing cells suggested that there is no significant effect of the degradation of PG on *pmf*-dependent transport of lactose via LacY.

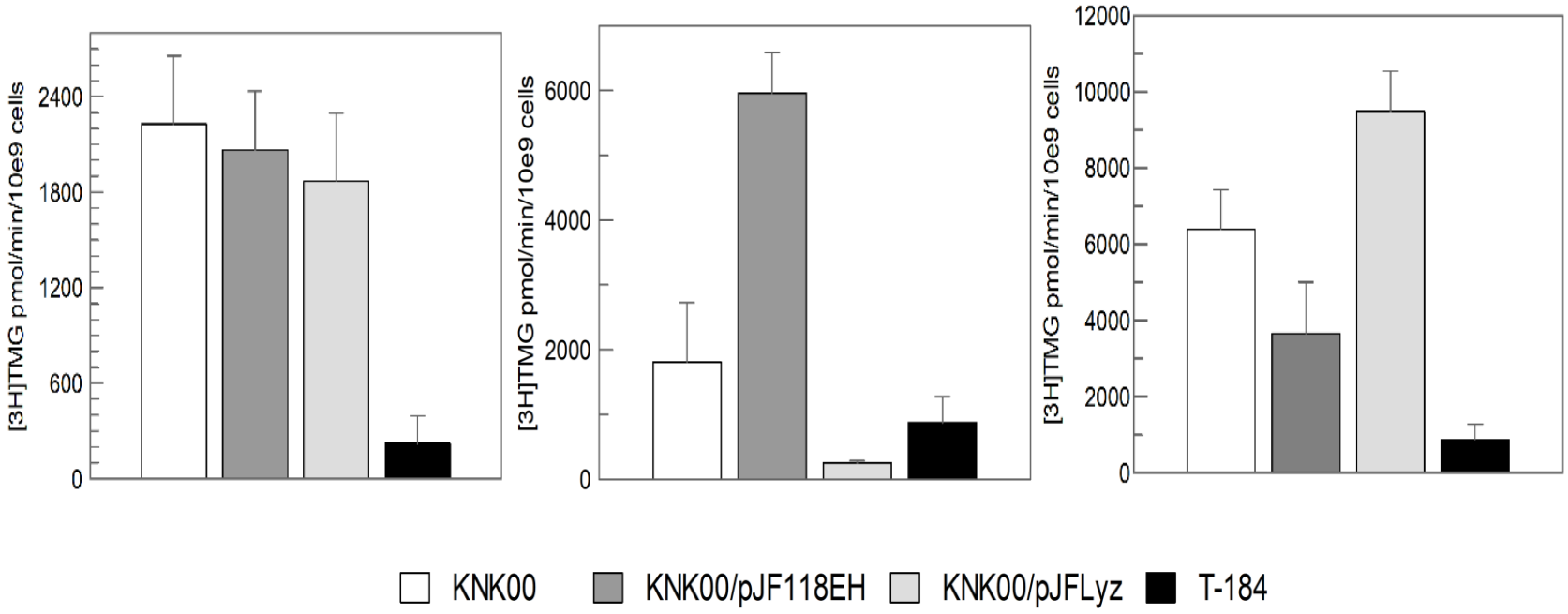

Fig. 4-13: Vmax transport of [^{3}H]TMG by KNK00 whole cells and spheroplasts. Data shown is the transport occurring in three separate experiments. Cells were subcultured in MOPS, treated with 0.1 mM IPTG to induce LacY expression and then exposed to 0.4 mM final concentration of [^{3}H]TMG. Aliquots were filtered at time points 5 seconds and 3 minute 5 seconds to obtain amount of substrate transported/minute at the saturating substrate concentration. Transport rates show large day-to-day variation in the different strains making it difficult to conclude any trend in the data.

A.

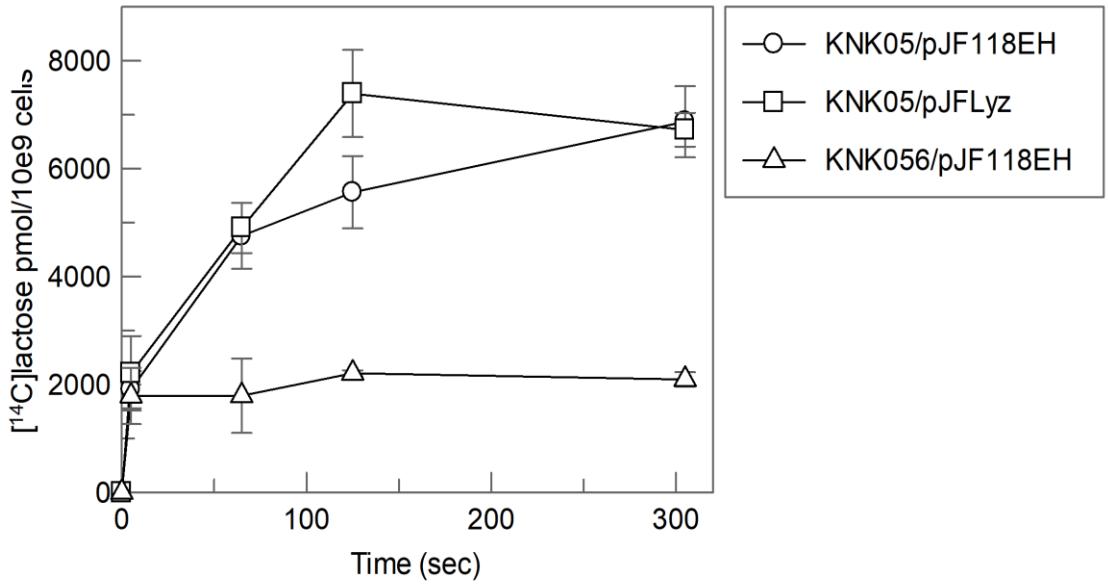

B.

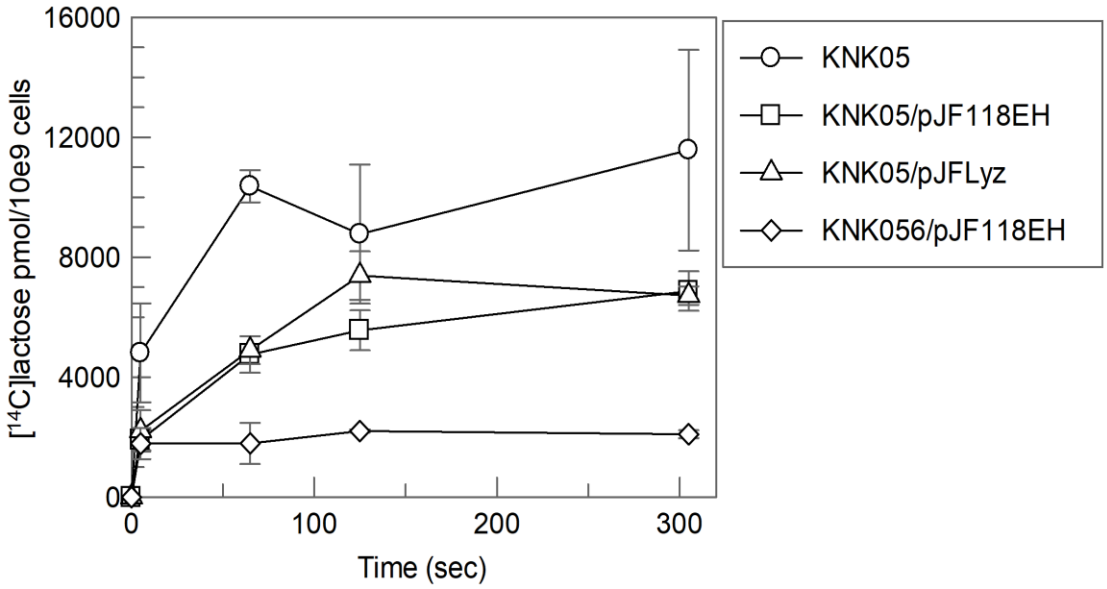

Fig. 4-14: Accumulation of [^{14}C]lactose in KNK05 whole cells and spheroplasts. Data was obtained from the average of three experiments. Cells and spheroplasts grown in NB that were used for [^{59}Fe]Ent studies, were exposed to 10 mM final concentration of [^{14}C]lactose and aliquots were filtered at 5, 65, 125 and 305 seconds and rinsed with LiCl/0.1M KPi (pH5.5). A) Radioactive substrate transported by KNK05/pJF118EH (□) whole cells and KNK05/pJFLyz (Δ) spheroplasts

were at identical levels and significantly higher than the KNK056/pJF118EH (◊) negative control. B) However, both strains accumulated less than KNK05 (○) not containing any plasmid.

4.3.6 iPALM/dSTORM observation of FepA and TonB

The ability of super resolution microscopy to observe individual molecules within cellular structures allowed us to visualize, for the first time ever the two Gram-negative bacterial membrane proteins FepA and TonB. We observed the localization of the extrinsically labeled FepA and the intrinsically fluorescent mEos-TonB molecules in the OM and IM respectively and also assessed whether the two proteins co-localized due to interaction during ligand transport. We also made similar observations in *E. coli* cells converted in to spheroplasts with the hypothesis that degradation of PG may prevent any co-localization, if any.

We collected images of the same field one color at a time and then performed algorithms to overlay the two colors to obtain the final image displaying FepA molecules lining the OM and mEos-TonB distributed throughout the IM. Starting from the bottom of the cell that is attached to the coverslip, the z-sections up to 800 nm represents the cell. Beyond this range, the instrument fails to collect data due to the proximity of the two objectives to the coverslip. We counted the total number of FepAs and mEos-TonB in different cells and in each cell, the number of FepAs appear to be 3-5 times more than mEos-TonB. The maximum number FepA molecules per cell ranged from 3000-5000, whereas the number of mEos-TonB ranged between 750-1500. These numbers are far less than those predicted biochemically. In many of the cells visualized, both FepA and TonB appeared to be present in clusters of variable sizes. We zoomed in to such clusters and counted the number of protein molecules in each cluster. Table 4-2 summarizes the

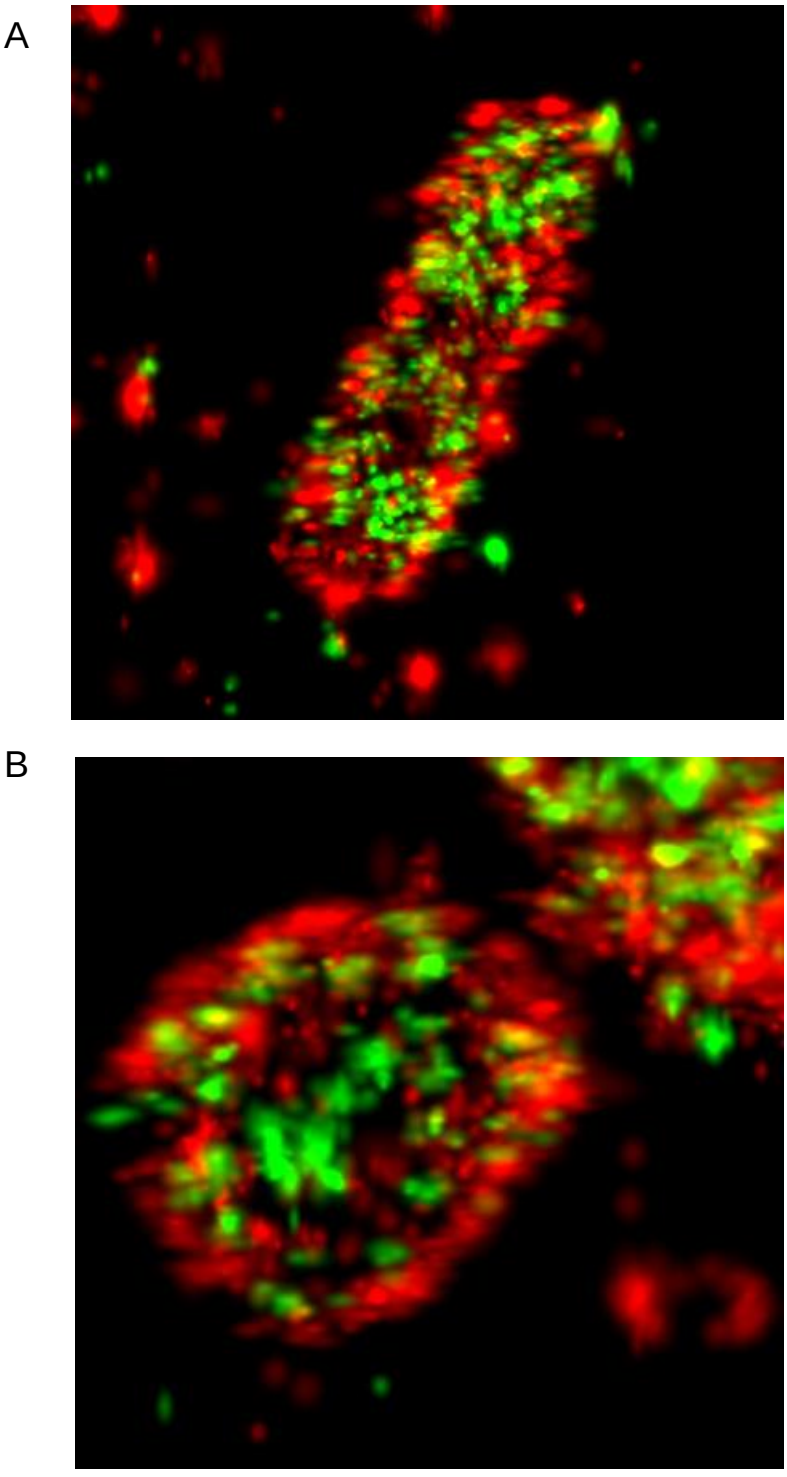

Fig. 4-15: iPALM/dSTORM observation of FepA and TonB in whole cells (A) and spheroplasts (B). The FepA is represented in red and is visible in the outer membrane while the mEos-TonB is represented in green and is present along the inner membrane. The bacterial cells ranging from

1-2 μ in size, the resolution rendered color up to 5nm per pixel shows FepA and TonB molecules in close proximity and some resolution between individual molecules is lost.

count of number of clusters of FepA and TonB with respect to their size in 25 cells studied across different fields obtained from two separate days of experiments. We compared the cluster size and number in the absence or presence of FeEnt addition in both whole cells (KNK013/pETFA698C) and spheroplasts (KNK013/pETFA698C/pJFlyz). We did not notice any predictable pattern in the way the clusters appeared either in whole cells or spheroplasts. Iron transport did not seem to make any noticeable difference either.

Table 4-2: Number of clusters of FepA or mEos-TonB per cell vs cluster size in whole cells and spheroplasts without or with addition of FeEnt.

Type	Sample no.	-FeEnt				+FeEnt			
		No. of clusters/cell		Cluster size		No. of clusters/cell		Cluster size	
		FepA	TonB	FepA	TonB	FepA	TonB	FepA	TonB
Whole cells	1	10.8± 4.6	4.8± 2.3	74.9± 27	40.2± 16.8	7.6± 3.2	5± 2.3	55.6± 12.7	44.3± 22.2
	2	11.4± 1.14	3± 1.5	80.1± 11.4	42.2± 22.5	14.6± 3.5	4± 1.4	151.4± 63.4	66.3± 21.5
Spheroplasts	1	8.6± 3.1	3.8± 2.9	56.2± 10.9	39.6± 20.8	3.8± 2.1	3.4± 1.1	90.2± 33.4	62.2± 30.3
	2	13.2± 5.2	4.2± 2.1	76.5± 19	29.6± 7.9	8.8± 5.4	2.4± 1.1	115.8± 48.8	79.4± 13.5

4.4 Discussion

The cell envelope architecture is under-appreciated in the context of TonB-dependent metal transport in Gram negative bacteria. The affinity of the TonB C-terminus for the PG positions it directly underneath the OM since, the murein sacculus is closely associated with the outermost layer of the cell envelope (Sonntag, et al., 1978). Even, repeated detergent extractions of OM proteins do not completely remove the proteins connecting

the PG to the OM (Schnaitman et al., 1973; Schmitges, Henning, 1976) suggesting a structure-function relationship of this association. The oligosaccharide network of N-acetylglucosamine (NAG) and N-acetylmuramic acid (NAM) of PG provides a structural framework for the assembly of the OM and its proteins. In the VS model of PG structure, as suggested by Meroueh et al., the PG matrix is formed of hexagonal cells which are appropriately sized to house OM proteins, as well the dimeric and monomeric TonB CTD that reaches out from the IM. This arrangement makes the tenets of the ROSET model of TonB action mechanistically simpler compared to the contrasting PN model of PG arrangement. The goal of this study was to explore this structural role of the PG in TonB-dependent uptake of the Fe^{3+}-siderophore FeEnt through FepA and thereby validate or refute the concept of dependency of TonB function on its association with PG (Kaserer et al, 2008; Klebba, 2016). The use of PG-deficient live *E. coli* cells allowed us to test the function of the LysM domains of TonB CTD in its overall localization in the cell envelope and its significance in energized rotational motion of TonB that proposedly drives metal uptake by OM transporters.

Conventionally, “cell wall-less” spheroplasts of Gram negative bacteria are prepared by treatment of sensitive species with lysozyme (Weibull 1958; Brenner et al., 1958) or with penicillin and analogous antibiotics that block PG cross-linking in rapidly dividing cells (Lederberg, 1956: Leibermester & Kellenberger, 1956). Our approach involved plasmid encoded expression of the PG-disrupting agent from within the cell. The SAR endolysins, identified as a separate class of enzymes involved in the lytic infection cycle of some phages, differ from the canonical lytic process of phages in several aspects (Young et al., 2014; Sao-Jose et al.,2000). Contrary to canonical endolysins, which leak into the

periplasm through large holes created by holins in the cytoplasmic membrane, SAR endolysins are secreted through the sec translocon of bacterial secretory system into the periplasm. There they accumulate in inactive, IM-tethered forms by virtue of N-terminal Signal-Arrest Release (SAR) peptide sequence. Another set of transmembrane viral proteins, pinholins, deposit in the IM and bring about membrane depolarization in an enzyme-specific manner. This releases the membrane-bound endolysins and activates them to attack the PG. Lysis of the OM is then brought about by another class of phage proteins called spannins. Interestingly, plasmid-encoded SAR endolysin of phage P1 (P1Lyz) was found to accumulate in membrane-form in considerable amounts (Xu et al., 2004). We took advantage of this observation for creating PG-lacking viable *E. coli* cells with intact cytoplasmic and outer membranes by inducing expression of the SAR endolysins from high-copy plasmids. P1Lyz expressed by the plasmid pJFLyz in MG1655 cells secrete out into the periplasm using bacterial transport proteins, where they concentrate and attack the murein backbone without the necessity of membrane depolarization. In the absence of phage-derived spannins, the OM disintegration step is blocked leaving “wall-less” Gram negative bacterial spheroplasts that require iso-osmotic conditions to remain stable for extended periods of time.

Working out ideal conditions for preparing and maintaining stable spheroplasts created by expressing SAR endolysins, turned out to be considerably tricky and time-consuming. One downside of expressing lethal genes in high-copy plasmids under control of “leaky” promoters like p_{tac} was that it led to basal level of endolysin synthesis even in uninduced conditions, turning increasing number of cells into spheroplasts. Some of the spheroplasts would lyse leaking out contents of the cytoplasm loaded with ampicillinase that would de-

activate the ampicillin added to the external medium. Ultimately, a fraction of cells would be cured of the SAR endolysin-encoded plasmid leading to poor yield of spheroplasts upon induction. Using fresh transformants from plates or small aliquots of frozen stocks prepared from scraps of freshly transformed colonies appeared to alleviate this problem. Adding of 0.2% glucose to transformation plates as well as starter cultures of pJFLyz harboring cells, also helped to curtail the uncontrolled expression of P1Lyz. Growing starter cultures in LB broth for not more than 14 hours appeared to be crucial for obtaining healthy, reproducible growth rates of the P1Lyz expressing strains once we subcultured from LB into NB or MOPS media. Using low concentrations of IPTG to induce expression of P1Lyz in cells growing in NB, produced spheroplasts that remained stable and viable over several hours (Fig). From confocal microscopic images, spheroplasts appeared to be more stable when subcultured in NB compared to MOPS. Composition of the OM proteins is found to vary considerably between nutrient-rich and minimal media, possibly being the factor responsible for this difference in stability of the spheroplasts prepared in the two media. Identification of a buffer at physiological pH with ideal isosmolar strength was crucial for our [^{59}Fe]Ent and [^{14}C]lactose transport experiments. Literature suggests that spheroplasts remain viable for long periods in buffers containing salts like NaCl or sugars like sucrose at pHs below 7.0 (Gnarpe and Edebo, 1970), that we corroborated in our experiments with spheroplasts suspended in different buffers (Fig). However, LacY being a galactoside/H^+ symporter, in buffers with pH as low as 5.0, the cell interior is too acidic reversing the direction of proton flow across the cytoplasmic membrane, that ultimately prevents cells from accumulating [^{14}C]lactose (Kaback, 2015, Jiang et al. , 2014). Hence, 100 mM NaCl/20 mM Tris-Cl at pH:5.0 was not useful to us. Addition of

8% PEG-6000 (Melechen et al., 1972) to Kpi buffer which was regularly used by Kaback et al. (Kaback, 1974) for [^{14}C]lactose transport experiments, allowed us to get stable spheroplasts (Fig. 4-6).

Epifluorescence observation of KNK013 cells expressing pJF118EH (empty vector) and pGTFA698C plasmids repeated our previous observation of GFP-TonB's restricted localization at the center of the cells. In opposition, the re-distribution of GFP-TonB throughout the cell in the PG degraded spheroplasts hints towards uneven thickness or cross-linking of the PG layer across the cell with higher thickness near the poles. A neutron small-angle scattering study suggested that the maximum thickness (7±0.5 nm) of the murein sacculus prepared from exponential phase *E. coli* cells was enough to consist of a partially triple-layered structure, with about 75-80% being single-layered across its surface and the rest triple-layered. A partial multi-layered structure structure of the murein sacculus at polar caps is favored by the intercalation-type growth model of PG proposed by Burman & Park (Burman & Park, 1984) where new PG strands and PG-binding enzymes are incorporated to growing strands in a helical path around the cell. PG at poles is found to be metabolically inert with addition of new materials or turnover as in the lateral walls in both Gram negative and positive bacteria. Additionally, some evidence suggests that mobility of periplasmic proteins is restricted at cell poles and potential sites of cell division (Foley et al., 1989). Hence, TonB with its periplasm-spanning structure could potentially have restricted access to the polar caps of the cell. However, this raises questions against the fundamental proposition of the TonB ROSET model that direct protein-protein interactions between TonB and FepA (LGPs) facilitate energy-transduction for siderophore internalization. X-ray crystallographic structures reveal the

TonB CTD in close association with the TonB box of LGPs (Shultis et al., 2006; Pawelek et al., 2006). Therefore, if TonB is unable to access the TonB box of LGPs located at the poles, then how do they transport? Alternatively, FepAs located ta poles may be mostly inert and do not participate in cellular uptake of FeEnt. However, biochemical evidence suggests otherwise. Post-uptake binding measurements of FeEnt transport revealed rates that reflect transport by all FepAs present in an *E. coli* cell (Newton et al., 2012). Real time fluorescence quenching and recovery upon FeEnt binding upon A546M bound FepAs and consequent transport also show uniform uptake of the siderophore throughout the cell (Smallwood et al., 2014) underlining our biochemical findings of OM transport rates. This infers one of two possibilities: i) The ROSET hypothesis is untrue and incapable of explaining how TonB transduces energy to LGPs, particularly in all parts of the cell that is, energy transmission by the TonB complex occurs by a mechanism that is difficult to envision with the current knowledge base, ii) TonB may be present at the poles of Gram negative cells but in far less numbers than the rest of the rod-shaped bacteria, limiting epifluorescence visualization of the protein. The few TonBs in these regions perhaps may be enough to drive transport through FepAs present at the poles. Single-molecule resolution microscopy technique may potentially make TonB fusion proteins observable in the polar caps circumventing the problem of diffraction-limited resolution of conventional light microscopy. Nevertheless, focusing on observations that are unambiguous, we now know that the PG layer is indeed responsible for the scarcity of TonB in the polar regions of the Gram negative cell envelope and its arrangement within the two membranes also plays a role in the TonB-dependent uptake of metals.

Siderophore nutrition tests provide an excellent assessment of the status of siderophore uptake by cells based on the nature of the halo of bacterial growth obtained around the filter disc. As the Fe^{3+}-siderophore diffuses into the agar that was made iron-deficient by the iron-chelating agent, bacteria with intact iron transport capabilities reproduce in large numbers around the disc forming small, intense halos. KNK00 and BN1071 strains formed such halos in our experiments. Both strains harboring the SAR endolysin plasmids showed similar halos also when there was no prior induction with IPTG. However, once IPTG was added before plating these cells in the soft agar as well as when small concentrations of IPTG was added to the agar, the halos that appeared were either larger in diameter or less intense, or both in some cases (Fig. 4-4). This indicated reduced uptake of the siderophores FeEnt or FeFc in those strains. Consistent appearance of diffuse halos in strains KNK00/pJFLyz and BN1071/pZE-R21 encouraged us to test them for quantitative uptake of [^{59}Fe]Ent. P1Lyz expressed in different MG1655 strains showed drastic reduction in the ability to accumulate the radiolabeled siderophore over time underscoring the importance of an intact PG in TonB-dependent metal uptake through LGPs like FepA. Comparable levels OM FepA expression in spheroplasts and uninduced cells of KNK00/pJFLyz and KNK00/pJF118EH, permitted us to attribute the reduced uptake of [^{59}Fe]Ent to the degradation of PG. The similar levels of the OM protein in both whole cells and spheroplasts prepared under identical growth conditions also suggested a largely intact OM in the spheroplasts. Close association of the outer and inner membranes in spheropalsts resuspended in SM buffer, as seen in images obtained from confocal microscopy, as well as iPALM/dSTORM, re-assessed the mechanistic significance of TonB's affinity and association with the murein sacculus. The arrangement

of the GFP-TonB or mEos-TonB in the cytoplasmic membrane in close contact with the OM bilayer in those images counter-argued against any possibility of the reduced ligand uptake arising from unnatural separation of the FepA and TonB proteins in the outer and inner membranes respectively. Interestingly, the uptake of [^{59}Fe]Ent was not completely abolished in the spheroplasts. This possibly suggests that even after the cell's transition into spheroplast, the degradation of PG by P1Lyz is not complete and chunks of the murein backbone remain intact, which might be allowing FepAs and TonBs to interact in those regions. Future experiments involving simultaneous observation of the FepA and TonB proteins and the PG in cells and spheroplasts could potentially shed light on this.

Concomitant with the studies of the impact of degradation of PG on TonB-dependent siderophore uptake is the exploration of any influence of such perturbation of the cellular envelope on IM transporters which also function based on the electrochemical gradient. Cells capable of utilizing lactose ferment MacConkey agar thereby reducing the pH and turning the neutral red indicator pink to give rise to pink/red colonies. Appearance of pink/red colonies of spheroplasts of KNK00/pJFLyz that recovered in the MacConkey Top agar suggested at least preliminarily that degradation of PG does not affect other pmf-dependent transport processes such as uptake of lactose via LacY.

Quantitative measurements of Vmax at saturating concentrations of the non-utilizable lactose analog [^{3}H]TMG although showed differential uptake of the radiolabeled substrate compared to the negative control T-184, the variability in the uptake rates of the different strains is difficult to explain. Switching over to [^{14}C]lactose as the radiolabeled substrate, to study accumulation over time, we saw differential uptake of the cells and spheroplasts compared to the KNK056/pJF118EH negative control. Comparable levels of

accumulation by both whole cells and spheroplasts, suggested that *pmf*-dependent transport through IM lactose permease is independent of the integrity of the murein layer. This supported the hypothesis that an intact PG underlying the OM is essential for *pmf*-driven TonB-dependent OM uptake of Fe^{3+}-siderophores but not for TonB-independent phenomenon occurring in the IM.

The aims of the iPALM/dSTORM experiments were not only to observe FepA and TonB at the level of single molecule resolution, but also to observe their localization in the membranes under conditions of iron starvation and iron transport. Such observations could potentially verify the idea of FepA and TonB coming in close proximity for interaction during FeEnt transport. The experiments with the spheroplasts would assess whether degrading the PG would exert any changes in the patterns of localization in the whole cells under similar conditions. However, there were several discrepancies in the data that were difficult to explain. First, the number of FepA and TonB per cell turned out to be much lower than predicted from biochemical analysis (35,000 FepA to 1,000 TonB) (Klebba, 2003; Newton et al., 2010). Second, FepA and TonB appeared to be present in clusters of variable sizes and frequency throughout the membranes in both whole cells and spheroplasts. There was no pattern in the distribution of these clusters, nor did they appear to colocalize induced by FeEnt transport. Hence, we were not able to deduce any conclusion in connection to FepA and TonB interactions promoting ligand transport.

Possible explanations behind these discrepancies include: i) since we are imaging ~50-75% of the cell volume, we are undercounting the fluorescent molecules, ii) due to instrumental limitations, not all blinks are counted, iii) comparatively fast photobleaching of A647M, resulted in loss in signal, iv) quenching of fluorescence of FepA molecules that

are at the surface of the cells adsorbed to the coverslip by the poly-L-Lys coating. After personal communications with Prof. Hiroshi Nikaido, we learnt that attachment of cells using poly-L-Lys not only causes loss of fluorescence intensity but also considerably deforms the OM morphology due to the interaction of the charges. The use of poly-L-Lys to coat coverslips for cellular adsorption prior to fixation is a common practice in fluorescence microscopy techniques. Hence our discoveries using this method came as a surprise and ultimately it is difficult to draw any conclusions from these data. Never the less we achieved single molecule visualization of FepA and TonB in *E. coli* cells and their distribution in the cell envelope. For future studies we plan to raise mouse antibodies against outer envelope of the bacteria and use it to coat over the poly-L-Lys in order to circumvent the adverse effects of the latter on bacterial cell morphology and fluorescence.

Chapter 5: Concerted loop motion triggers induced fit of FepA to ferric enterobactin

Smallwood CR, Jordan L, Trinh V, Schuerch DW, Gala A, Hanson M, Shipelskiy Y, Majumdar A, Newton SM, Klebba PE. *The Journal of General Physiology*. 2014;144(1):71-80. doi:10.1085/jgp.201311159.

5.1 Introduction

Ligand specificity and binding affinity of FepA and its ligand-gated homologs like BtuB, FhuA, require conformational changes in the transporters themselves. Although, ligand specificity is conferred by certain residues in the protein, structural similarities among the paralogous proteins suggest common modes of conformational motion and ligand transport mechanism. Binding of FeEnt to FepA involves hydrophobic interactions with aromatic residues of the FepA external loops (Cao et al., 2000, Annamalai et al., 2004) and electrostatic interactions with basic residues deeper in the vestibule atop the N-domain (Scott et al., 2002, Annamalai et al., 2004). Conformational motion of the external loops then converts the protein to a 'closed' conformation in which FeEnt is at binding equilibrium and poised for transport upon subsequent energization.

The ability to fluoresceinate cysteine sulfide residues on native FepA in living cells or outer membrane fragments, allowed us to study binding and transport reactions with FeEnt. When FeEnt binds, surface loops of FepA close around the ligand and this alters the environment around the attached fluorophore leading to collisional quenching of fluorescence intensity (Scott et al., 2002, Cao et al., 2003). In energized *tonB*+ cells, as FeEnt is transported inside of cells, the fluorescence intensity recovers to original levels. To evaluate the nature of the conformational motion in the surface loops, we used maleimide fluorophores that specifically modify surface exposed free Cys sulfides at <pH:

6.8 to label seven out of eleven loops. This enabled us to study interactions of the individual loops with FeEnt during transport. The target residues showed variability in extent of fluorophore accessibility, fluorescence quenching and motion during ligand binding. Our data indicated a hierarchy of loop motion where individual loops close around the ligand at different rates, analogous to fingers closing around a tennis ball while catching it.

Our observations extrapolate to a model of induced-fit leading to high-affinity binding which is a common interaction in enzyme-catalyzed reactions (Koshland, 1958). In this process, the enzyme is not initially in its catalytic conformation and initial substrate associations expedite change to a catalytically-stable binding conformation. The concept of induced-fit is also applicable to ligand-receptor interactions in membrane proteins and transporters in which conformational change is innately involved in protein function. This work helps to elaborate the nature of the dynamic actions of the extracellular loops of FepA and homologous LGPs, during ligand binding and transport atop of further defining fluorescence spectroscopic methods of measuring membrane transport.

5.2 Methods

To study dynamic changes in the surface loops during FeEnt binding, we selected specific residues for making new Cys substitutions and screened existing mutations for fluorophore accessibility. To label cells, we grew the FepA Cys mutants in iron-deficient media to late-log phase (10^9 cells/ml), washed and resuspended them in labeling buffer (50 mm sodium hypophosphate, 0.9% sodium chloride, pH: 6.5) and exposed the cells to either 5 µM fluorescein-5-maleimide (FM) or Alexa Fluor 488 maleimide (A488M) for 5

min at 37ºC. We stopped the reaction with 100 mM β-mercaptoethanol, pelleted the cells, washed and finally resuspended in 1X PBS with 0.4% glucose.

We monitored the phenotypes of the mutants for unaltered FepA function by siderophore nutrition tests, colicin B killing assays as well as quantitative [^{59}Fe]Ent uptake measurements of FepA before and after fluorescence labeling. We compared the extent of FM labeling relative to the level of FepA expression to determine the efficiency of labeling. We ran protein samples resuspended in sample boiling buffer with 3% βME on SDS-PAGE and scanned the gel on a Typhoon Scanner at 520 nm, then transferred the proteins to nitrocellulose membrane and made quantitative measurements of FepA protein in the samples using [^{125}I]-proteinA to develop the immunoblots.

For fluorescence observation and quenching experiments, we used a SLM AMINCO 8000 fluorescence spectrometer upgraded with an OLIS operating system. We performed quenching experiments at 2ºC by adding FeEnt to 2.5 X 10^7 labeled cells in 3 mL PBS with glucose with stirring. To monitor the time course of fluorescence quenching and recovery at 520 nm emission wavelength, we performed similar experiments at 25ºC. We measured binding kinetics using fluorescent FepA in OM fragments instead of whole cells by rapid-mixing with FeEnt in a stopped-flow set-up. We analyzed fluorescence quenching data using Grafit software to fit the curves in either single or double exponential decay equations with offset. We used single exponential decay equation to fit -log (F/F_0) data for calculating recovery half-times of each labeled loop.

Fluorescence microscopy observations were made using a Carl Zeiss Laser Scanning 700 Microscope of a strain encoding FepAS271C and GFP-TonB fusion on plasmids. We grew the cells in iron-deficient conditions, labeled FepA with Alexa fluor

546 maleimide (A546M) and adhered cells to poly-L-Lysine coated, 8-well microslides and observed GFP and A546M by sequentially exciting with 488 nm and 555 nm laser lights, respectively. We observed $5X10^8$ cells in 350 µL of PBS before and after addition of 5 nm FeEnt. Images were captured over a time course of 23 minutes with 20 second scanning time at 100X magnification.

5.3 Results and Discussion

5.3.1 Site-directed fluorescence labeling of Cys substitutions in the surface loops of FepA

OM proteins of gram negative contain few free Cys residues. The sole two Cys in FepA on Loop7, C487 and C494 are disulfide bonded and do not react with maleimide fluorophores unless reduced (Liu et al., 1994). This allows specific labeling of FepA at engineered Cys residues that we utilized to determine the reactivity of Cys sulfhydryls at various positions in FepA towards different fluorophore maleimides like FM, A546M, A555M, and A680M. We created Cys mutant derivatives of the plasmids pITS23 or pITS47 (both carrying WT *fepA* in pHSG575 plasmid) and expressed them in OKN3 (BN1071 *ΔfepA*) and OKN13 (BN1071 *ΔfepA ΔtonB*). FM labeled live cells grown in iron-deficient media with satisfactory selectivity and sensitivity with 1-5 µM concentration at pH 6.5 which limited reactivity towards Lys. Both 0ºC and 37ºC showed comparable reactivity of Cys (Fig. 5-1).

The method achieved specific labeling of cell surface sulfhydryls with the maleimide fluorophores along with labeling of Cys substitutions on the internal rim of the β-barrel (S150, T666) and the underside of the N-domain (I14, T30, T32, A33) (Fig. 5-2). Fluors like FM which are smaller than the size exclusion limit of the OM, labeled

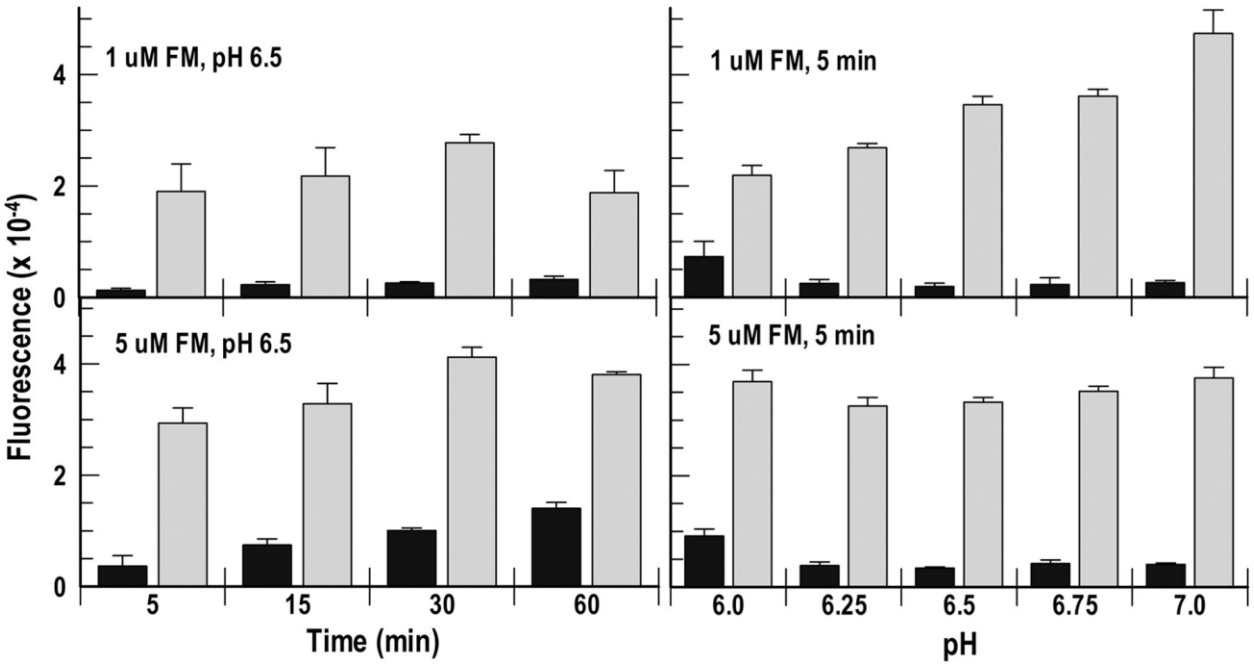

Fig. 5-1: FM labeling reactions. E. coli OKN3/*pfepA*+ (black bars) and OKN3/*pfepAS271C* (gray bars) labeled with 1 or 5 µm FM and incubated in different pH buffers for indicated times (Smallwood et al. 2014).

periplasmic targets weakly at low concentrations (1-5 µM) used in the protocol. At higher concentration of 300 µM, FM quantitatively labeled periplasmic residues, but selectivity was compromised as background labeling of other proteins increased. Alexa Fluors being of higher MW than FM were size-excluded of the OM porin channels and did not label residues on the periplasmic face.

We tested expression and functionality of single cys mutants by measuring their binding and transport capabilities. In most cases, FepA expression and function were unaffected, particularly, loop residues showed least effect due to substitution. They were intensely labeled with FM at 5 µM and fluorescence modification did not affect their functionality except in some cases where binding and transport of [^{59}Fe]Ent was reduced. In comparison, residues in the protein interior and N-domain although expressed at WT

levels, showed considerable impairment of binding and transport capabilities before and after fluoresceination. Based on these observations, we selected seven Cys mutants for investigation of dynamics of the surface loops: T216 (Loop2), S271 (L3), A322 (L4), A383 (L5), S490 (L7), T550 (L8), and A698 (L11) (Fig. 5-2).

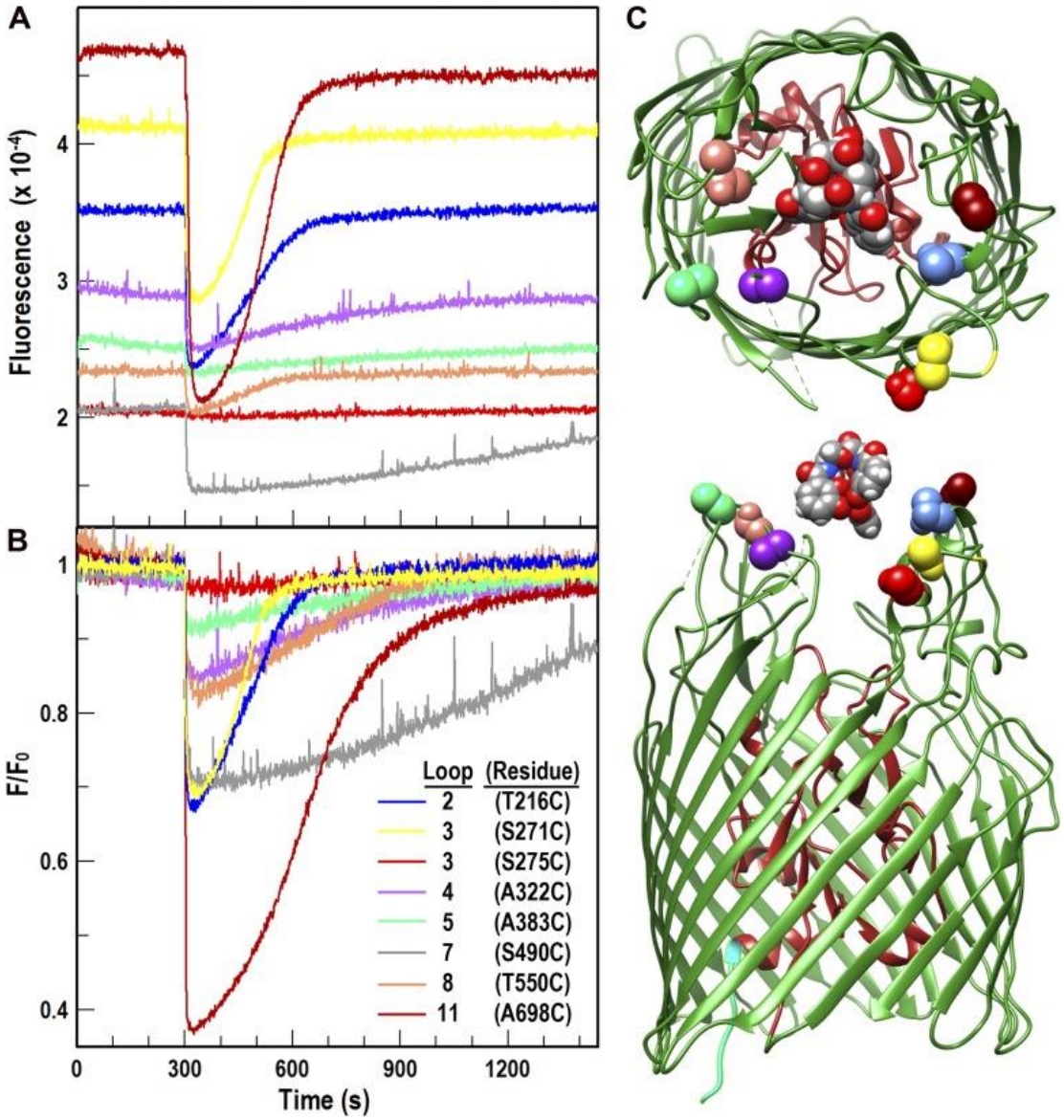

Fig. 5-2: FeEnt-induced quenching of FepA surface loop–FM fluorescence, and recovery from FeEnt transport. A) Raw fluorescence intensity readings showing characteristic extents of quenching and recovery for each FepA Cys substitution. B) Normalized F/F0 data showing

relative extent of quenching and rates of recovery. C) Schematic representation of location of residues (Smallwood et al. 2014).

5.3.2 Loop motion during FeEnt binding and transport by FepA

Using the stable, high quantum yields of FM labeled FepA Cys mutants suspended in PBS at pH:7.4, we characterized fluoresceination, quenching due to FeEnt binding and recovery from transport, of the seven FepA loops. The different mutants at a density of 2.5 x 10^7 cells/mL in a 3 mL cuvette showed a range of initial fluorescence intensities. Labeling efficiency corresponded to the level of FepA expression combined with the accessibility of the Cys targets in the native FepA structure (Fig. 5-2C). Consistent with this idea, residues A698C (L11) and T216C (L2) which are comparatively more surface-exposed on the loops, showed maximum expression and labeling intensities.

Addition of 10 nM FeEnt at 300 seconds led to quenching of fluorescence intensities up to 10-60% of the original values. This reflected binding of the siderophore to the labeled protein and interactions of the individual fluorophore labeled loops with the ligand. The extent of quenching was more in L2, L3, and L11 and less in L4, L5, L7, and L8. Under physiological conditions, the cells transported FeEnt at different rates from solution and the fluorescence reverted to initial levels. This observation depended on the energized and *tonB*+ state of the cells and the half time of fluorescence recovery ranged from 70 to 700 seconds suggesting some extent of impairment of FepA function at some sites. The time required for fluorescence rebound also depended on the concentration of FeEnt added (Fig. 5-3). Concentrations >1 nM FeEnt resulted in >10% detectable quenching (expect in L5).

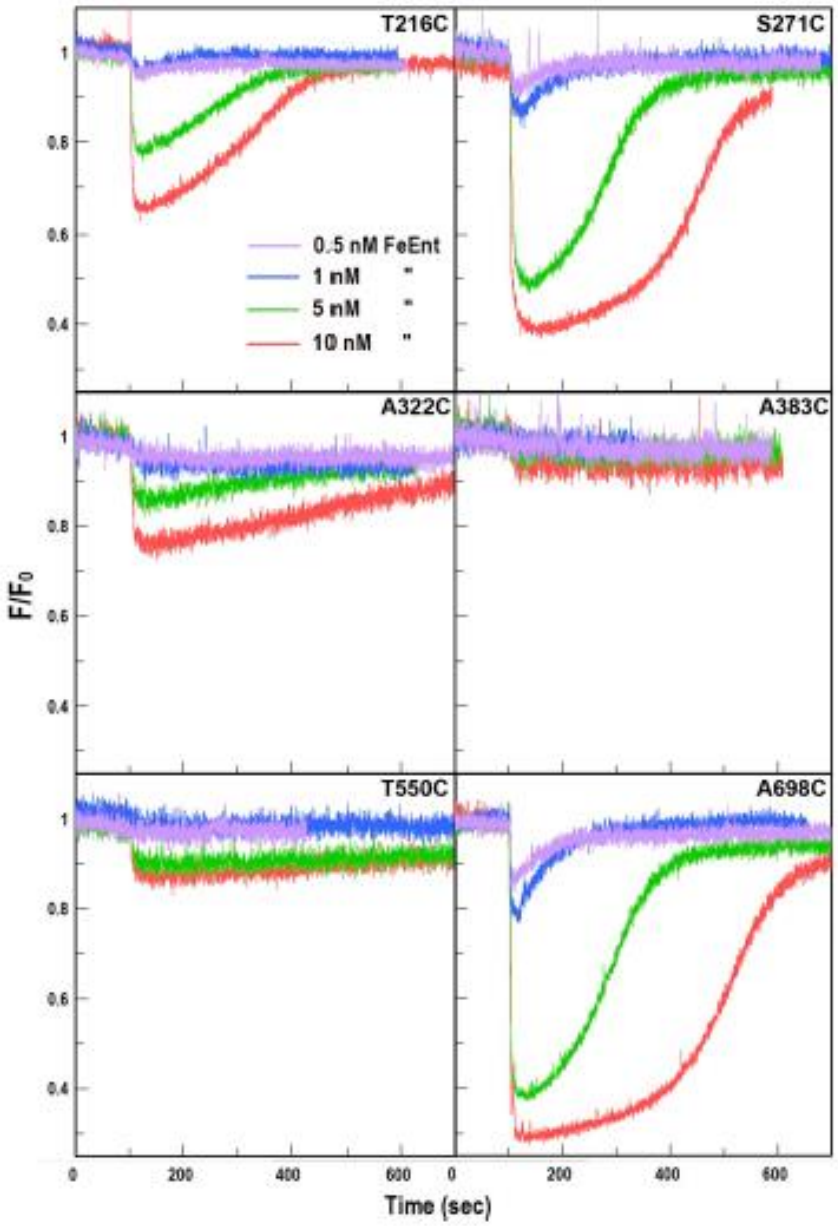

Fig. 5-3: Concentration dependence of FeEnt quenching and recovery (Smallwood et al. 2014).

5.3.3 Correspondence between fluorescence spectroscopic and radioisotopic measurements of FeEnt uptake

FM being a comparatively small fluorophore, is less likely to interfere with binding and transport functions of the protein. The transport rates of the individual fluoresceinated loops can be obtained from the $t_{1/2}$ of the elapsed time of recovery. We compared these to measurements of K_d, K_M and V_{max} of Cys mutants before and after fluoresceination

determined using conventional radioisotopic techniques in relation to WT binding and transport rates.

Table 5-1: Binding and transport by cells expressing FepA Cys substitutions (Smallwood et al. 2014.)

Site	Loop	Binding				Transport				
		<FM		>FM		<FM		>FM		
		K_d	Cap	K_d	Cap	K_M	Vmax	K_M	Vmax	$t_{1/2\ Rrecovery}$ (rank)
fepA+	NA	1.5	110.8	2.2	111.7	1.2	124	2.2	99.7	NA
T216C	2	0.8	27.8	5.22	18.5	2.1	86	2.1	40.6	103 (2)
S271C	3	2.1	97.8	4.0	90.4	1.5	93.5	2.3	67	69 (1)
A322C	4	2.9	65.4	4.3	30.7	1.7	68.8	4.3	21	193 (4)
A383C	5	6.7	91.9	4.7	20.7	3.0	50.4	6.2	35.6	630 (6)
S490C	7	15	64	90	22	8.9	65	57	35	700 (7)
T550C	8	1.7	53.2	3.3	30.7	2.2	125.7	2.9	29.5	315 (5)
A698C	11	1.1	18.5	4.7	36.7	1.9	124.2	2.8	96.3	165 (3)

These values also reflected the effect of the Cys substitutions by themselves (Table 5-1). These comparisons showed that the Cys substitutions had little impact on FepA binding affinity and transport in most cases. Three mutants, A322C, A383C and S490C transported at about half maximal rates even before fluoresceination. Modification by FM decreased affinity by <4-fold relative to WT except in for S490C-FM where affinity was drastically reduced (K_d = 90 nM; K_M = 57 nM). However, treatment with FM caused large reductions of 10-80% in Vmax values in almost all mutants compared to WT rate of ~100 pmol/min/10^9 cells. A698C and S271C were the least affected in transport capabilities and these findings corresponded with the relatively fast or slow recovery rates of the mutants in the spectroscopic data. Overall, the slight effect of FM modification on binding affinities of the mutants do not hinder us from making accurate measurements of rates of loop motion that lead to high-affinity binding. Impaired transport rates likely reflect steric interactions experienced by the FM-modified residues due to conformational changes in the protein during ligand internalization.

5.3.4 Effects of *ΔtonB* on ligand adsorption to FepA in vivo

Ligand binding in FhuA was reported to be TonB-dependent. We examined this nature of loop motion in case of FepA using fluorescence spectroscopy in *ΔtonB E. coli* cells. We expressed the seven loop Cys mutants (pITS23 variants) in OKN13 (*ΔfepA*, *ΔtonB*) and compared fluorescence observations upon FeEnt treatment with the OKN3 (*ΔfepA*) host strains. OKN13 strains harboring the Cys mutants always showed less quenching than the respective *tonB*+ strains suggesting loop motion is influenced by TonB. However, upon further investigation the lower level of quenching in *ΔtonB* bacteria was found to be related to the lesser expression of the FepA Cys mutants in *ΔtonB* cells compared to the OKN3 background. This led to decreased fluoresceination of FepA cysteines relative to the background labeling ultimately resulting in the perception of TonB-dependent loop motion.

5.3.5 Rates of FM quenching in different loops of FepA

Previously we had observed biphasic quenching of fluorescence in L3 when we monitored purified FepA E280C-FM in detergent solution (Payne et al., 1997). This suggested two phases of conformational motion. To study conformational motion of the other loops of FepA, we observed quenching of the seven FM labeled surface loops upon treatment with FeEnt. We tried two approaches: first we mixed FeEnt in to live bacteria in a cuvette by stirring. However, in this technique reagent mixing time made kinetic studies difficult because the individual quenching rates were too rapid to differentiate. Secondly, we attempted rapid mixing of FM labeled cells in a stopped-flow device. This method was rarely successful because high turbidity of the bacterial suspension hindered sufficient fluorescence intensity measurements. Hence, instead of using live cells, we generated outer membrane fragments of concentrated bacterial cultures by French pressing.

Thereby, we obtained clarified solutions of FM labeled FepA in native outer membrane environment. Upon rapid mixing with FeEnt, we observed much faster rates of ligand binding to FepA than previously reported (k = 0.8-6.4 s^{-1}) (Payne et al., 1997).

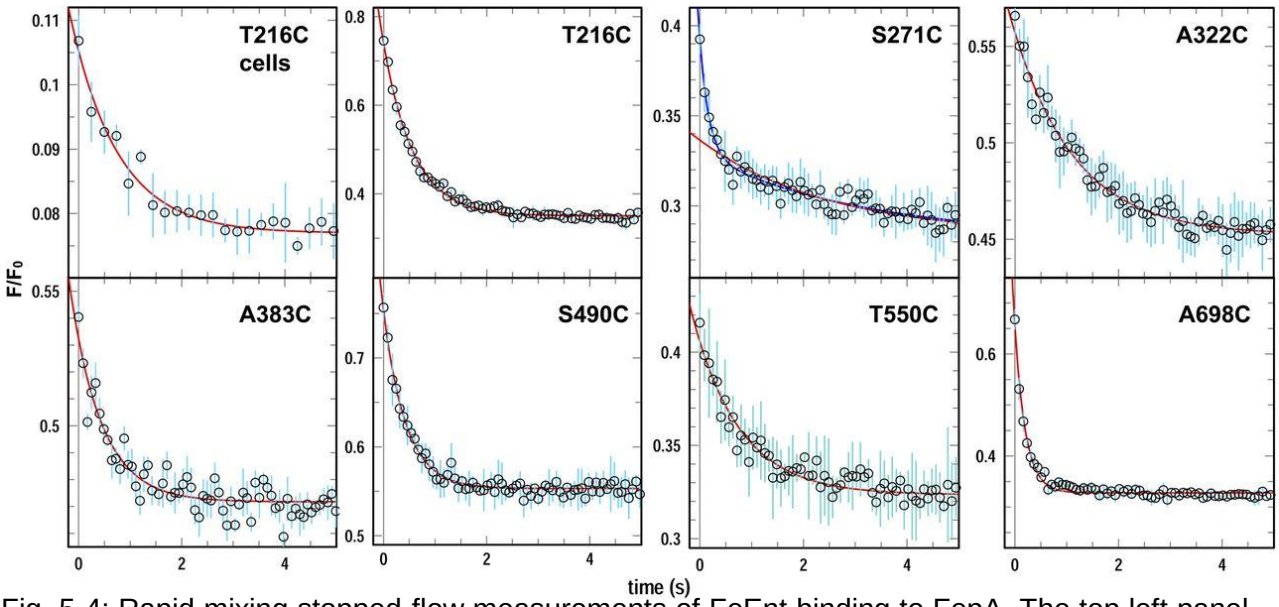

Fig. 5-4: Rapid mixing stopped-flow measurements of FeEnt binding to FepA. The top left panel shows data for FepAT216C-FM cells whereas the other panels show data obtained from rapid-mixing and stopped-flow experiments with outer membrane preparations (Smallwood et al. 2014).

Additionally, rates of FM quenching of the different loops varied, revealing a hierarchy of surface loop motion: S271C (L3) > A698C (L11) > S490C (L7) > T216C (L2) > T550C (L8) > A383C (L5) > S322C (L4) (Table 5-2). Fluorescence quenching data when fitted into exponential decay equations repeated our prior observation of biphasic kinetics. Conversely, all other loops showed single exponential decays (Fig. 5-4). The complex, two-stage closing mechanism of L3 may represent its interactions with other loops such as, adjacent L2 and L7 across the vestibule, as these loops come close to the ligand at slower rates while approaching binding equilibrium. Different loops close around FeEnt at different rates ultimately binding the ferric siderophore within a second or two.

Table 5-2: Differential rates of FM quenching in extracellular loops of FepA (Smallwood et al. 2014.)

Mutant	Loop	k (SE)	$t_{1/2}$	Rank
		s^{-1}	s	
T216[a]	2	1.08 (0.08)	0.64	7
T216	2	1.73 (0.04)	0.40	4
S271C[b]	3	5.72 (0.81); 0.31 (0.04)	0.12; 2.23	1
A322C	4	0.84 (0.05)	0.83	8
A383C	5	1.64 (0.15)	0.43	5
S490C	7	2.32 (0.13)	0.30	3
T550C	8	1.09 (0.06)	0.64	6
A698C	11	4.90 (0.18)	0.14	2

5.3.6 Bulk observations of FeEnt transport in living cells

Previously, fluorescence microscopic observation of labeled FepA and GFP-TonB fusion proteins in cells revealed an uneven distribution of TonB across the cell. TonB were localized to the center of the cell although FepA were present all over the cell surface. This raised questions on how polar FepAs transport FeEnt since mechanistically, the receptor interacts directly with TonB during transport (Cadieux et al., 2000; Pawelek et al., 2006). Hence, we attempted to use fluorescence microscopy to observe transport activity of FepA proteins at different locations of the cell in alignment with our fluorescence spectroscopic studies. Bulk observation of OKN13 (*ΔfepA*, *ΔtonB*) cells with expressing FepAS271C labeled with A546M and GFP-TonB after addition of 5 nM FeEnt showed uniform decrease of fluorescence intensity upon binding and consequent recovery over time at the same rate all over the cell surface (Fig. 5-5). GFP-TonB were again absent at the poles and presented at lower frequency and hence lower fluorescence intensity in the cells. Thus, uniform uptake rates of FeEnt by FepA across the cell with centrally restricted

TonB suggests further complexities in the mechanism of FepA-TonB interaction than yet understood.

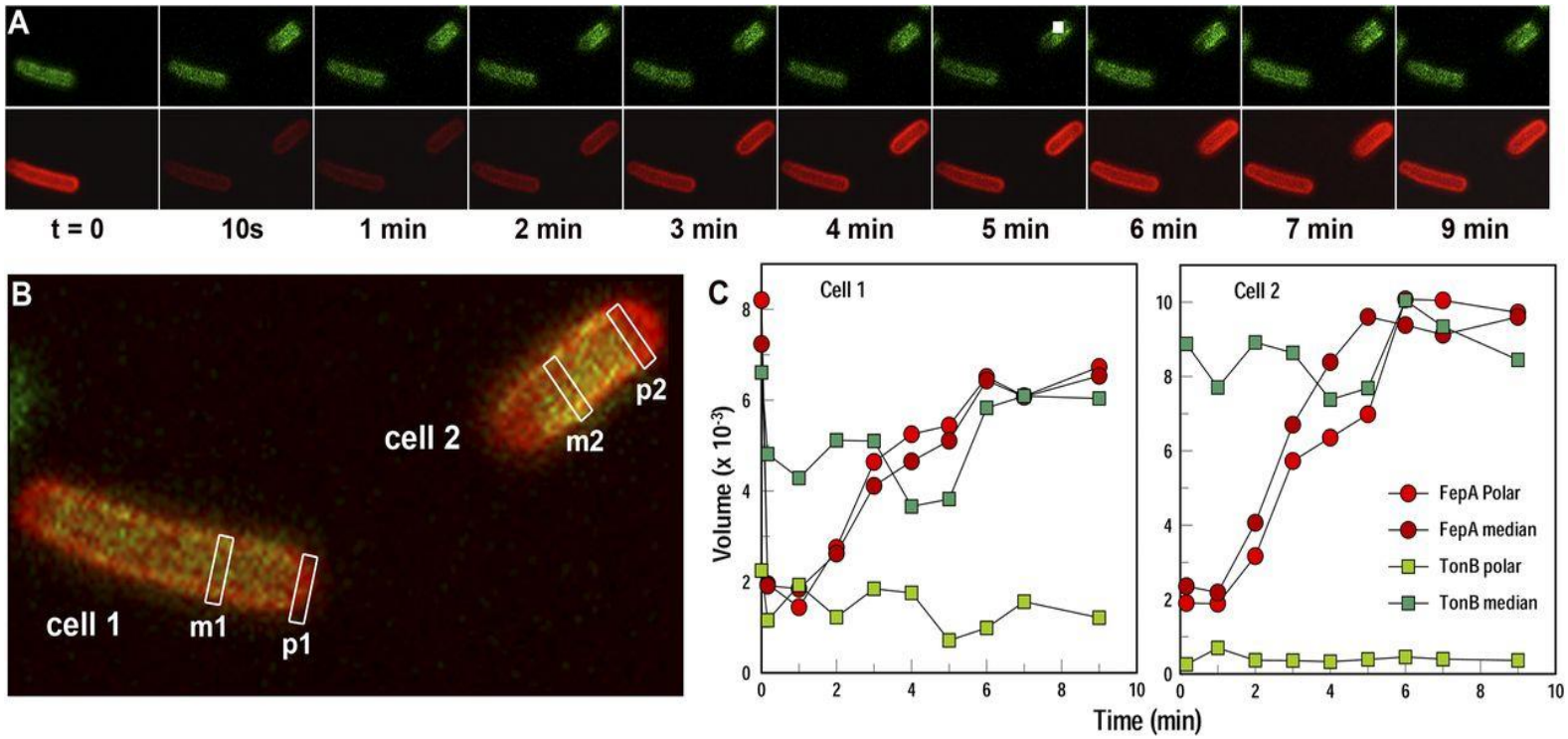

Fig. 5-5: Observation of FeEnt binding and transport in single cell by Confocal microscopy. A) Shows the response of GFP-TonB and FepAS271C-FM (top and bottom respectively) when 10nM FeEnt was added to the system at t = 0 minute. B) The two-colored images were superimposed at a 6-minute time point. The polar region of the cell is designated as ‘p’ and the median as ‘m’. C) Fluorescence intensity analysis of the image in ImageQuant revealed that the TonB dependent iron transport by FepA occurs with same kinetics throughout the OM despite the apparent absence of TonB from the poles of the cells (Smallwood et al. 2014.).

Chapter 6: TonB-Dependent Heme/Hemoglobin Utilization by *Caulobacter crescentus* HutA

Balhesteros H, Shipelskiy Y, Long NJ, Majumdar A, Katz BB, Santos NM, Leaden L, Newton SM, Marques MV, Klebba PE. J Bacteriol. 2017 Mar 15; 199(6): e00723-16.

6.1 Introduction

Caulobacter crescentus is a free-living Gram-negative, fresh-water aquatic α-proteobacterium growing in oligotrophic environments. It is a popular productive model organism for the study of bacterial cell-cycle regulation and asymmetrical cell division owing to its dimorphic form of life cycle differentiating into sessile, stalked and motile, flagellated forms (Jenal et al., 2002). The bacterium is also interesting from possessing 62 putative TBDTs in a similar sized genome as E. coli (Nierman et al., 2001). In comparison, E. coli encodes only 8, all of which are involved in transport of metals. Abundance of TBDTs in bacteria in aquatic environment is not uncommon. Members of the marine bacterial genera *Citromicrobium* and *Sphingomonas* have been reported to also possess large number TBDTs in their genomes (Tang et al., 2012). Hence, TBDTs have been implicated in the scavenging of carbohydrates substrates such as maltose, sucrose, xylan, N-acetyl glucosamine, N-acteyl chitin oligosaccharides (Neugabaeur et al., 2005; Blanvillain et al., 2007; Lohmiller et al., 2008; DeJean et al., 2013; Eisenbeis et al., 2008), molecules which are likely to be found in aquatic oligotrophic environments. In the absence of micromolar levels of these substrates that is required for passage by general or facilitated diffusion, TBDTs might be able to promote better acquisition of nutrients.

Detailed descriptions of the iron-uptake systems in *C. crescentus* are lacking. Genomic and bioinformatic analyses predict the presence of TBDTs involved in iron transport, but biochemical data on the transporters are very limited. Previously, *C. crescentus* was reported to utilize two hydroxamate siderophores Ferrioxamine B and Ferric-rhodotorulate (Neugabaeur et al., 2005) although the genome lacks presence of recognizable siderophore biosynthesis genes (Nierman et al., 2001). The large number of predicted TBDTs in the OM, hinted on the likely presence of more Fur regulated TBDTs of iron in this bacterium.

Our work shed more light on iron transport in *C. crescentus*. By screening a library of ferric siderophores for uptake by NA1000, the synchronizable derivative of wild-type *C. crescentus* CB15, we identified that it utilizes several ferric hydroxamates, mixed chelates as well as the iron porphyrins, heme/hemin and hemoglobin. Interestingly, *C. crescentus* did not show uptake of ferric catecholates allowing us to exploit apo-enterobactin as a specific chelator for iron deprivation in complex media. Using such growth conditions, we performed MS analysis of cell envelope proteins and identified five TBDTs that are iron-modulated. Deletion of one of the loci *Ccr 02277* led to loss of hemin/hemoglobin uptake capability in the strain. We named this protein HutA, as an outer membrane TBDT of the hemin/hemoglobin utilization system in *Caulobacter crescentus*.

6.2 Methods

We extensively used siderophore nutrition tests to survey siderophores utilized by *C*. *cresentus* NA1000. After overnight growth in NB containing 0.5mM $Cacl_2$, we subcultured the strain in NB and grew till OD_{600}nm ~0.3 by shaking at 30°C. We mixed 200µL of bacteria in 20mL NB top agar containing either 200µM 2,2'-bipyridyl (BP) or

100µM enterobactin (Ent) and poured in standard petri plates. Once the agar solidified, we placed 6 or more sterile paper discs on the surface and added 10µL of a 50µM solution of Ferric-siderophore to each disc. After 24hour incubation at 30°C, we measured the diameter of the halos of bacterial growth around the discs.

To monitor growth of *C. cresentus*, we diluted overnight cultures in NB to an OD_{600}nm of 0.05 and continued growing till OD_{600}nm of 0.2. At this point we divided the culture into aliquots, added either BP to 50, 100 or 200 µM final concentrations, or 100µM Ent and left one without addition as a control. We took OD_{600}nm measurements at regular intervals and after 18 hours we again split the cultures into equal halves and added ferrichrome to 10µM to one half of the cultures. By taking further OD_{600}nm measurements we could study growth rates in iron replete and iron deficient conditions.

For [^{59}Fe]Fc binding and transport determinations, we followed similar methods as used in E. coli. We grew cells in NB with Ent added to 100 µM at OD600nm 0.3 and grew them for another 3 hours. For binding measurements, we spun down the cells, chilled them on ice for 1 hour and measured Kd and capacity by fitting the amount of radioactivity bound by filtered aliquots of cells exposed to a range of concentrations of [^{59}Fe]Fc for 5 seconds into Grafit software. For Km and Vmax measurements, we directly used the cells at 30°C without chilling and filtered aliquots of cells exposed to different concentrations of [^{59}Fe]Fc at 5 second and 185 second to measure transport over a 3 minute period. We repeated each experiment thrice to obtain Sd and SE values. Since in E. coli uptake of ferric citrate (FeCit) is induced by the presence of extracellular citrate, we grew NA1000 in NB in the presence of both Ent and Cit at 100 µM for 3 hours. We then washed the cells twice in phosphate-buffered saline (PBS) containing 0.2% glucose. To study

accumulation of radioactive ligand over time, we added 1 µM [^{59}Fe]Cit (50-fold molar excess) and filtered cells in triplicate at different time points for 1 hour. To determine Km and Vmax we performed similar filter-binding assays as for [^{59}Fe]Fc.

To perform bioinformatic analyses of sequences, we aligned complete sequences of putative TBDTs of *C. crescentus*, from homology to E. coli FepA using CLUSTALW2. We then analyzed sequence relationships among the proteins by separate CLUSTALW2 comparisons of their TonB boxes, N-domains, C-domains and full-length mature proteins to separate them out into different clads. Deletion of locus Ccr02277 to make strain MM90 was done by homologous replacement in NA1000 by the Marquilis lab in Universidade de Sa Paulo, Brazil.

We performed detergent extractions of cell envelope proteins of *C. crescentus* cells grown in NB either 50 µM $FeSO_4$ (iron-replete condition) or 100 µM enterobactin (iron-deficient condition). We lysed the cells by passing through French Press at 14,000 psi twice, separated the membranes by high-speed centrifugation and resuspended the pelleted membranes in PBS. We then treated them with 0.1 to 0.5% sodium sarcosinate (Sarkosyl) for 20 minutes at 4ºC to solubilize cell envelope proteins. Following centrifugation at 13,000 rpm for 1 hour we separated the sarkosyl-soluble (supernatant) and sarkosyl-insoluble (pellet) fractions. Lysate and cell envelope proteins were then analyzed on SDS-PAGE after staining with Coomassie Blue. We excised protein bands of interest from the stained gels and subjected them to Matrix-assisted Laser Desorption Ionisation-Time of Flight (MALDI-TOF) mass spectrometry analysis using a 2,5-dihydroxybenzoic acid matrix. We processed the data using mMass software (http:

://www.mmass.org) and identified protein candidates by matching with similar peptides from BLASTP analysis of *C. crescentus* genome (KEGG strain NA1000).

6.3 Results and Discussion

6.3.1 Siderophore nutrition tests with *C. crescentus*

From preliminary siderophore nutrition tests with 200 µM 2,2'-bipyridyl as the non-utilizable iron chelator in NB, we were able to identify the siderophores utilized by *C. crescentus* (Fig. 6-1) The data revealed that *C. crescentus* utilizes several hydroxamate siderophores like Ferrichrome but not catecholates like Ferric enterobactin. This finding allowed us to employ enterobactin in complex media to render *C. crescentus* iron deficient. Enterobactin being a specific chelator of Fe^{3+} compared to bipyridyl which complexes many cations, yielded more well-defined, denser halos when included in siderophore nutrition tests in NB medium. We found that *C. crescentus* also utilizes the iron porphyrins, hemin and hemoglobin.

Fig. 6-1: Siderophore nutrition tests with *C. crescentus*. Strain NA1000 was grown in NB to mid-log phase, and 100 µl of the culture was plated on an NB plate in NB top agar containing enterobactin (100 µM). After solidification of the top agar, filter discs were placed on the surface

of the agar, and 10 µl of 50 µM solutions of ferric siderophore complexes were applied to the discs: 1, asperchrome B1; 2, ferrichrome; 3, ferrichrome A; 4, malonichrome; 5, ferrioxamine B; 6, tetraglycyl ferrichrome; 7, rhodotorulate; 8, aerobactin; 9, $FeS0_4$; 10, hemin; 11, hemoglobin (15 µM); 12, dimerum acid; 13, mycobactin; 14, schizokinen; 15, coprogen; 16, vibriobactin; 17, corynebactin; and 18, agrobactin. Re-produced with permission from American Society for Microbiology.

6.3.2 Growth in iron-deficient media

We studied growth of NA1000 in NB media that we rendered iron-deficient by adding either bipyridyl or enterobactin. On increasing the concentration of bipyridyl, the maximum growth retardation was seen at 200 µM while, enterobactin was effective at 100 µM in reducing the growth rate by 4 hours. Compared to control cells (no addition), both compounds reduced growth rates in 18 hours to 70%. The increased doubling time was relieved from 10 hours to 4 hours by adding 10 µM ferrichrome after 18 hours to the enterobactin added cultures. However, the bipyridyl treated cultures did not recover emphasizing on the effects of non-specific chelation of divalent cations such as Ca^{2+} by bipyridyl which is essential for growth in NA1000 (Fig. 6-2).

6.3.3 Identification of potential iron transporters

Using the 8 ferric siderophore and porphyrin receptors of E. coli as a basis for comparison in CLUSTALW2 alignments of protein sequences, we found that the 62 TBDTs in the *C. crescentus* fall in 4 different phylogenetic branches. The full-length TBDTs of E. coli, which are all metal transporters, sub-divided into 2 clades or branches of the phylogenetic tree. The catecholate transporters FepA and Cir, the porphyrin

receptor BtuB and the ferric aerobactin receptor LutA segregated into one branch whereas, the ferric hydroxamate receptors FhuA, FhuE,

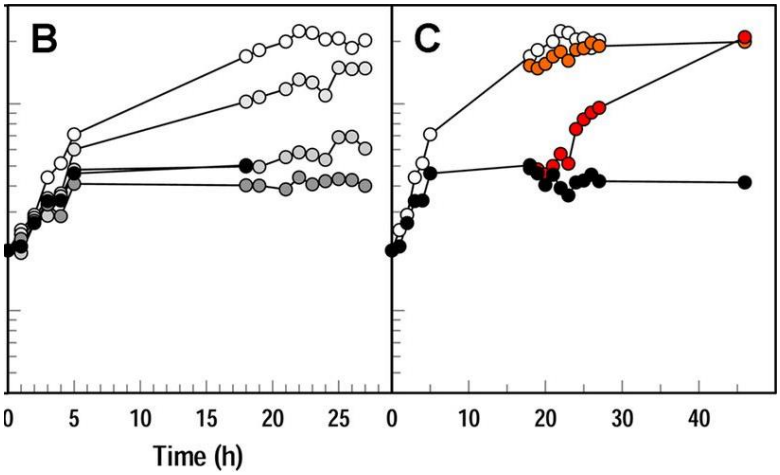

Fig. 6-2: Growth of *C. crescentus* NA1000 in iron-deficient media. Panel (B) from the original figure shows concentration dependence of inhibition of growth by BP. White circles show growth in NB; darkening shades of gray circles show the effects of 50, 100, and 200 μM BP, and black circles show the effects of 100 μM enterobactin, added at 5 h. Panel (C) show addition of ferrichrome restores growth. We added ferrichrome (10 μM) to NA1000 growing in NB (○) or NB plus 100 μM enterobactin (•) (from panel B) at 19 h (orange and red circles), and it restored the original growth rates. adapted in part with permission from American Society for Microbiology.

FecA and Fiu fell in another branch. Alignment of N-domain sequences of E. coli TBDTs, yielded same results as the full-length proteins, and C-domain alignments clustered all the iron transporters in one branch and only the Vit.B12 transporter BtuB in another one. Finally, all TonB box sequences of E. coli TBDTs fell in one branch distinct from those of the *C. crescentus* TBDTs. *C. crescentus* overexpresses TBDTs in both iron-deficient and iron-replete conditions. Such transporters are also under negative and positive regulation

respectively by Fur (da Silva et al. 2009). The TBDTs that are overexpressed in iron-depleted conditions, 00028, 00138, 02277 and 03023 fell in two branches of the CLUSTALW2 comparisons with E. coli TBDTs. These four proteins contain 20 -25% overall sequence identity with E. coli TonB-dependent OM porins and also a recognizable TonB box sequence near their N-termini. Ccr02277 bears closest homology with and falls in the group containing the E. coli catecholate transporters FepA and Cir and porphyrin receptor BtuB. On the other hand, Ccr00028, Ccr00138 and Ccr03023 bear closest relationship to the E. coli hydroxamate receptors. This comparative analysis pointed towards the structural identities of 00028, 00138, 02277, 03023 with ferric siderophore transporter which combined with their Fur-regulated, enhanced expression under iron-deficient conditions, suggest that these proteins are iron transporters in *C. crescentus*. TBDTs which show upregulation in iron-replete conditions (Ccr 00210) or downregulation under iron-limitation or in *fur* mutant (03263, 03444, 01042, 03574, 03227) (daSilva) with the exceptions (01155 and 02895), all lie together in a separate branch exclusive of any E. coli iron transporters. At present, it is difficult to predict physiological functions of these transporters.

6.3.4 Iron-regulated cell envelope proteins

Based on bioinformatic prediction of TonB dependent OM proteins of *C. crescentus*, we performed extraction of cell envelope proteins to identify the iroregulated OM porins. We grew NA1000 in NB in either iron-sufficient or iron-deficient conditions, and harvested the cells, lysed them, and pelleted the membranes by spinning and finally solubilized the membrane proteins with Sarkosyl. The percentage of sarkosyl used and the incubation time, played crucial roles in the efficient separation of OM proteins from

the IM ones. Use of 0.1% Sarkosyl for 20 minutes at 4ºC showed ideal separation of TBDTs (OM proteins) as an insoluble pellet compared to 0.5% sarkosyl for 30 minutes at 25ºC. Treatment with Sarkosyl improved resolution of the proteins on SDS-PAGE and revealed numerous iron-regulated cell envelope proteins in iron-deprived cultures. We also attempted to separate IM and OM proteins by isopycnic sucrose-gradient centrifugation but despite apparent separation of the two fractions, we did not see efficient fractionation of the proteins in SDS-PAGE. Both lanes on the polyacrylamide gels showed very similar profiles, suggesting inefficient separation of membranes.

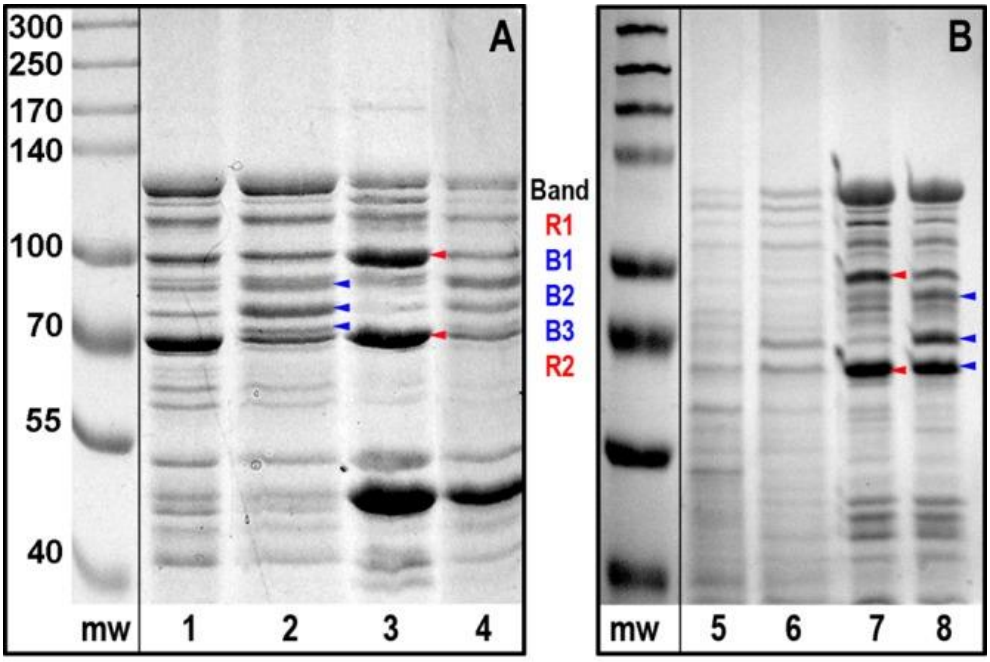

Band	Mass	Coverage (%)	Intensity (%)	Identity
R1	85,581	65.0	66.0	00210
B1	78,234	59.1	51.5	00028
B2	75,525	70.7	48.6	02277
B3	74,322	83.9	50.9	03023
R2	69,198	65.7	15.4	01196

Fig.: 6-3: SDS-PAGE showing expression of iron-regulated proteins in NA1000 grown in iron-replete (odd lanes) or iron-deficient (even lanes) media. In panel A) cell envelope fractions were solubilized in 0.5% Sarkosyl and in panel B) with 0.1%. Re-produced with permission from American Society for Microbiology.

To identify proteins related to iron transport, we excised bands from the gels, trypsin-treated and subjected them to MALDI-TOF/MS analysis. We matched them to predicted tryptic digestion patterns of *C. crescentus* TBDTs which revealed several iron-regulated proteins in the samples. As observed before, 00028, 02277, and 03023 were over-expressed in iron-deficient conditions (da Silva et al., 2013). The predicted masses of the three mature proteins also matched with their expected positions on SDS-PAGE. Two proteins were overexpressed in iron-replete condition: 00210 and 01196. Previously, 00210 has been identified as an iron-regulated TBDT but 01196 was described as a virulence protein. It showed 18% identity with EcoFepA which combined with its upregulated expression in iron-rich conditions, led us to identify it as an iron-regulated TBDT as well.

6.3.5 Ccr02277 (HutA) is a receptor for heme/hemoglobin

Ccr02277, which showed overexpression in iron-starvation conditions as well as in a Fur mutant (DaSilva Neto et al., 2009) bears 25% sequence identity with EcoCir. Identity with EcoFepA and EcoBtuB were only slightly less at 23% and 22% respectively and it also included a distinctive TonB box sequence (DKVTVTAT). These data hinted at Ccr02277 being a TonB dependent OM transporter. Consequently, we engineered a precise deletion of ccr02277 to create the strain MM90. MM90 was deficient in acquisition of hemin or hemoglobin in siderophore nutrition tests. We confirmed the deletion by lack of the 75.5 KDa band on SDS-PAGE gels of Sarkosyl extracted cell envelopes (Fig. 6-4). This led us to name the locus *hutA* for its role in hemin/hemoglobin utilization.

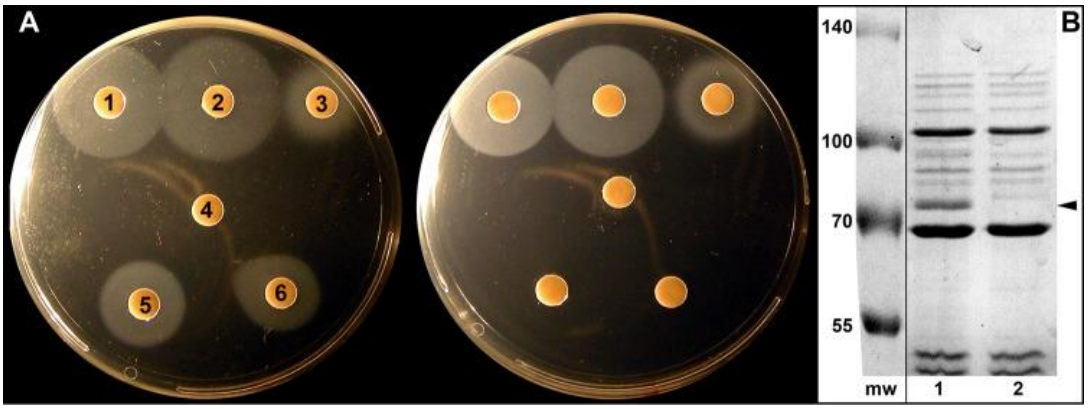

Fig. 6-4: Siderophore nutrition test showing inability of ccr_02277 (ΔhutA) to utilize heme and hemoglobin (A) and SDS-PAGE gel lacking the ccr_02277 band in the deletion mutant. Re-produced with permission from American Society for Microbiology.

6.3.6 Radioisotopic measurements of iron binding and transport

We performed quantitative measurements of the binding and transport of [^{59}Fe]apo-Ferrichrome ([^{59}Fe]Fc) by NA1000. By performing filter binding assays at a range of substrate concentrations at 0ºC, we were able to measure K_D and binding capacity of [^{59}Fe]Fc binding by *C. crescentus*. It showed high-affinity recognition of substrate with K_D and capacity being 1.4 nM and 26 pmol/10^9 cells respectively. I performed similar filtration assays at 37ºC to determine transport rate Vmax and Km of [^{59}Fe]Fc by *C. crescentus*. I mixed measured quantities of cells with different amounts of radioactive substrate in duplicate and filtered one of the mixtures at 5 sec and the other at 185 sec. By subtracting the radioactivity accumulated on the filters at these two time points, I was able to determine the transport occurring over 3 minutes. By fitting the data in an enzyme kinetics curve in the Grafit software, I obtained Km and Vmax values as 0.03 nM and 19 pmol/10^9 cells. This experiment was performed twice to obtain statistical validation of the data. The transport rate was comparable to chromosomally encoded uptake rate of Ferrichrome by *E. coli*.

The *C. crescentus* NA1000 chromosome encodes four potential TBDTs with N-terminal homology to E. coli FecA suggesting potential for capability of Ferric citrate uptake. We characterized uptake of [^{59}Fe]-citrate ([^{59}Fe]Cit) by NA1000 through filter binding assays. Since, in E. coli expression of FecA is induced by external FeCit, we grew NA1000 in the presence of enterobactin and/or 100 µM citrate. This led to comparable uptake of [^{59}Fe]Cit by the strain like [^{59}Fe]Fc with Km of 5 nM and Vmax of 29 pmol/min/10^9 cells). Inhibition of uptake by 0.5 mM carbonyl m-cholorophenyl hydrazine (CCCP) indicated the TonB-dependent nature of the process.

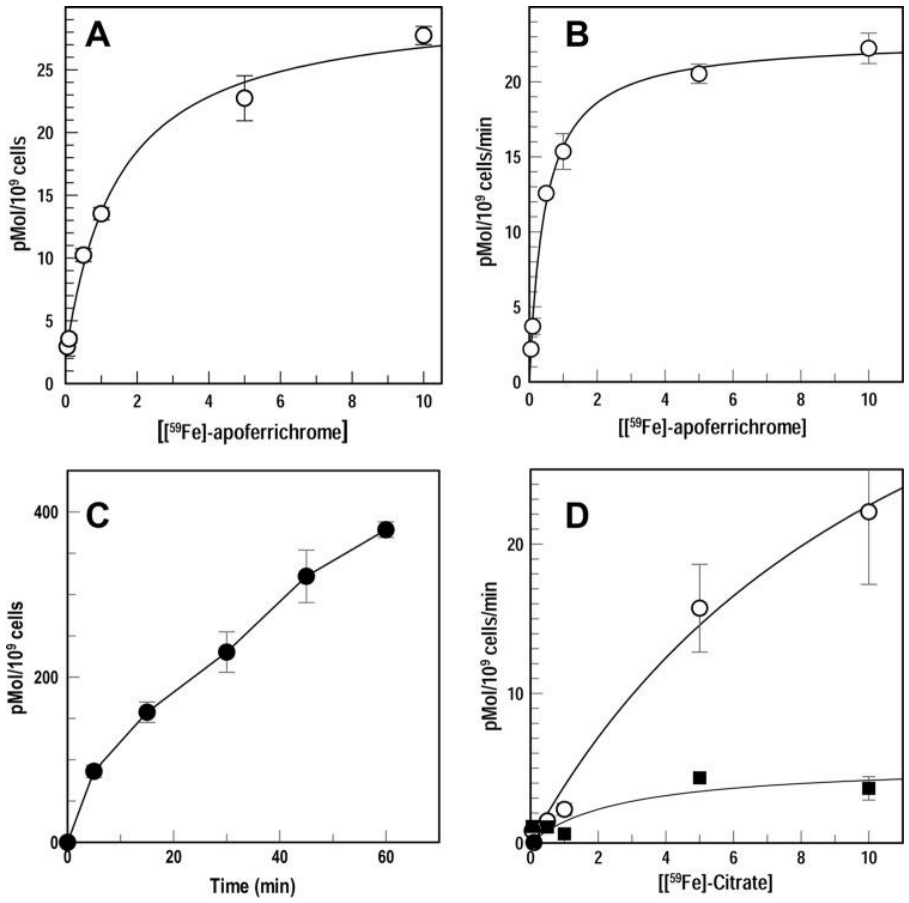

Fig. 6-5: Binding and uptake of [^{59}Fe]Fc and [^{59}Fe]Cit by *C. crescentus*. We measured binding (A) and uptake (B) of [^{59}Fe]Fc by filtration assays (C) We exposed NA1000 to [59Fe]Cit and measured accumulation of the radionuclide for 1 h. (D) Lastly, we measured the uptake of increasing

concentrations of [^{59}Fe]Cit by NA1000 in the absence (circles) or presence (squares) of 0.5 mM CCCP. Re-used with permission from American Society for Microbiology.

Chapter 7: Fluorescence High-Throughput Screening for Inhibitors of TonB Action

Nairn BL, Eliasson OS, Hyder DR, Long NJ, Majumdar A, Chakravorty S, McDonald P, Roy A, Newton SM, Klebba PE. J Bacteriol. 2017 May 15; 199(10): e00889-16.

7.1 Introduction

Bacteria often elaborate multiple iron-acquisition strategies to overcome the challenge of extremely low concentrations of iron in the host environment. Most Gram-negative bacteria utilize siderophores all of which, require energy-dependent transporters to import the iron-bound siderophores across the cell envelopes against the concentration gradient. Energy is also necessary to induce conformational changes in the OM ligand-gated transporters to open their occluded channels. Since, the only feasible source of energy in the Gram-negative OM is the *pmf* of the IM, which can be transduced to the OM by TonB and its accessory proteins ExbBD, these LGPs are invariably TonB-dependent. Hence, inhibition of the TonB complex can possibly mitigate universal effects on siderophore-mediated iron acquisition in bacteria.

A surge of antibiotic resistance among bacteria has evoked search for novel antimicrobials against alternative targets. Particularly, the CRE/ESKAPE pathogens which include Carbapenem-resistant *Enterobacteriaceae*/*Enterococcus faecium*, *Staphylococcus aureus*, *Klebsiella pneumoniae*, *Acinetobacter baumannii*, *Pseudomonas aeruginosa* and *Enterobacter* species, are often multi-drug and pan-drug resistant in nosocomial environment making them serious threats to human health and disease management. Iron acquisition pathways in bacteria is a promising target for

inhibitory drugs since, perturbation of these mechanisms can exert bacteriostatic effects making it easier for conventional antibiotics to effectively fight infection.

Fluorescence labeling of site-directed Cys sulfhydryls in FepA, the TonB-dependent transporter of the ubiquitous catecholate siderophore ferric enterobactin, allows real-time spectroscopic observation of FeEnt transport in live cells. Binding of FeEnt, quenches the fluorescence of labeled FepA since conformational changes in FepA extracellular loops relocalizes the fluor to a quenching environment (Cao et al., 2002, Smallwood et al., 2014). But as the bacteria internalize the FeEnt and gradually deplete it from solution, the fluorescence rebounds. Agents such as ionophores which disrupt IM *pmf* and interferes with TonB function, prevents the recovery of fluorescence. With the ability to detect transport of even nanomolar concentrations of FeEnt, spectroscopic observation of ligand binding-mediated quenching of fluorescence and subsequent recovery, can identify compounds that prevent TonB-dependent, FeEnt uptake by FepA and hence interfere with fluorescence recovery in a dose-dependent fashion.

Using this assay, previously optimized by Hanson et al. (2015) to high-throughput screening (HTS) standards, we screened 17,441 compounds to identify inhibitors of TonB-dependent transport of FeEnt by FepA in live E. coli cells. The experiments revealed numerous compounds that also interfered with the ability to transport FeEnt and Ferrichrome as well as Colicin B and Ia killing, all of which are dependent on TonB-ExbBD activity. We verified their TonB-dependent nature by excluding perturbation of lactose transport which is also dependent on *pmf* thereby, distinguishing between energy poisons and TonB inhibitors. We extended the application of this method to the Gram negative ESKAPE pathogen *Acinetobacter baumanii* which is causes a range of infections in

intensive-care units worldwide and is a leading cause of ventilator-associated pneumonia. It forms persistent biofilms on abiotic surfaces in nosocomial environments (Vidal et al., 1996) and the high-incidence of multi– and pan-drug resistant strains makes it a priority threat (Doyle et al., 2011; Durante-Mangoni et al., 2011). *A. baumanii* utilizes FeEnt under iron-limiting conditions and FepA (AbaFepA) is required for full virulence in a sepsis model of infection. We identified the *A. baumanii* fepA gene and characterized FeEnt transport by AbaFepA. We engineered Cys residues in AbaFepA and adapted the system for FLHTS in *A. baumanii*. We tested some of the compounds identified in the E. coli screen in *A. baumanii* and showed the validity of FLHTS strategy against even distantly-related Gram-negative pathogens.

7.2 Methods

We grew E. coli MG1655 and BN1071 derivatives and A. baumanii ATCC strain 17978 or its *ΔfepA* derivative in LB at 37°C with aeration. For iron-deprivation, we used MOPS media to grow cells.

For generation of the *A. baumannii ΔfepA* derivative, we PCR amplified approximately 1000 bp of DNA in both upstream and downstream of the ORF and stitched them together with the PCR-amplified suicide-vector pFLP2 using the NEBuilder HiFi cloning kit (New England Biolabs) for Gibson assembly method (Gibson et al., 2009). After verifying the resulting construct by sequencing, we electroporated it into A. baumanii and selected integrants on LBAmp500 agar. We selected for merodiploids by patching transformants onto LBAmp500 or LB with 10% sucrose; merodiploids were Amp^R and sucrose sensitive. To excise the integrated plasmid, we grew the merodiploid strains overnight in LB at 37°C with shaking, then serially diluted the cultures, and plated them

for single colonies on LB agar with 10% sucrose. We patched the transformants on LBAmp500 and LB agar and the screened the Amp^S colonies obtained for the loss of *fepA* by PCR.

For site-directed mutagenesis and fluorescence labeling of Cys, we used a QuikChange II XL mutagenesis kit and expressed FepA in WT or complemented strains by growing in MOPS media. We labeled the live bacteria with fluorescein maleimide following protocols used for E. coli. For fluorescence spectroscopy, we used an upgraded version of the SLM/OLIS spectrofluorometer at emission/excitation wavelengths 490/520nm and collected readings for cells diluted to 2.5 X 10^7/mL in 2 mL of PBS plus 0.4% glucose or sodium acetate. We added FeEnt to the desired final concentration, and monitored changes in fluorescence emissions during its binding and transport in absence or presence of inhibitor molecules. We optimized the procedure in microtiter format using the Tecan GENios microplate reader (TECAN, Switzerland) using fresh or frozen labeled cells to black, round-bottom 96-well or 384-well plates to a 190 µL or 95 µL total volume in same buffer as in SLM. For all fluorescence assays, we normalized raw fluorescence volts readings (F) with respect to the initial fluorescence (F_0) and calculated Z' factor for the positive and negative controls: $Z' = 1 - (3*\sigma_{+c} + \sigma_{-c})/(|\mu_{-c} - \mu_{+c}|)$.

The FLHTS assay was carried out at the University of Kansas HTS facility. We reconstituted frozen cells in PBS plus or minus CCCP prior to the assay and then used 2 X 10^7 cells/mL in a 384-well format to screen a total of 17,441 compounds in the BioTek Synergy microplate reader measuring initial fluorescence (F1), quenched fluorescence 1 min after FeEnt addition (F2) and recovered fluorescence 60 to 80 min following addition of FeEnt and incubation at 37°C (F3). We included labeled cells plus FeEnt and 100 µM

CCCP on the same plate. To identify primary hits, we calculated Z' scores for each plate and plotted a scattergram of all compounds to determine the median and standard deviation. We cherry-picked 165 compounds that showed greater than 2 SD from the mean of all compounds which we further categorized into three types based on the percentage of inhibition. We performed secondary analysis of 20 compounds which showed >30% inhibition.

For secondary screening of the 20 compounds, we analyzed their effects in siderophore nutrition tests. We performed the tests with same protocol as before, but with the addition of 100 µM final concentration of each compound into the agar before placing the filter discs and addition of 10 µL of 50 µM FeEnt or Fc to the discs. DMSO, which was used to dissolve the compounds was tested alongside as well as a positive control with 15 or 20 µM CCCP added to the agar. To assess the influence of primary hits on colicin killing tests, we determined the titer of each of the colicins B and Ia in absence and presence of the 20 hit compounds. To perform the assay, we serially diluted MG1655 cells sub-cultured in MOPS to a concentration of 1 X 10^4CFU/mL and incubated a sub-toxic concentration of each compound with 100 µL aliquots of cells for 15 minutes at 37°C. We added a predetermined amount of ColB or Ia to the mixture and and incubated it for another 15 minutes, followed by plating on LB agar. After incubation at 37°C for 16 hours we counted the number of colonies and determined the number of colicin hits per cell. We performed each experiment three times and expressed the data as average of either percentage of killing or percentage of survival.

We determined Minimal Inhibitory Concentrations (MICs) of compounds in E. coli MG1655 or *A. baumannii* ATCC17987 by sub-culturing 1% overnight cultures in LB in a

range of concentration in a 2-fold dilution series: 0.25 – 512 µM. Untreated E. coli and E. coli with added DMSO in corresponding volumes acted as controls.

To monitor growth of *A. baumannii* WT and *ΔfepA* strains we subcultured the bacteria in MOPS with or without 100 µM apo-FcA and measured OD600nm at regular intervals over 8 hours. To evaluate growth in presence of FeEnt as an iron source, we added 1 µM FeEnt to the MOPS medium and measured growth over 8 hour period.

We performed [^{59}Fe]Ent accumulation and transport kinetics assays in *A. baumannii* in the same way as described before for E. coli. We replaced glucose with 50 mM sodium acetate as the carbon source in minimal media for *A. baumannii*. To determine effect of target compounds we incubated the E. coli MG1655 cells with respective concentrations of inhibitors for 0.5 hour at 37°C immediately before adding 1 µM [^{59}Fe]Ent and filtering the cells. To distinguish TonB dependent inhibitors from proton ionophores, we grew MG1655 cells in MOPS with 0.4% sodium succinate as the carbon source for 3.5 hours, induced with isopropyl-β-D-thiogalactopyranoside (IPTG) to 0.1 mM with shaking for another 2 hours. We spun down the cells, resuspended in same volume of Kpi (pH:7.0) with 10 mM MgSO4 and then added respective concentrations of the target compounds. Immediately afterwards, we added [14C]-lactose to 10 mM and filtered aliquots of cells at 5, 15, 30 and 45 minutes at 37°C in triplicate and washed with 5 mL of 100 mM Kpi (pH:5.5)/100 mM LiCl and counted the radioactivity accumulated in the cells.

7.3 Results and Discussion

7.3.1 FLHTS for inhibitors of TonB-dependent FeEnt transport by FepA

We attempted to identify small molecule inhibitors of TonB-dependent ferric siderophore transport by the FLHTS approach in the 384-well format. We spectroscopically observed transport of FeEnt in fluorescein labeled FepA in live cells. The specific response of fluorescence quenching by addition of FeEnt and subsequent recovery after transport into $TonB^+$ cells, allowed us to evaluate the effect of small molecule inhibitors that abrogate or hamper the transport process. We customized the assay to the 384-well format to increase efficiency and used cryopreserved cells, which behaved in the same way as freshly labeled cells, to conduct small-scale FLHTS of 17,441 compounds (4 compound libraries) at the University of Kansas High-Throughput Screening Laboratory (KU-HTSL). We included controls in each plate: no bacteria (16 wells; blank), untreated bacteria (8 wells; negative control), bacteria treated with 8 μM CCCP (8 wells; positive control). We obtained fluorescence readings at time zero (initial fluorescence), 1 minute (extent of quenching) and 60 minute (extent of recovery) after addition of 10 nM FeEnt. Across all plates the Z' factor was 0.87 ± 0.02 which was indicative of a sufficiently high success of the procedure. We chose 165 compounds that inhibited greater than and or equal to 2 SD from the median for validation of primary screens. Here we conducted the fluorescence assay in presence of 0, 2.5, 5, 10 and 20 μM of each compound and sub-divided them into 3 groups based on percentage of inhibition caused: <20%, 20-30% and >30%. True primary hits were 94 compounds that showed ≥20% inhibition. This excluded out chemicals that quenched fluorescence before

addition of FeEnt (1st read) possibly by specific or non-specific adsorption to FepA or energy transfer from spectral overlap with fluorescein (Table 7-1).

Table 7-1: Summary of primary screen results

Library	Total no. of compounds	No. cherry-picked[a]	No. with >30% inhibition	No. with 20–30% inhibition	No. with <20% inhibition	Hit rate[b] (overall)
CMLD	5,208	61	4	30	27	0.19
TimTec Actiprobe 5K	5,000	39	9	9	21	0.10
FDA/Bioactives	5,233	37	15	6	16	0.12
Microsource Spectrum	2,000	28	16	5	7	0.12
Total	17,441	165	44	50	71	0.54

[a]Compounds were cherry-picked by selection of any compounds whose percent inhibition at read 3 was ≥2 SD from the median (15% cutoff).
[b]The hit rate represents the number of compounds with >20% inhibition out of the total number of compounds.

Secondary screens were necessary to validate effects of the compounds on TonB-dependent phenomena such as, transport of FeEnt and Fc through FepA and FhuA, respectively in siderophore nutrition tests, and ColB and ColIa killing through FepA and Cir, respectively. Among 44 compounds that inhibited >30%, we purchased 20 for secondary screening tests. In siderophore nutrition tests (Fig. 7-1A), inclusion of 100 µM of test compounds in the top agar led to variable rates of inhibition by different chemicals which was apparent from the larger and fainter halos of bacterial growth around the disc containing either FeEnt or Fc. The positive control CCCP abolished uptake at 20 µM. We considered compounds that caused >10% increase in diameter as valid inhibitors in this test. Five compounds entirely abrogated growth at 100 µM, prompting us to test them at lower concentrations, where they responded in a dose-dependent fashion establishing them as inhibitors of TonB-dependent iron transport and not inherently toxic.

Various colicins, including ColB and ColIa utilize OM transporters such as FepA and Cir to penetrate the OM in a TonB-dependent fashion before depolarizing the IM. Compounds that inhibit TonB function will potentially block Colicin mediated killing.

Compounds that increased survival by >10% (Table 7-2) were considered as true inhibitors.

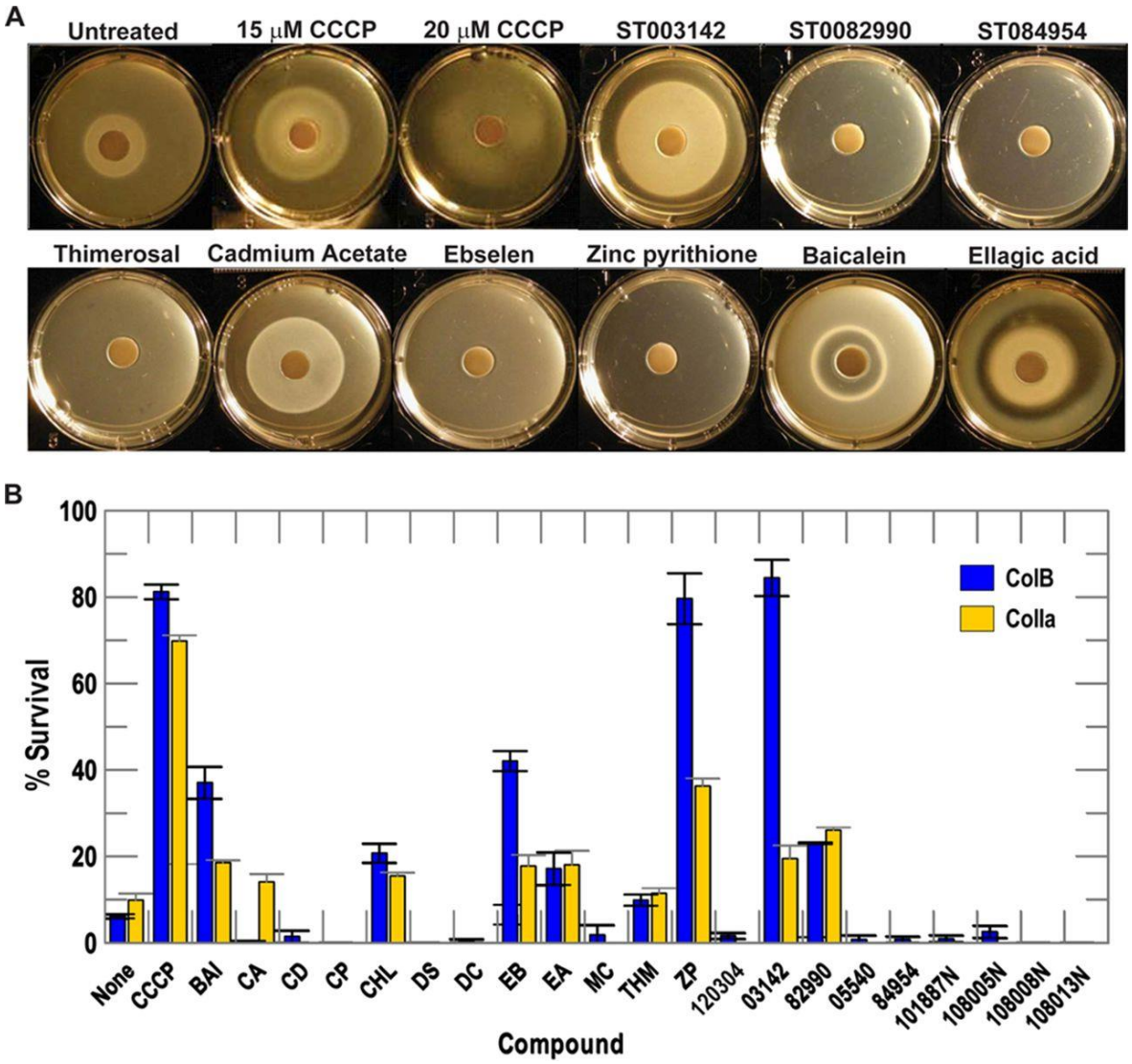

Fig. 7-1: Secondary screening for TonB-dependent inhibitors. A) Siderophore nutrition assays with FeEnt and B) Colicin killing tests in the presence of 20 selected hits from primary screening. Re-used with permission from American Society for Microbiology.

Overall, we identified six compounds that inhibited in all four TonB-dependent secondary screening assays. These were baicalein, ST003142, Thimerosal, Zinc pyrithione, Ebselen and ST0082990. Simultaneous blockage of FeEnt and Fc transport

excluded the possibility of an inhibitor creating steric hindrance on ligand absorption as TBDTs are very specific and inhibitory effects on both siderophore uptake and colicin killing excluded inhibitors that might be affecting periplasmic carriers or IM ABC-type transporters or ATP hydrolysis, as colicin killing does not involve these processes. However, none of these tests eliminate proton ionophores which disrupt IM *pmf* from consideration necessitating further tests to distinguish between chemicals that directly inhibit TonB-ExbBD from *pmf* depleting agents.

Table 7.2: Secondary screening of top 20 selected compounds against *E. coli* and *A. baumannii*

	E. coli							*A. baumannii*	
Treatment	FeEnt (cm)[b]	Fc (cm)[b]	ColB hits/cell[c]	Colla hits/cell[c]	[^{59}Fe]Ent uptake[d]	[^{14}C]lactose uptake[e]	MIC (μM)[f]	FeEnt (cm)[g]	MIC (μM)[f]
None	1.5 ± 0.1	1.5 ± 0.1	1.0	1.0	1.0	1.0	NA	1.2 ± 0.1	NA
CCCP	2.0 ± 0.1	1.9 ± 0.1	0.1 ± 0.0	0.2 ± 0.0	0.2	0.2	NT	1.5 ± 0.1	NT
Baicalein	1.7 ± 0.1	1.7 ± 0.1	0.3 ± 0.1	0.7 ± 0.0	1.0	1.0	—	1.2 ± 0.1	—
Cadmium acetate	2.2 ± 0.1	2.1 ± 0.4	1.1 ± 0.2	0.8 ± 0.1	NT	NT	512	0	256
Carbidopa	1.6 ± 0.1	1.6 ± 0.1	1.4 ± 0.5	NT	NT	NT	—	1.1 ± 0.0	—
Carboplatin	1.5 ± 0.0	1.6 ± 0.0	1.1 ± 0.1	NT	NT	NT	—	1.1 ± 0.1	—
p-Chloranil	1.5 ± 0.2	1.6 ± 0.1	0.7 ± 0.1	0.8 ± 0.0	NT	NT	—	1.1 ± 0.0	—
Dideoxyscleroin	1.6 ± 0.1	1.7 ± 0.2	1.1 ± 0.2	NT	NT	NT	—	1.2 ± 0.0	—
Dequalinium-Cl	1.4 ± 0.1	1.6 ± 0.1	1.1 ± 0.1	NT	NT	NT	—	1.1 ± 0.0	—
Ebselen	0[h]	0[h]	0.6 ± 0.1	0.8 ± 0.1	0.18	0.68	128	0	32
Ellagic acid	1.6 ± 0.1	1.4 ± 0.2	0.6 ± 0.1	0.7 ± 0.1	NT	NT	—	1.1 ± 0.0	256
3-Methoxycatechol	1.5 ± 0.1	1.6 ± 0.5	0.9 ± 0.3	NT	NT	NT	—	1.1 ± 0.0	—
Thimerosal	0[h]	0[h]	1.1 ± 0.1	1.1 ± 0.1	0.2	0.2	2	0	1
Zinc pyrithione	0[h]	0[h]	0.0 ± 0.0	0.5 ± 0.0	0.2	0.2	4	0	16
120304	1.6 ± 0.1	1.6 ± 0.1	1.0 ± 0.2	NT	NT	NT	—	1.2 ± 0.1	—
ST003142	2.7 ± 0.3	2.1 ± 0.0	0.0 ± 0.0	0.7 ± 0.1	1.0	1.0	256	1.7 ± 0.4	512
ST005540	1.6 ± 0.2	1.7 ± 0.2	1.2 ± 0.2	1.2 ± 0.1	NT	NT	—	1.1 ± 0.0	—
ST082990	0[h]	0[h]	0.6 ± 0.0	0.7 ± 0.0	0.44	0.74	128	0	16
ST084954	0[h]	0[h]	1.3 ± 0.3	1.1 ± 0.1	1.0	1.0	32	1.4 ± 0.1	256
KUC101887N	1.4 ± 0.1	1.5 ± 0.1	1.1 ± 0.3	NT	NT	NT	—	1.1 ± 0.1	—
KUC108008N	1.5 ± 0.0	1.6 ± 0.0	1.3 ± 0.3	NT	NT	NT	—	1.1 ± 0.0	—
KUC108005N	1.5 ± 0.1	1.6 ± 0.1	1.0 ± 0.0	NT	NT	NT	—	1.1 ± 0.0	—
KUC108013N	1.5 ± 0.1	1.6 ± 0.1	1.3 ± 0.3	NT	NT	NT	—	1.1 ± 0.0	—

[a]NA, not applicable; NT, not tested. —, MIC exceeded 512 μM.

Since, both TonB-dependent OM transport and IM lactose transport are dependent on *pmf*, we tested the effect of different concentrations of the 6 compounds from the secondary screen on [^{59}Fe]Ent and [^{14}C]lactose uptake. Surprisingly, baicalein and ST003142 did not show any effect on either [^{59}Fe]Ent and [^{14}C]lactose uptake at concentrations as high as 0.5 mM. Thimerosal and zinc pyrithione on the other hand, affected both [^{59}Fe]Ent and [^{14}C]lactose transport in a concentration-dependent fashion

almost similar to CCCP. Thimerosal being an organomercurial might be reacting with protein amino and sulfhydryl groups to modify key functional residues such as His20 in TonB. Lastly, ebselen and ST0082990 showed potential as specific inhibitors of TonB-ExbBD function. Both compounds inhibited [^{59}Fe]Ent uptake to levels comparable to CCCP (25 µM) although at a 10-fold higher concentration. They inhibited [^{14}C]lactose uptake at 250 µM but to a much less extent than CCCP. Importantly, there was a large differential in the extent of their iron uptake to that of lactose transport (Fig. 7-2). This resulted in an overall hit rate of 0.054% potentially TonB inhibitors which allows us to expect hundreds of such non-proton ionophore, TonB antagonists when extrapolated to larger compound libraries. To evaluate the bactericidal activity of the 20 chemicals, we performed MIC tests in LB as well as MOPS media up to 512 µM. Both ebselen and ST0082990 showed MICs of <128 µM (Table 7-2).

7.3.2 Identification and characterization of FeEnt transporter in *A. baumannii*

A. baumannii encodes Fur-regulated TBDTs for ferric-siderophores from different species apart from the ones it synthesizes. By PCR amplifying genomic locus that encodes a disrupted fepA ortholog in *A. baumannii* ATCC 17987 strain, we found that the locus is not split as annotated in the genome. We precisely deleted the loci A1S_0980 and A1S_0981 to create a ***ΔfepA*** strain and tested its ability to utilize FeEnt in MOPS minimal medium with or without the apo-siderophore, apo-ferrichromeA as an iron-sequestering agent. *A. baumannii* ***ΔfepA*** and WT were able to grow equally well under both conditions but the ***ΔfepA*** strain was unable to use FeEnt as the sole iron source in siderophore nutrition tests; it was able to utilize Fc normally indicating that the deleted

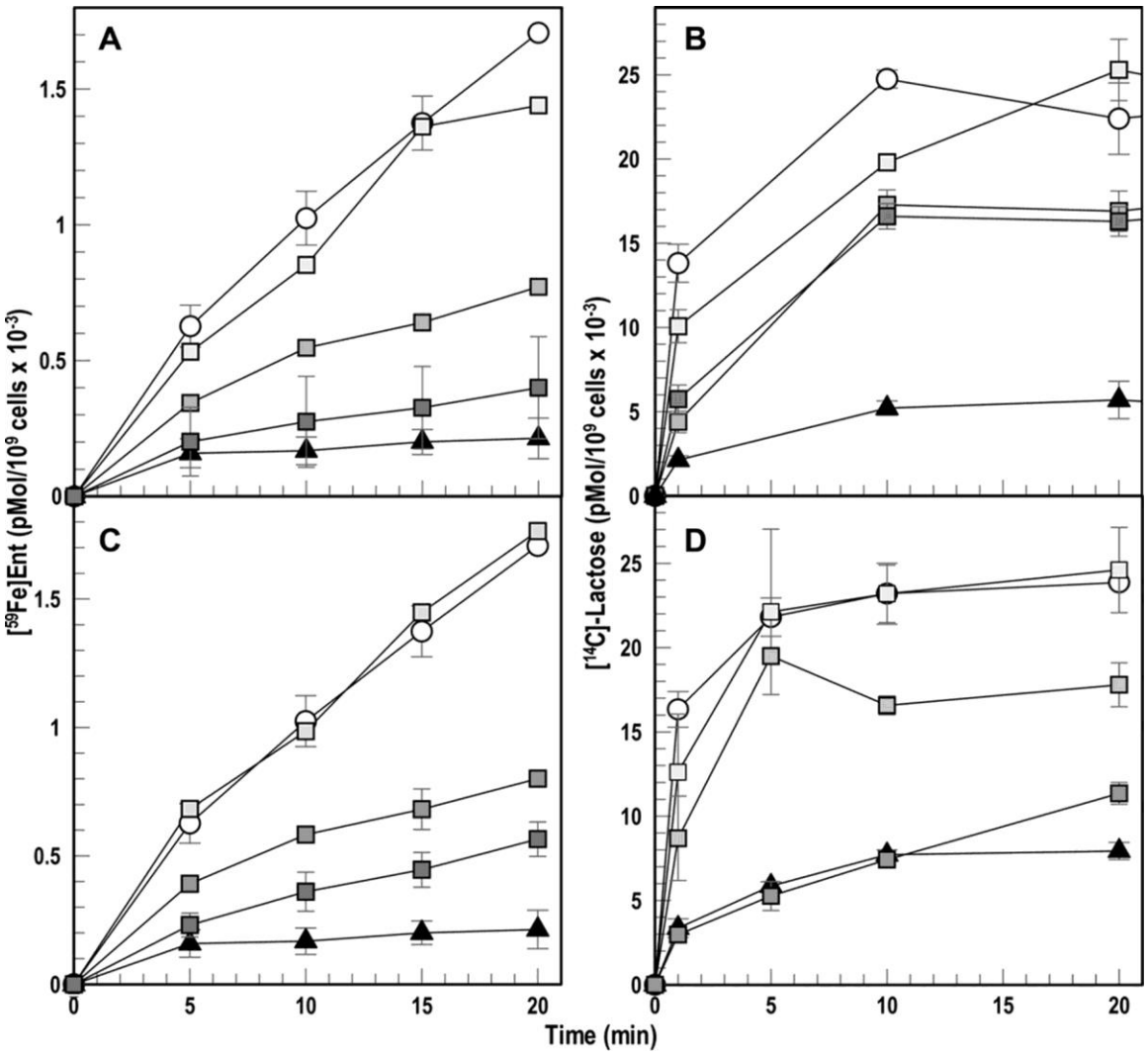

Fig. 7-2: Inhibition of [^{59}Fe]Ent and [^{14}C]lactose uptake in E. coli MG1655. We assayed accumulation of [^{59}Fe]Ent (A and C) and [^{14}C]lactose (B and D) in the presence of ebselen (A and B) and ST0082990 (C and D) in the absence of inhibitor (circles), in the presence of 25 µM CCCP (triangles), in the presence of ebselen at 25 µM (light grey square), 200 (medium grey square) and 250 (dark grey square) or in the presence of ST0082990 at 25 µM (light grey square), 100 (medium grey square) and 250 (dark grey square).

loci encoded FepA. Phenotype was restored by complementing with plasmid encoded FepA under control of its native promoter (pAbaFepA) as well as under an exogenous

promoter (p2682proAbaFepA) (Fig. 7-3 C, D). Comparison of [^{59}Fe]Ent uptake rates of WT, *ΔfepA* and complemented strains showed much lower uptake compared to both WT and complemented strains (Fig. 7-3 E) suggesting that this loci encodes the primary FeEnt transporter. We also characterized its transport kinetics parameters, Km = 14.6 nM and Vmax = 413.05 pmol/10^9 cells/min (Fig. 7-3 F).

7.3.3 Fluorescence observations of FeEnt transport with AbaFepA Cys mutants

To test the adaptability of the FLHTS approach in other bacteria, we decided to engineer Cys substitutions in the external loops of AbaFepA similar to EcoFepA. Since, crystal structure of AbaFepA is unavailable, we used a predicted (Chimera program) architecture, based on its 46% identity of primary structures with EcoFepA, to identify ortholgous residues on AbaFepA loops that may be potentially fluoresceinated. By site-directed mutagenesis we created the sites: T223C, S279C, A326C, T383C, T482C, T562C, S665C, and S712C (Fig. 7-4 A, B). We expressed the AbaFepA Cys mutants in the ΔfepA strain, labeled them with fluorescein maleimide. All the mutants were strongly expressed and specifically labeled as evident from SDS-PAGE and fluorescence imaging, like EcoFepA S271C. Although all of the mutants were positive in siderophore nutrition tests, they showed variable uptake rates of [^{59}Fe]Ent. S279C, T562C and T665C showed 30-75% uptake rates compared WT even in fluoresceinated state making them suitable candidates for use in FLHTS.

Spectroscopic observation of FeEnt binding to the candidate fluorescienated FepA mutants showed 10-20% quenching which is less than EcoFepA Cys mutants (60%).

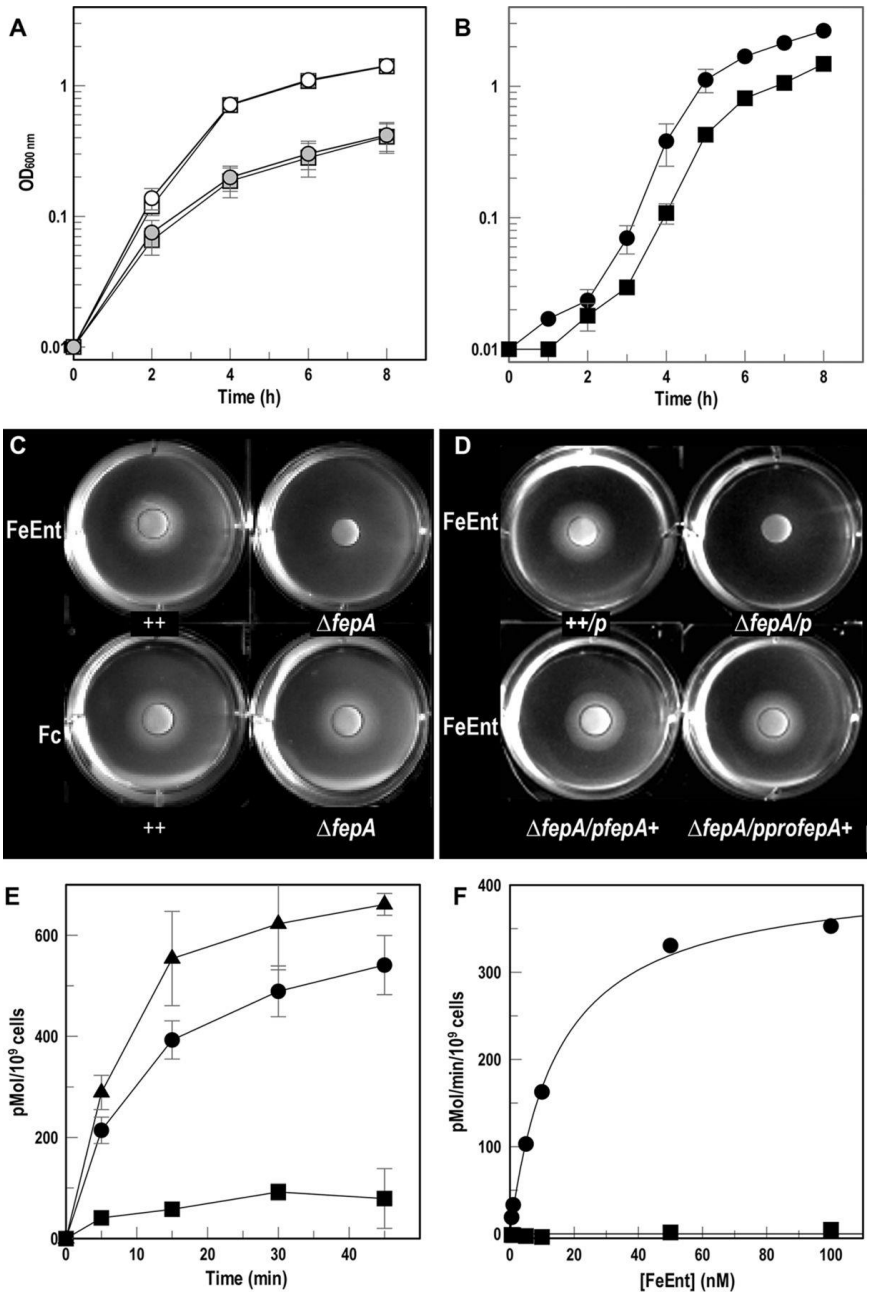

Fig. 7-3: FeEnt transport by *A. baumannii.* A) Growth of 17978 (circles) and its ΔfepA derivative (squares) in MOPS with or without apo-FcA. B) The ΔfepA (■) derivative grows to about half the WT (●) in MOPS in presence of FeEnt. C) and D) Siderophore nutrition assays with 17978, the ΔfepA strain and the complemented strain expressing pfepA. E) Accumulation of [^{59}Fe]Ent by WT (●), ΔfepA (■) and the complemented strain (▲). F) Transport of [^{59}Fe]Ent by *A. baumannii* 17978 (●), or its ΔfepA derivative (■).

Nevertheless, quenching and recovery occurred in a dose-dependent fashion. 10 to 20 nM FeEnt showed the best quenching and the fluorescence recovered completely in 10 min (Fig. 7-4C). Transport by AbaFepAS279C-FM was also blocked by CCCP as expected, but at ~5-fold less concentration than required to abolish transport by EcoFepA, underlining the consistency of the physiological system (Fig. 7-4D). Lower levels of quenching might point out that the residues we engineered were not optimum sites for fluor attachment. The sites we targeted may not be ideal for tracking changes in protein conformation since, fluorescence quenching is brought about by movement of loops with attached fluorophores translocating to altered environments. It may also arise from presence of extended hydrophilic surfaces on pathogenic *A. baumannii* cells from a more complex, full-length LPS O-antigen and capsule layer in its cell envelope, than found in E. coli K-12. This may give rise to collisional quenching, and thereby limit the extent of further quenching upon FeEnt binding to FepA. Finally, we tested the applicability of the three most promising mutants in the 96-well format where we observed 14 and 18% quenching in the ΔfepA/pAbafepAS279C or -T562C mutants respectively upon addition of 20 nM FeEnt to 5 X 10^7 cells and recovery was nearly complete. Ultimately, we obtained Z' factors of 0.6 to 0.8 after 8 to 15 min.

In summary, through this small-scale FLHTS study we discovered novel antagonists of TonB function in E. coli and demonstrated the efficacy of this method in the ESKAPE pathogen *A. baumannii*. In the light of increasing antibiotic-resistance among bacterial pathogens, pilot studies such as this acts as a methodological template for identification of drugs against clinically-relevant bacterial strains.

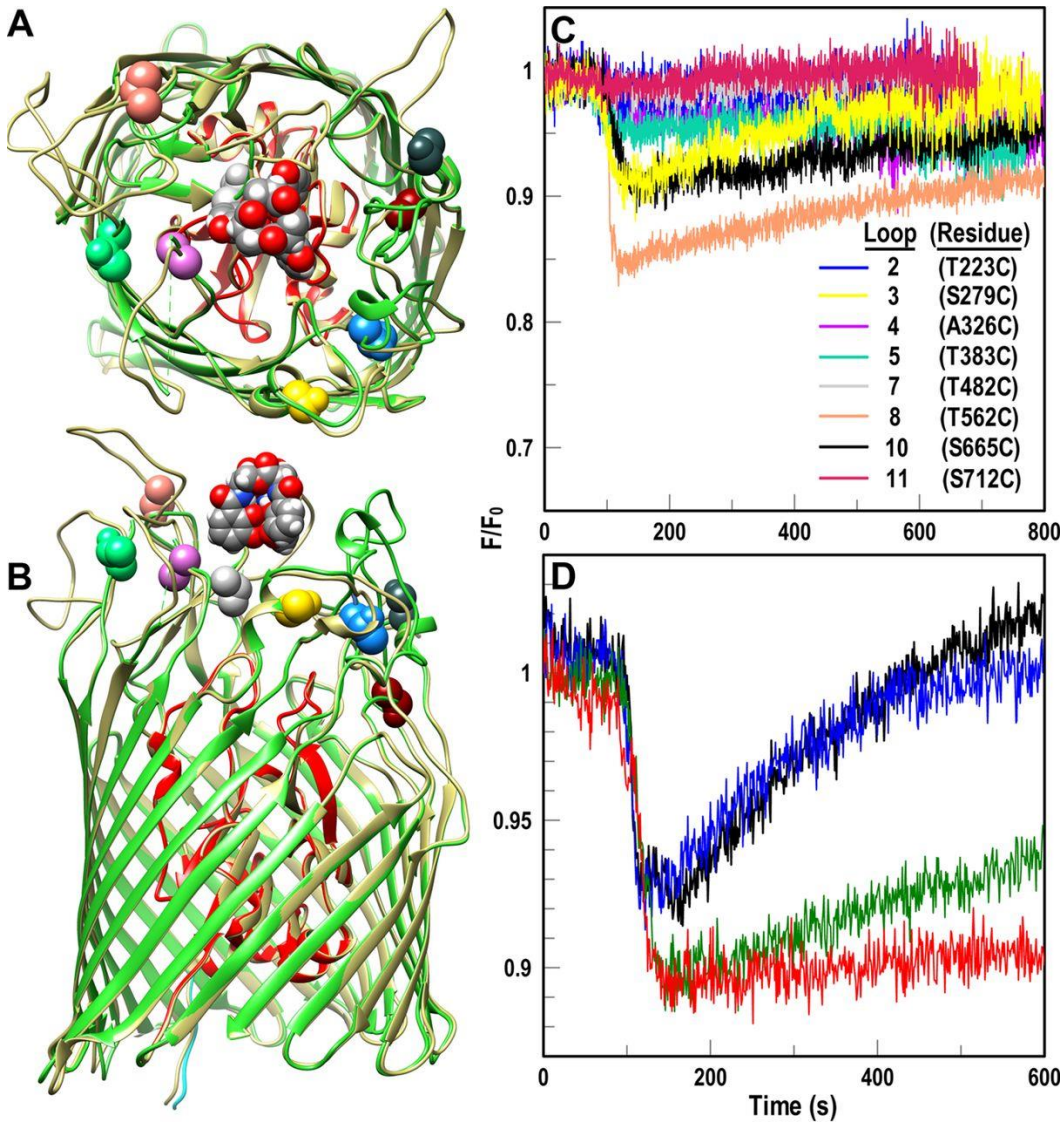

Fig. 7-4: The proposed Cys residues in the Aba FepA (dark beige) were determined by aligning it against Eco FepA (lime green) in CHIMERA (A and B). The real-time uptake of FeEnt observed by fluorescence spectroscopy in each of the labeled Cys substituted mutants (C) indicated that the optimum quenching and recovery was observed in 17978 ΔfepA/pAbafepAS279C. Normalized fluorescence against time in absence (black) and presence of increasing concentration of inhibitor (CCCP: blue, 2.5μM; green, 5 μM; red, 10 μM) of the labeled 17978 ΔfepA/pAbafepAS279C is depicted in D).

References

Abergel, R.J., Warner, J.A., Shuh, D.K. and Raymond, K.N. (2006) Journal of the American Chemical Society **128**, 8920-31.

Aisen, P., Leibman, A. and Zweier, J. (1978). Journal of Biological Chemistry. **253,** 1930–1937.

Beddek, A.J., Sheehan, B.J., Bosse, J.T., Rycroft, A.N., Kroll, J.S. and Langford, P.R. (20004) Infection and Immunity **72**, 701–708. DOI. 10.1128/IAI.72.2.701-708.2004.

Beeby, M., Gumbart, J.C., Roux, B. and Jensen, G.J. (2013) Molecular Microbiology **88**, 664 – 672.

Bleuel, C., Grosse, C., Taudte, N., Scherer, J., Wesenberg, D., Krauss, G.J., Nies. D.H. and Grass, G. (2005) Journal of Bacteriology **187**, 6701-6707.

Bos, C., Lorenzen, D. and Braun, V. (1998) Journal of Bacteriology **180**, 605–613.

Bullen, J.J., Rogers, H.J. and Griffiths, E. (1978) Current Topics in Microbiology and Immunology **80**, 1–35.

Cadieux, N, Bradbeer, C., and Kadner, R.J. (2000) Journal of Bacteriology **182**, 5954-5961.

Charbit, A., Clement, J.M., Hofnung, M. (1984) Journal of Molecular Biology **175**, 395–401.

Cope, L.D., Hrkal, Z. and Hansen, E.J. (2000) Infection and Immunity **68**, 4092–4101.

Cornelissen, C.N. and Sparling, P.F. (1994) Methods in Enzymology **235**, 356–363.

Cornelissen, C.N. and Sparling, P.F. (1994) Molecular Microbiology **14**, 843–850.

da Silva Neto, J.F., Lourenco, R.F. and Marques, M.V. (2013) BMC Genomics **14**, 549.

de Lorenzo, V., Giovannini, F., Herrero, M. and Neilands, J.B. (1988) Journal of Molecular Biology **203**, 875–884.

Di Masi, D.R., White, J.C., Schnaitman, C.A. and Bradbeer, C. (1973) Journal of Bacteriology. **115**, 506-513.

Escolar, L., Pe´rez-Martı´n, J. and de Lorenzo, V. (1998) Journal of Molecular Biology **283**, 537–547.

Evans, J.S., Levine, B.A., Trayer, I.P., Dorman, C.J., and Higgins, C.F. (1986) FEBS Letters **208**, 211–216.

Ferguson, A.D., Chakraborty, R., Smith, B.S., Esser, L., van der Helm, D. and Deisenhofer, J. (2002) Science **295**, 1715–1719.

Furrer, J.L, Sanders, D.N., Hook-Barnard, I.G. and McIntosh, M.A. (2002) Molecular Microbiology **44(5)**, 1225-34.

Greenwood, K.T. and Luke, R.K. (1978) Biochimica et Biophysica Acta **525**, 209-218.

Gudmundsdottir, A, Bell, P.E., Lundrigan, M.D., Bradbeer, C. and Kadner, R.J. (1989) Journal of Bacteriology **171**, 6526-33.

Gumbart J.C., Beeby, M., Jensen, G.J. and Roux, B. (2014) PLoS Computational Biology **10**, e1003475.

Hall, H. K. and Foster. J.W. (1996) Journal of Bacteriology **178**, 5683–5691.

Hantke, K. (1976) FEBS Letters **70**, 109-112.

Heidinger, S., Braun, V., Pecoraro, V.L. and Raymond, K.N. (1983) Journal of Bacteriology **153**, 109–115.

Hickman, S.J., Cooper, R.E.M., Bellucci, L., Paci, E. and Brockwell, D.J. (2017) Nature Communications **8**, 14804.

Horiyama, T and Nishino, K (2014) PLoS One. **9(9)**, e108642.

Huang, B., Ru, K., Yuan, Z., Whitchurch, C.B. and Mattick, J. (2004) Journal of Bacteriology **186**, 4387–4389. DOI. 10.1128/JB.186.13.4387-4389.2004.

Jenal, U., and Stephens, C. (2002) Current Opinions in Microbiology. **5**, 558–563.

Jiang, X., Payne, M.A. Cao, Z., Foster, S.B., Feix, J.B., Newton, S.M. and Klebba, P.E. (1997) Science **276**, 1261–1264.

Karjalainen, T.K., Evans, D.G., Evans, D.J., Graham, Jr. D.Y., and Lee. C.H. (1991) Microbial Pathogenesis. **11**, 317–323.

Kaserer, W.A., Jiang, X., Xiao, Q., Scott, D.C., Bauler, M., Copeland, D., Newton, S.M.C. and Klebba, P.E. (2008) Journal of Bacteriology **190**, 4001–4016.

Koch, A.L. (1998) Research in Microbiology **149**, 689–701.

Kretchmar, S.A., Reyes, Z.E. and Raymond, K.N. (1988) Biochimica et Biophysica Acta **956**, 85–94.

Letoffe, S., Ghigo, J.M. and Wandersman, C. (1994) PNAS **91**, 9876–9880.

Létoffé, S., Nato, F., Goldberg, M.E. and Wandersman, C. (1999) Molecular Microbiology **33(3)**, 546-55.

Litwin, M. and Calderwood, S.B. (1993) Clinical Microbiology Reviews **6**, 137–149.

Locher, K.P., Rees, B., Koebnik, R., Mitschler, A., Moulinier, L., Rosenbusch, J.P. and Moras, D. (1998) Cell **95**, 771–778.

Makemson, J. C. and Hastings, J.W. (1982) Current Microbiology. **7**, 181–186.

Martin, R.B., Savory, J., Brown, S., Bertholf, R.L. and Wills, M.R. (1987) Clinical Chemistry **33**, 405–407.

McCarter, L. and Silverman, M. (1989) Journal of Bacteriology **171**, 731–736.

Morton, D.J., Seale, T.W., Madore, L.L., VanWagoner, T.M., Whitby, P.W. and Stull, T.L. (2007) Microbiology **153**, 215–224.

Motley, S.T., Morrow, B.J., Liu, X., Dodge, I.L., Vitiello, A., Ward, C.K. and Shaw, K.J. (2004) Cell Microbiology **6**, 849–65.

Noinaj, N., Guillier, M., Barnard, T.J. and Buchanan, S.K. (2010) Annual Review of Microbiology **64**, 43-60.

Neilands, J.B. (1995) Journal of Biological Chemistry **270**, 26723–26726.

Neilands, J.B., Konopka, K., Schwyn, B., Coy, M., Francis, R.T., Paw, B.H. and Bagg, A. (1987) in Iron Transport in Microbes, Plants and Animals (Winkelmann, G., van der Helm, D., and Neilands, J. B., eds) pp. 3–33, VCH Press, Weinheim.

Newton, S.M., Igo, J.D., Scott, D.C. and P. E. Klebba. (1999) Molecular Microbiology **32**, 1153–1165.

Niederhoffer, E. C., Naranjo, C.M, Bradley, K.L. and Fee, J.A. (1990) Journal of Bacteriology **172**, 1930–1938.

Nikaido, H. and Vaara, M. (1985) Microbiological Reviews **49**, 1–32.

Nuss, A.M., Beckstette, M., Pimenova, M., Schmühl, C., Opitz, W., Pisano, F., Heroven, A.K. and Dersch, P. (2017) PNAS. DOI. 10.1073/pnas.1613405114.

Occhino, D.A., Wyckoff, E.E., Henderson, D.P., Wrona, T.J.and Payne, S.M. (1998) Molecular Microbiology **29**,1493–1507.

Ochsner, U.A., Johnson, Z. and Vasil, M. L. (2000) Microbiology **146**, 185–198.

Perkins-Balding, D., Ratliff-Griffin, M. and Stojiljkovic, I. (2004) Microbiology and Molecular Biology Reviews **68**, 154–171.

Pilsl, H. and Braun, V. (1995) Journal of Bacteriology **177**, 6973–6977.

Pilsl, H., Glaser, C., Gross, P., Killman, H., Olschläger, T. and Braun V. (1993) Domains of colicin M involved in uptake and activity. Molecular and General Genetics **240**, 103–112.

Poole, K., Zhao, Q., Neshat, S., Heinrichs, D.E. and Dean, C.R. (1996) Microbiology **142**, 1449-1458. DOI. 10.1099/13500872-142-6-1449.

Rabsch, W., Ma, L., Wiley, G., Najar, F.Z., Kaserer, W., Schuerch, D.W., Klebba, J.E., Roe, B.A., Laverde Gomez, J.A., Schallmey, M., Newton, S.M. and Klebba, P.E. (2007) Journal of Bacteriology **189**, 5658-5674.

Reniere, M.L., Torres, V.J. and Skaar, E.P. (2007) Biometals **20**, 333–345.

Roof, S.K., Allard, J.D., Bertrand, K.P., and Postle, K. (1991) Journal of Bacteriology **173**, 5554–5557.

Schaible, U.E. and Kaufmann, S.H.E. (2004) Nature Reviews Microbiology **2**, 946-953

Scott, D.C., Newton, S.M. and Klebba, P.E. (2002) Journal of Bacteriology **184**, 4906–4911.

Sharp, K.H., Schneider, S., Cockayne, A. and Paoli, M. (2007) Journal of Biological Chemistry **282(14)**, 10625-106231.

Smith, A.D. and Wilks, A. (2015) Journal of Biological Chemistry **290**, 7756 –7766.

Stock, J.B., Ninfa, A.J. and Stock, A.M. (1989) Microbiological Reviews **53**, 450-490.

Stojiljkovic, I., Ba¨umer, A.J. and Hantke, K. (1994) Journal of Molecular Biology **236**, 531–545.

Struyve, M., Moons, M. and Tommassen, J. (1991) Journal of Molecular Biology **218**, 141–148.

Szafranska, A.K., Oxley, A.P.A., Chaves-Moreno, D., Horst, S.A., Roßlenbroich, S., Peters, G., Goldmann, O., Rohde, M., Sinha, B., Pieper, D.H., Löffler, B., Jauregui, R., Wos-Oxley, M.L. and Medina, E. (2014) mBio ***5*(6)**, e01775–14.

Thulasiraman, P., Newton, S.M., Xu, J., Raymond, K.N., Mai, C., Hall, A., Montague, M.A. and Klebba, P.E. (1998) Journal of Bacteriology **180**, 6689–6696.

Verwer, R.W.H., Nanninga, N., Keck, W. and Schwarz, U. (1978) Journal of Bacteriology **136**, 723 – 729.

Wiener, M., Freymann, D., Ghosh, P. and Stroud, R.M. (1997) Nature **385**, 461–464.

Worst, D.J., Maaskant, J., Vandenbroucke-Grauls, C.M. and Kusters, J.G. (1999) Microbiology **145**, 681–688.